Title
Variability in wildfire emissions of nitrogen oxides as observed from space

Author
Mebust, Anna

Publication Date
2013

Peer reviewed|Thesis/dissertation

Variability in wildfire emissions of nitrogen oxides as observed from space

By

Anna Kristina Mebust

A dissertation submitted in partial satisfaction of the

requirements for the degree of

Doctor of Philosophy

in

Chemistry

in the

Graduate Division

of the

University of California, Berkeley

Committee in charge:

Professor Ronald C. Cohen, Chair
Professor Kristie Boering
Professor Inez Fung

Fall 2013

Variability in wildfire emissions of nitrogen oxides as observed from space

Abstract

Variability in wildfire emissions of nitrogen oxides as observed from space

by

Anna Kristina Mebust

Doctor of Philosophy in Chemistry

University of California, Berkeley

Professor Ronald C. Cohen, Chair

Wildfires are a significant source of nitrogen oxides ($NO_x \equiv NO + NO_2$) to the global atmosphere, representing approximately 15% of the total NO_x budget. Fire conditions that govern NO_x emission vary significantly from fire to fire, resulting in highly variable emissions. Emissions from fires burned in a laboratory setting fail to reproduce the conditions in which large wildfires occur, such as fire size and meteorology; however, *in situ* measurements of fire emissions are challenging to make, in part due to the destructive nature of large wildfires. As a result, systematic variability of NO_x emissions—even when normalized for biomass burned—across or within biomes is poorly understood and documented.

In this dissertation, I demonstrate that the high spatial and temporal coverage of space-based observations can be used to greatly increase the number and scope of available observations of actively burning wildfires. I derive a method to estimate NO_x emission coefficients (ECs in g NO_x MJ^{-1}) using NO_2 column densities from the Ozone Monitoring Instrument (OMI) and fire radiative power from the Moderate Resolution Imaging Spectroradiometer (MODIS), two Earth-observing satellite instruments. I show that this method, when applied in California and Nevada, reproduces differences in fire emission factors (EFs in g NO_x kg^{-1}) between fuel types that have been previously observed using in situ measurements. I then identify and explore sources of variability in NO_x ECs in fires across the globe. I compare mean ECs for fires in different locations but similar biomes (e.g. grasses) and find that while most ECs cover a relatively narrow range, ECs for several locations are significantly different from the mean biome EC. I examine seasonal variability in ECs, finding that ECs in African woody savannas have a strong seasonal dependence that is not observed in open savannas; this behavior may be related to reallocation of nitrogen to below ground during the fire season by plants and/or the seasonal variation of fire fuel composition in woody savannas. I also find that this behavior extends to other woody savanna regions in South America and Australia, and that ECs in several biomes exhibit a dependence on wind speed.

Table of contents

List of Figures

List of Tables

Acknowledgements

This work would not have been possible without the contributions of many individuals. I want to thank my advisor, Ron Cohen, for his guidance and support throughout my time at Berkeley. I have had the pleasure of working with many brilliant colleagues within my research group, and I particularly would like to acknowledge Ashley Russell, Lukas Valin, Rynda Hudman, Sally Pusede, and Jill Teige for their contributions, direct and indirect, to my work. Thanks also to my dissertation committee members, Inez Fung and Kristie Boering, and to the Berkeley Atmospheric Sciences community. I gratefully acknowledge financial support from the National Aeronautics and Space Administration, grants NNX08AE566 and NNX12AB79G, and from the Department of Energy Office of Science Graduate Fellowship Program (DOE SCGF), made possible in part by the American Recovery and Reinvestment Act of 2009, administered by ORISE-ORAU under contract no. DE-AC05-06OR23100. All opinions expressed in this dissertation are my own and do not necessarily reflect the policies and views of DOE, ORAU, or ORISE.

Chapter 1

Overview

1.1 Background and summary

Fires represent ~15% of total global nitrogen oxide ($NO_x \equiv NO + NO_2$) emissions and are similar in magnitude to other natural or partly natural sources of NO_x—i.e., soils and lightning (Denman et al., 2007). These emissions are a major component of the nitrogen (N) cycle, releasing N from the biosphere to the atmosphere where it affects the composition of the atmosphere on global scales and is ultimately returned to the biosphere via deposition. Yearly global biomass burning emission estimates from the Global Fire Emission Database version 3 (GFEDv3) range from 7.41 to 13.93 Tg N yr^{-1} over a 15-year span (1997-2011), indicative of the high interannual variability in these emissions (van der Werf et al., 2010). Given the episodic nature of fires, these emissions are even more variable on smaller temporal (e.g., days to weeks) and spatial (local, regional) scales. Biomass burning estimates like those provided by GFEDv3 are highly parameterized estimates; it is generally understood that these estimates are tuned to capture a statistical ensemble and not the emissions from an individual fire and that there are limited observational constraints on regional biases. This underlines the basic lack of understanding in the scientific community with respect to the processes that govern variability in fire emissions.

Factors considered in most current treatments of fire emissions of NO_x are fire size and fuel type. Emissions are estimated as the product of the total biomass burned in the fire or fires (in kg) and an "emission factor" (EF in g kg^{-1}) derived from measurements of an individual fire or several fires that are assumed to be representative of fire conditions for a particular fuel type (Andreae and Merlet, 2001). These EFs are typically based on in situ measurements of fire emissions, or occasionally laboratory measurements. While there is a growing body of laboratory EF measurements for increasingly specific fuel types (e.g., McMeeking et al., 2009), there remain questions with respect to the extrapolation of these measurements to the scale of a wildfire where the relative contributions of specific fuels are not characterized. Estimates of emissions in this framework are linearly dependent on fire size and discretely dependent on fuel type, with EFs derived independently for only a few (3-7) biomes (Andreae and Merlet, 2001; Hoelzemann et al., 2004; van der Werf et al., 2010; Akagi et al., 2011). These estimates neglect any potential for differences in emissions per unit mass between fires from a single biome type, and strategies that incorporate known variability in biomass burn rates on time scales shorter than monthly (e.g., diurnal and daily variability) have only recently been proposed (Mu et al., 2011).

The major question with respect to biomass burning emissions of NO_x (and, indeed, for many other species emitted in fires) is what governs the variability in emissions (outside of fire size) and whether that variability is predictable. It is well-established that EFs for NO_x are highly

variable from fire to fire, but the processes governing this variability are poorly understood. Proposed factors include the N content of the fuel and the modified combustion efficiency (MCE) of the fire (Andreae and Merlet, 2001). MCE is an index describing the relative contributions of flaming and smoldering combustion to a fire: an MCE of 1 indicates completely flaming combustion, with lower values indicating an increasingly important smoldering component (Battye and Battye, 2002). Theoretically, since NO_x is formed via oxidation of N in the fuel, the more N available to be oxidized during combustion, the greater the NO_x emissions; similarly, high MCE indicates a larger fraction of flaming combustion, which is more oxidizing than smoldering combustion, suggesting high NO_x emissions at high MCE as a fraction of all N-containing compounds—e.g., NH_3, HCN, etc. (Andreae and Merlet, 2001). However, we note that observational support for the effects of these processes on emissions remains limited. Unlike many carbon-containing species which show a clear linear dependence on MCE, NO_x is only weakly dependent on MCE with extremely low correlation coefficients ($R^2<0.2$) (Battye and Battye, 2002; Yokelson et al., 2011). Fuel N is almost never measured in combination with EFs either in the laboratory or for wild or prescribed fires. When measured, there tends to be a strong correlation of fuel N with EFs (Lacaux et al., 1996). Thus it is unclear whether fuel N and MCE fully explain the variability in EFs, leaving open the possibility that other processes might play an important but as-yet unidentified role in emission variability. These processes potentially (or even probably) vary throughout the fire season or between different fire seasons, and so temporally resolved EFs might provide a clearer picture of the relevant processes; however, prior to this dissertation only two studies have performed such an analysis for NO_x (both focused on seasonal variations), and both were extremely limited in scope (Lapina et al., 2008; Yokelson et al., 2011).

To improve understanding of fire NO_x emissions, a dramatic enhancement in the number of measurements of fires (often in remote locations) is needed. Instruments deployed on sun-synchronous, polar-orbiting satellites offer a unique opportunity to make these observations because unlike ambient measurements, space-based observations are distributed evenly across the globe and include remote locations where in situ measurements are financially or logistically difficult. Satellite instruments generally sample continuously throughout the year, providing measurements of seasonal variability in emissions, and observational records span several years, covering a range of different environmental conditions that might impact emission behavior. Current instruments provide observations at high enough spatial resolution that individual emission plumes from point sources can be observed (Mebust et al., 2011; Chapter 2). When measuring fire emissions via satellite instruments, calculation of an "emission coefficient" (EC in g MJ^{-1} of fire radiative energy) is often chosen over an EF (Ichoku and Kaufman, 2005; Jordan et al., 2008; Vermote et al., 2009). This is because estimation of total biomass burned from a fire via satellite requires the combination of several observational products along with other assumptions that significantly increase uncertainties, while fire radiative power (FRP in MJ s^{-1}) is directly measured by several instruments and so ECs are calculated with generally lower uncertainties. Studies have shown that the total radiative energy released by the fire is proportional to the biomass burned, indicating that ECs are proportional to EFs and thus can provide similar information with respect to fire emission processes (Wooster, 2002; Wooster et al., 2005; Freeborn et al., 2008).

In this dissertation, I apply satellite observations to examine variability in NO_x ECs across the globe. Using tropospheric NO_2 column densities from the Ozone Monitoring Instrument

(OMI) and fire radiative power (FRP) from the Moderate Resolution Imaging Spectroradiometer (MODIS), I develop a method to measure NO_x ECs; I then apply it to study within- and across-biome ECs and also examine seasonal behavior in ECs. This work provides an especially comprehensive picture of systematic similarities and differences in ECs and identifies remaining uncertainties that are opportunities for future research.

In Chapter 2, I describe the development of the method used to infer ECs from space-based observations of fires. I use observations of FRP from MODIS and tropospheric NO_2 columns from OMI to derive NO_2 ECs for three land types over California and Nevada. Retrieved emission coefficients are 0.279±0.077, 0.342±0.053, and 0.696±0.088 g MJ^{-1} NO_2 for forest, grass and shrub fuels, respectively. I find that these emission coefficients reproduce ratios of emissions with fuel type reported previously using independent methods. However, the magnitude of these coefficients is lower than prior estimates. While it is possible that a negative bias in the OMI NO_2 retrieval over regions of active fire emissions is partly responsible, comparison with several other studies of fire emissions using satellite platforms indicates that current emission factors may overestimate the contributions of flaming combustion and underestimate the contributions of smoldering combustion to total fire emissions. I find that in California and Nevada, 67% of the variability in emissions between individual fires is accounted for by FRP and fuel type.

In Chapter 3, I extend this analysis to the global scale. I infer mean emission coefficients (ECs in g NO MJ^{-1}) from fires for global biomes, and across a wide range of smaller-scale ecoregions. Mean ECs for all biomes fall between 0.250 – 0.362 g NO MJ^{-1}, a range that is smaller than found in previous studies of biome-scale emission factors. The majority of ecoregion ECs fall within or near the range of biome-scale ECs observed here, implying that under most conditions, mean fire emissions per unit energy are similar regardless of fuel type or location. In contrast to these similarities, I find that about 24% of individual ecoregion ECs deviate significantly ($p<0.05$) from the mean EC for the associated biome (e.g., boreal forest fires in Asia vs. global boreal forest fires), showing that there are some regions where fuel type-specific global emission parameterizations will fail to capture local mean fire NO_x emission behavior.

In Chapter 4, I show that satellite observations can be applied to identify and examine seasonal patterns in ECs and EFs, and demonstrate that these patterns can provide some information regarding the specific drivers of these patterns. I show that in Africa, ECs for NO_x exhibit a pronounced seasonal cycle in woody savannas, with early-season ECs 20–40% above and late-season ECs 30–40% below the mean, while no cycle exists in nonwoody savannas. I discuss several possible mechanisms of the observed cycle, including seasonal differences in fuel N content and modified combustion efficiency.

In Chapter 5, I discuss some examples of temporal behavior and specific meteorological drivers of ECs. I examine seasonal variability in ECs in woody savanna and savanna biomes on the global scale. I find that the seasonal pattern demonstrated in Chapter 4 also holds for important tropical savanna and woody savanna regions in South America and Australia, with ECs for woody savanna fires decreasing strongly throughout the fire season and ECs for savanna fires exhibiting little or no seasonal dependence. This pattern is not matched by woody savanna fires in regions outside of the tropics, which typically have much lower rates of fire occurrence,

suggesting that the behavior could be the result of a biome-specific adaptation to frequent fire. I also find that ECs in all global biomes are correlated with high wind speeds, consistent with a mechanism proposed previously that remained untested by observations.

In Chapter 6, I conclude with a discussion of opportunities for future research. Areas of focus include greater investigation of temporal variability (e.g., broader assessment of seasonality, examination of interannual variability) and identifying and quantifying relationships with potential meteorological drivers of variability (e.g., precipitation). I also comment on the future of space-based observations of fires and how improvements to technology and sampling in the upcoming generation of satellite instruments might positively contribute to efforts to characterize wildfire emissions from space.

Chapter 2

Characterization of wildfire NO_X emissions using MODIS fire radiative power and OMI tropospheric NO_2 columns

This chapter has been adapted from the following peer-reviewed publication: A. K. Mebust, A. R. Russell, R. C. Hudman, L. C. Valin, and R. C. Cohen, Characterization of wildfire NO_x emissions using MODIS fire radiative power and OMI tropospheric NO_2 columns, Atmos. Chem. Phys. 11, 5839-5851, 2011.

2.1 Introduction

Emissions from vegetation fires are a significant source of trace gases (e.g. CO, NO_x, VOCs) and particulate matter to the atmosphere (Andreae and Merlet, 2001); formation of secondary pollutants occurs as a result of these emissions with consequences that range from local to global in scale (e.g. Val Martin et al., 2006; Cook et al., 2007; Pfister et al., 2008; Hudman et al., 2009). NO_x ($NO + NO_2$) emissions play a major role both in the production of ozone, a monitored pollutant and tropospheric greenhouse gas, and in the regulation of oxidant concentrations. NO_x emissions from biomass and biofuel burning contribute approximately 5.9 Tg N y^{-1} to the atmosphere, roughly 15% of the global NOx budget (Denman et al., 2007), with total emissions from wildfires fluctuating from year to year due to interannual variability in fire frequency and intensity. However, there are significant uncertainties associated with biomass burning budgets due to the large uncertainties in NO_x emission factors and global biomass burned. For example, Jaeglé et al. (2005) partitioned yearly GOME satellite NO_2 data to determine budgets for individual NO_x sources in 2000; while a priori and top-down global inventory totals for fire emissions agreed, regional differences of up to 50% between these two inventories were noted and attributed to uncertainties in regionally resolved NO_x emission factors used in the study. Laboratory studies also indicate that biomass burning NO_x emission factors can vary greatly–even among plants from similar ecosystems or categorized as similar under current emissions inventories, e.g. extratropical forest (McMeeking et al., 2009). These wide variations on regional scales raise questions as to whether existing parameterizations capture the mean emissions from the range of recent fires, and whether a more detailed parameterization could capture some of the variability in emissions.

Biomass burning emissions have generally been estimated using a bottom-up approach (Wiedinmyer et al., 2006):

$$M_X = M_T \times EC_X \quad (1)$$

where M_X is the mass of a species X emitted by the fire, M_T is the total biomass burned, and EF_X is the empirically measured emission factor (EF) for species X, expressed as the ratio of pollutant mass emitted to the total biomass burned. NO_x emissions vary greatly based on individual fire conditions, such as differences in the flaming vs. smoldering fraction of the fuel burned and its nitrogen content; most NO_x EFs used in atmospheric modeling applications are reported with high uncertainties (±50 %) as this variability is significant between different biomes and emissions in a given location are attributed to one of only a handful of biome categories (Andreae and Merlet, 2001; Battye and Battye, 2002). NO_x EFs are primarily based on airborne and occasionally local measurements from wildfires or prescribed fires (e.g. Laursen et al., 1992; Goode et al., 2000; Yokelson et al., 2007; Alvarado et al., 2010), or measurements from small fires burned under controlled laboratory conditions (e.g. Goode et al., 1999; Freeborn et al., 2008; Yokelson et al., 2008; McMeeking et al., 2009). Airborne measurements, while precise for a given fire, face obvious limitations with respect to the number and size of fires that can be sampled, limiting their ability to characterize variability in fire emissions on regional scales; these measurements may also exhibit a bias toward emissions from flaming combustion (Andreae and Merlet, 2001; Yokelson et al., 2008; van Leeuwen and van der Werf, 2011). Laboratory fires, on the other hand, do not accurately recreate several characteristics of typical large-scale natural wildfires including size, fuel moisture, flaming and smoldering fractions, and structural and meteorological characteristics, among others. Satellite measurements offer an opportunity to bridge the gap between global analyses that identify a need for representative emission factors at regional scales and observations at the fuel and individual fire level.

In the mass-burned formalism M_T is estimated as

$$M_T = A \times B \times C \qquad (2)$$

where A is the burned area, B is the available fuel per unit area, and C is the combustion completeness, or fraction of available fuel that was burned (Seiler and Crutzen, 1980; Wiedinmyer et al., 2006). Poor knowledge of A, B and C leads to large uncertainties in the mass of pollutant emitted, and the lack of temporal and spatial resolution prevents air quality forecasting of individual fires in real time (Ichoku and Kaufman, 2005). In recent literature, a linear relationship between the biomass burned in a fire and the radiative energy released by the fire has been established (Wooster, 2002; Wooster et al., 2005; Freeborn et al., 2008), leading to a new expression of pollutant mass emission:

$$M_X = EC_X \times E_R = K \times EF_X \times E_R \qquad (3)$$

where EC_X is an "emission coefficient" (EC) expressed as the mass of pollutant emitted per unit of radiative energy, E_R is the total radiative energy, and K is an empirically measured coefficient with reported uncertainties of approximately 10–15% (Ichoku and Kaufman, 2005; Wooster et al., 2005; Vermote et al., 2009). E_R can be measured remotely and so may have lower uncertainties than estimates of mass burned for larger fires; thus some recent studies of fire emissions have focused on directly establishing EC_X for pollutants of interest (Ichoku and Kaufman, 2005; Freeborn et al., 2008; Jordan et al., 2008; Vermote et al., 2009). Although NO_x ECs have been measured for small experimental fires (Freeborn et al., 2008), they may not accurately represent emissions for larger scale natural fires, and only a small number of fuel types are represented. Satellite observations with relatively high spatiotemporal resolution

provide us the opportunity to directly measure NO_x ECs and to gather statistics of variation among wildfires using observations from a large number of fires.

Here we show that satellite observations of fire activity and NO_2 can establish statistical properties of NO_2 ECs. We evaluate emissions from 1960 fires in California and Nevada over the years 2005–2008 to derive NO_2 ECs for three land cover classes (forest, shrub and grass) by combining NO_2 columns from the Ozone Monitoring Instrument (OMI) aboard NASA's EOS-Aura satellite, wind vectors from the North American Regional Reanalysis (NARR), and measurements of fire radiative power (FRP) from the Moderate Resolution Imaging Spectroradiometer (MODIS) instrument on NASA's EOS-Aqua satellite. Although not considered a major contributor to global biomass burning emissions, this region has a number of fires over diverse land types which can aid our understanding of variations in emissions with fuel type. Further, emissions from individual fires in this region can significantly perturb NOx levels over the natural background, leading to local and regional degradation of air quality (Pfister et al., 2008). We note that in this work, the phrases "NO_2 emissions" and "NO_2 ECs" refer to emissions and ECs derived from the observed NO_2 columns, and thus represent total NO_2 present in plumes at NO-NO_2 photostationary state, as opposed to direct NO_2 emissions from fires.

2.2 Datasets

The MODIS instruments reside on the NASA EOS-Terra and EOS-Aqua satellites, measuring spectral radiance from Earth; the MODIS fire detection algorithm employs infrared spectral channels at 4 and 11 μm (Kaufman et al., 1998). We use daytime fire detections at 1 km nominal resolution from the MODIS Aqua Thermal Anomalies Level 2 Collection 5 data product, MYD14 (Giglio et al., 2003). FRP is provided for each fire pixel via an empirical relationship using the 4 μm band brightness temperatures (Kaufman et al., 1998; Justice et al., 2002). Sensitivity studies indicate that the theoretical average standard error associated with this relationship is ±16 %, and is higher for small fires and lower for more energetic fires (Kaufman et al., 1998). Independent validation byWooster et al. (2003) using the Bi-spectral InfraRed Detection satellite instrument found that the two instruments agreed to within 15% for some fires but that MODIS underestimates FRP by up to 46% for fires where some of the less intensely radiating fire pixels are not detected by the MODIS algorithm. To identify the primary land type for each fire pixel we use the MODIS Aqua+Terra Land Cover Level 3 Collection 5 (MCD12Q1) product, which provides yearly land cover classification at 500m×500m resolution (Friedl et al., 2010).

To measure NO_2 emissions we use tropospheric vertical column densities of NO_2 obtained from the OMI NO_2 standard product (Level 2, Version 1.0.5, Collection 3) available from the NASA Goddard Earth Sciences (GES) Data and Information Services Center (DISC). OMI is a nadir-viewing spectrometer, measuring backscattered solar radiation from earth at UV and visible wavelengths (270–500 nm) with a spectral resolution of ~0.5 nm. OMI employs differential optical absorption spectroscopy (DOAS) to measure NO_2; the tropospheric vertical columns of NO_2 and corresponding standard errors used in this work are retrieved as described by Boersma et al. (2004), Bucsela et al. (2006), and Celarier et al. (2008). With daily global coverage at a spatial resolution of 13 km×24 km at nadir, OMI has the highest resolution of any

remote instrument measuring NO_2 columns. In this work, only the 40 inner pixels out of 60 total (in the across-track direction) were used, minimizing effects of poor resolution in the outer, larger pixels. OMI pixels with cloud fractions greater than 20% were not included in our analysis to reduce uncertainties associated with cloud cover (Boersma et al., 2002; Celarier et al., 2008).

We use wind fields at 900 hPa (~1 km) from NARR, a data assimilation system that provides meteorological variables at 32 km horizontal resolution and 45 vertical layers every three hours from 1979–present (Mesinger et al., 2006). MODIS, OMI and NARR data for each fire were collocated in time to within one hour.

2.3 Methods

We follow the method outlined by Ichoku and Kaufman (2005), which computes regional ECs globally for smoke aerosol, with modifications to calculate ECs for NO_2. We begin with a brief summary of the method presented in the aforementioned study.

Ichoku and Kaufman (2005) first collocated MODIS aerosol pixels and MODIS fire detections. For each MODIS aerosol pixel identified as containing fire, a series of calculations were performed; first, the aerosol optical thickness (AOT) contributed by fire emissions was measured by subtracting the minimum AOT of the aerosol pixel containing fire and the eight surrounding aerosol pixels from the maximum AOT of these same pixels. Next, the authors converted AOT to column mass density. Ichoku and Kaufman (2005) then calculated the wind speed over the pixel and a characteristic length over which the wind must blow to clear the region of aerosol; this was given as the square root of the area of the aerosol pixel. Using this characteristic length and the wind speed to determine the clear time (defined below), the smoke mass emission rate is given as the total mass of aerosol contributed by fire emissions divided by the clear time. Ichoku and Kaufman (2005) then grouped aerosol pixels by their proximity and averaged these values for all pixels in a group.

For fire NO_x emissions, we began by collecting fire detections over California and Nevada and surrounding areas (31–44° N, 126–113° W) from 2005–2008. These fire pixels were assigned a primary fuel type of forest, shrub, grass or "other" (including sparsely vegetated, urban, or agricultural land) using the MODIS land cover product from the corresponding year (see Fig. 2.1a). For each day, OMI pixels and fire pixels were grouped into fire "events" such that adjacent OMI pixels containing fires were grouped together and rectangular regions were defined around each event (see Fig. 2.1b). Each event then represents all fire pixels in that location from a single day of observation, where the fire pixels are close enough to each other that the OMI spatial resolution cannot separately resolve their emissions.

The total mass emitted by each fire as measured by OMI was calculated as follows: total OMI tropospheric NO_2 columns for each event ($X_{NO_2,f}$) were obtained by averaging all columns in the rectangular region, weighted by pixel area, with the column standard deviation ($\sigma_{NO_2,f}$) equal to the weighted average of column standard deviations reported in the retrieval. OMI columns over the rectangular region were measured in a similar way for 60 days before and after the fire; the average of these columns yielded an event background NO_2 column ($X_{NO_2,b}$) with

corresponding background column standard deviation ($\sigma_{NO_2,b}$). Columns containing MODIS fire detections were eliminated from the background average. The total mass of NO_2 emitted by the fire M_{NO_2} (in kg) was then given by

$$M_{NO_2} = \left(M_{NO_2,f} - M_{NO_2,b}\right) \times A_R \quad (4)$$

where A_R is the regional area. The standard deviation for M_{NO2} is given by

$$\sigma_{NO_2} = \left(\sigma_{NO_2,f} - \sigma_{NO_2,b}\right) \times A_R . \quad (5)$$

As FRP is the rate of radiative energy release (MJ s^{-1}), the next step in the analysis was to determine the time over which the measured mass of NO_2 had been emitted. The time for emitted NO_2 to clear the region (t_c) was derived using wind speed (w) and direction from NARR wind fields at 900 hPa (~1 km):

$$t_c = d_c w^{-1}, \quad (6)$$

where d_c is the distance from the center of the fire to the edge of the region along the wind direction. Standard error in d_c was assumed to be at least 2 km (twice the nominal resolution of a MODIS pixel) and for larger fires, was given as the standard error associated with measuring the center of the fire; the center was found as an average of all fire pixel locations for that fire, weighted by FRP. Uncertainties in wind speed and direction for individual data points were difficult to assess and quantify, although we examine the effects of alternate wind data sets and assumptions about plume height in the discussion below; percent standard error in t_c was assumed equal to percent standard error in d_c. For each event, dividing M_{NO2} by t_c yielded a mass emission rate (MER) of NO_2 for the region, with percent standard error equal to percent standard error from t_c and M_{NO2}, summed in quadrature. Summing pixel FRP for each land type yielded the total event FRP for each land type (in MJ), with standard error estimated at 30 %, between 15% and 46% as reported in Wooster et al. (2003).

Satellite observations of fire emissions will necessarily contain a mixture of fresh and aged smoke, due to the spatial resolution of the observing instrument. NO_x is a relatively short-lived species; observations and theoretical studies both support the notion that NO_x concentrations in a fire plume will decay with time due to the formation of nitric acid (HNO_3) and NO_x reservoir species such as peroxyacetyl nitrate (PAN) (e.g. Jacob et al., 1992; Mauzerall et al., 1998; Leung et al., 2007; Real et al., 2007; Alvarado et al., 2010). Thus, the aged smoke present in satellite observations will bias our measured ECs low. To evaluate this effect, we consider a 1-D model of a fire plume, assuming a constant wind speed along the dependent axis; horizontal diffusion and vertical distribution of emissions are neglected. We also assume first-order reaction kinetics for NO_x, governed by a rate constant k; the lifetime is $\tau = k^{-1}$. The concentration of NO_2 as a function of distance from the fire is then:

$$C(x) = C_0 \exp\left(-kw^{-1}x\right), \quad (7)$$

where C_0 is the concentration immediately over the source (kg m^{-1} in our 1-D model) and x is the distance downwind from the source. Note that since we assume a constant wind speed, the age of

the smoke at x is given by $t = w^{-1}x$. The satellite will observe all NO_2 between the source and some point x_0 which represents the edge of the satellite pixel, and the total mass observed is equal to the integral of NO_2 concentration from the origin to x_0:

$$M_{NO_2} = \int_0^{x_0} C(x)dx = C_0 \int_0^{x_0} \exp(-kw^{-1}x)dx \\ = C_0 wk^{-1}\left[1 - \exp\left(-kw^{-1}x_0\right)\right] \quad (8)$$

Here, the clear time, t_c, is defined as the time required for transport from the source to the edge of the pixel: $t_c = w^{-1}x_0$. We also note that C_0x_0 corresponds to the total mass that would be observed had no decay in NO_2 occurred; thus $C_0x_0t_c^{-1}$ is equal to the mass emission rate that would have been measured with no decay, or equivalently, the initial mass emission rate at the fire source, MER_{init}. We can thus rewrite our total mass observed equation as:

$$M_{NO_2} = C_0 x_0 t_c^{-1} k^{-1}\left[1 - \exp\left(-kt_c\right)\right] \\ = \mathrm{MER}_{init}\tau\left[1 - \exp\left(-\tau^{-1}t_c\right)\right] \quad (9)$$

Dividing both sides by t_c yields our measured MER as a function of the initial MER, lifetime τ, and clear time t_c:

$$\mathrm{MER}_{meas} = \mathrm{MER}_{init} t_c^{-1}\tau\left[1 - \exp\left(-\tau^{-1}t_c\right)\right] \quad (10)$$

Although this 1-D model neglects diffusion, in most cases the width of the rectangular region is large enough that horizontal diffusion does not remove the fire-emitted NO_2 from the satellite field of view; thus this is a useful first order approximation of the relationship between initial and measured MER. We use this equation to apply a chemistry correction factor to each point in our analysis, assuming an appropriate lifetime.

Previous studies offer a range of NO_x lifetimes within fire plumes. Analyses have converged on lifetimes of less than 7 h with observationally constrained lifetimes closer to 2–3 h (Jacob et al., 1992; Yokelson et al., 1999; Alvarado et al., 2010). We select a lifetime of 2 h, which is in agreement with observations. A plot of MER decay for three different clear times (the time required to exit the satellite pixel) is shown in Fig. 2.2. These three clear times (5 min, 55 min, and 3 h) represent a short, average, and long clear time for our analysis, respectively. At a lifetime of 2 h, the apparent MER that would be inferred from the satellite observations for the average case is biased low by 20 %. Longer lifetimes result in less bias. Thus our choice of lifetime introduces at most a minor bias unless the lifetime is shorter than 45 min. We apply the correction to each point as a function of clear time, and assume an uncertainty from this correction equal to the percent difference between the measured and corrected MERs; overall uncertainty in the corrected MER is then obtained by summing in quadrature this uncertainty with the measured MER uncertainty.

To ensure that only high quality observations were included in the analysis, all events with a background column greater than 3.5×10^{15} molecules cm^{-2} were omitted from further analysis as it was difficult to distinguish fire emissions from variations in the NO_x background (361 points). Events with a clear time of greater than 3 h were removed to reduce errors associated with

changes in FRP or wind speed and direction during the transit time (199 points from the remaining dataset). Events from a region near Santa Barbara (34–35° N, 118–121° W) were also removed, due to errors in wind over this region that are likely associated with unresolved Santa Ana winds (37 points). Finally, points that had both high percent uncertainty (>100 %) and high absolute uncertainty (>1 kg s^{-1}) in MER were removed (430 points); this preserved points with MER near zero and a high percent uncertainty but low overall uncertainty. Overall, 34% of data points were removed via filtering; 1960 events remained for this analysis.

We identified several aspects of the study by Ichoku and Kaufman (2005) that did not translate to the OMI NO_2 observations. The method used by Ichoku and Kaufman (2005) to measure total and background mass overestimated emitted NO_2 when applied to our dataset, due to regional variation in NO_x concentrations on the spatial scale of an OMI pixel; hence our development of the method described above to account for these variations. This method analyzes several pixels at once, so there was also no need to include an averaging step at the end of the analysis. We also use a more precise determination of the characteristic length using the direction of the wind and the center of the fire, as well as a higher resolution wind dataset (NARR at 32 km resolution instead of the NCEP global reanalysis at 2°×2.5°). The study presented by Ichoku and Kaufman (2005) performed regional and subregional analyses over the globe, and assumed these subregions were representative of a single fuel type; we instead applied the MODIS Land Cover product to individual fire pixels. Finally, our correction to account for photochemical processing is necessary for NO_x but was not needed in the original study by Ichoku and Kaufman (2005).

2.4 Results and discussion

Figure 2.3 shows FRP vs. MER for all fires, as well as fires separated by their primary fuel type. Fires were identified as forest, grass, or shrub fires if at least 75% of FRP came from fire pixels of that fuel type. Best fit lines (with intercept fixed at zero) and R^2 values are shown. Distinctly different slopes are measured for all three fuel types, and with the exception of forest fires, analyzing emissions separated by fuel type improves the correlation coefficient. Forest fires exhibit more variability in emissions than other fuel types; this may be due to variations in the extent to which trees contribute to the fuel in forest-type fire pixels as opposed to underbrush and leaf litter, or greater variation in extent of flaming combustion during which most NO_x is emitted. The small number of larger fires (only four fires with FRP >5000 MJ s^{-1}) may also have an effect, as percent uncertainty in FRP is likely greater for small fires (Kaufman et al., 1998).

Limiting the analysis to individual fuel types reduces its statistical rigor. To obtain ECs with well-characterized uncertainties and including all of the data deemed reliable, a multiple regression with nonparametric bootstrap resampling was used. Since the emission parameterization scales linearly, the MER equation can be expanded to vary linearly with landtype:

$$\mathrm{MER} = \left(\mathrm{FRP_F} \times \mathrm{EC_F}\right) + \left(\mathrm{FRP_G} \times \mathrm{EC_G}\right) + \left(\mathrm{FRP_S} \times \mathrm{EC_S}\right) \qquad (11)$$

where F, G and S correspond to forest, grass and shrub land types. Points were randomly sampled with replacement and the multiple regression on land type FRP was performed 300,000 times; the resulting averaged ECs (in g MJ^{-1} NO_2) and their standard deviations (Table 2.1) were used to calculate predicted MERs for each fire measured in the analysis, as shown in Fig. 2.4. The best fit line (slope of 0.988) demonstrates that these ECs appropriately reproduce overall emissions. The correlation coefficient indicates that this parameterization method accounts for approximately 67% of the variability in emissions on this scale.

Previously, NO_x EFs of 2.5±1.2 for forests, 3.5±0.9 for grass and 6.5±2.7 (g kg^{-1}) for shrubs were reported for fires in North America by Battye and Battye (2002). As a ratio to the forest fire emissions, these reported NO_x EFs are 2.4 times higher for shrub fires and 1.6 for grass fires, mainly reflecting differences in the C:N ratios of the fuels and differences in typical combustion efficiency. Our analysis gives ECs that are 2.5 times larger for shrub fires and 1.2 times larger for grass fires than forest fires, consistent with those reported by Battye and Battye (2002). Globally averaged NOx EFs presented in Andreae and Merlet (2001) do not include a shrub category, but the ratio of the grassland EF to the extratropical forest EF is 1.3 to 1; the grassland number was later revised down by 40% (Hoelzemann et al., 2004), however, a number of papers have provided evidence that the extratropical forest EF should also be revised downward (Spichtinger et al., 2001; Cook et al., 2007; Alvarado et al., 2010).

To directly compare to previously reported NO_x ECs and EFs, we can convert using a photostationary state NO/NO_2 ratio and the aforementioned proportionality constant *K*, the ratio of biomass burned to FRE. For this comparison we assume that 75% of NO_x in the plume is present as NO_2, as the vast majority of fire plumes observed at OMI resolution are aged long enough for NO and NO_2 to reach photostationary state. This value is also consistent with previous observed and modeled values in fire plumes (Laursen et al., 1992; Alvarado and Prinn, 2009). We estimate that this value is accurate to within 20 %. We also use K = 0.41 kg MJ^{-1}, the average of two values measured in previous studies (Wooster et al., 2005; Freeborn et al., 2008). This value was used in Vermote et al. (2009) and the uncertainty estimated to be at least 10 %. The resulting NO_x EFs and ECs are presented in Table 2.1, in g NO_x (as NO); we note that the overall bias induced by these conversions may be as high as 25% in either direction.

Most reported NO_x emission factors are substantially larger than the ones we derive here. The NO_x EFs reported by Battye and Battye (2002) are roughly 3 times larger than our derived EFs. The grassland EF (2.32 g kg^{-1}) revised from Andreae and Merlet (2001) and given in Hoelzemann et al. (2004) is also roughly 3 times larger than our reported grassland EF and the extratropical forest EF (3.0 g kg^{-1}) from Andreae and Merlet (2001) is 5 times larger than our reported forest EF. Alvarado et al. (2010) used observations of NO_x in boreal forest fire plumes to obtain an emission factor for NO_x of 1.06 g kg^{-1}, almost twice our extratropical forest EF, with a reported uncertainty of ~100 %. Freeborn et al. (2008) report an overall NO_x EC of 1.19±0.65 g MJ^{-1} for laboratory fires of a number of different fuel types, 2–5 times greater than the NO_x ECs measured in this work (0.243–0.605 g MJ^{-1}).

A number of factors may be responsible for a bias in our measured values; these factors are presented in Table 2.2, and we discuss them here at length. First, we note that any assumptions we made about average fire behavior, such as NO_x lifetime within the plume, NO_2/NO_x ratio, or the value for *K*, are a possible source of systematic error, with under- and overestimation being

equally likely; however, each of these sources is expected to induce less than 20% error unless a typical NO_x lifetime in a fire plume is less than 1 h. A second source of systematic error is the diurnal cycle of fire behavior. A number of studies indicate that fire activity peaks in the afternoon (Giglio, 2007; Zhang and Kondragunta, 2008; Vermote et al., 2009). Data presented in Vermote et al. (2009) and Zhang and Kondragunta (2008) suggests that average activity increases roughly linearly from morning to peak activity. Our analysis assumes constant FRP throughout the time over which emissions were measured for each data point; while some fires will increase in FRP over this time and some fires will decrease, the diurnal cycles presented in these studies suggest that on average we are overestimating FRP by up to 20 %, depending on the average clear time.

To verify this effect, we tested all points in our analysis that were also detected during the morning overpass of MODIS on the Terra satellite, approximately 25% of the fires we studied, including the majority of large fires. For each point, we assumed FRP varied linearly from the Terra overpass to the Aqua overpass, and using the clear time, calculated the average FRP over the time of our measurement. Bootstrapping with these average FRPs instead of the Aqua FRP resulted in shrub and grass EFs approximately 15% greater than those presented in this work, indicating a small low bias. The forest EF increased by 40 %, a much larger effect, but it is not clear that this is statistically significant.

Another potential source of bias is from the use of NARR data at the selected wind level (900 hPa). Plume height varies significantly between individual fires; 900 hPa, which corresponds to approximately 1 km altitude, was selected as a result of data presented by val Martin et al. (2010) indicating that average fire plume heights in North America are less than 1 km, and that the majority of fire plumes remain within the boundary layer. As a result, we expect wind level selection to induce some random error for individual fires, but the choice should be appropriate for an average fire. However, any bias in NARR wind speed at this level would result in a bias in this work. Additionally, val Martin et al. (2010) note a correlation with plume height and measured FRP, although the correlation is weak and the relationship may not be applicable to our analysis since the data presented in the study was obtained in the morning as opposed to the early afternoon, when meteorology governing plume injection height is very different. Still, increases in injection height with FRP could induce a bias in our results due to differences in wind speeds through the troposphere. However, even when fire plumes inject emissions to heights of a few kilometers, the vertical distribution of emissions is not well known (val Martin et al., 2010); the majority of emissions may remain in the boundary layer.

We performed three separate tests to determine the magnitude of any possible bias due to wind selection. First, we repeated the analysis using 850 hPa wind (~1.5 km altitude) from NARR. Obtained NO_2 EC values were within 0.020 g MJ^{-1} of the values obtained using 900 hPa wind, less than a 10% change and well within our reported uncertainties. We concluded that small changes in wind level do not significantly bias the results. In the second test, we repeated the analysis using wind at 850 hPa from the NCEP Climate Forecast System Reanalysis, a global reanalysis and forecast produced at 0.5°×0.5° resolution (Saha et al., 2010). Differences in NO_2 EC values calculated via the two data sets were all less than 0.070 g MJ^{-1} and again were within the reported uncertainties for all three land types. This test ensured that there is no large bias as a result of using NARR values instead of an alternative reanalysis. Finally, we performed the analysis again using NARR wind at 700 hPa (~3 km) for fires with FRP greater than 5000 MJ s^{-1}

and NARR wind at 900 hPa for smaller fires. Due to increased wind speeds with increasing altitude in the troposphere, the use of this higher wind resulted in an increase in NO_2 ECs for all three land types, ranging from 20% to 50 %. Thus we consider our assumption of plume injection height a possible source of negative bias.

There are also some sources of systematic error that would bias our EFs high, including underestimation of FRP by MODIS due to clouds, smoke or canopy cover obscuring the satellite view of radiant fire energy (Vermote et al., 2009). The absence of coincident measurements of FRP from satellite and ground or airborne platforms prevents direct assessment of this uncertainty; however, OMI pixels used in this analysis are filtered for cloud fraction >20 %, largely eliminating fires that are partially obscured by clouds, or aerosol interpreted by the retrieval as cloud. We also note that comparison between FRP from other satellite platforms and FRP from MODIS suggests that when an individual fire is detected by both instruments, measured FRP is accurate to within 45%. For example, Roberts et al. (2005) compare FRP from MODIS to FRP derived from the Spinning Enhanced Visible and Infrared Imager (SEVIRI) instrument, and find that for fires in Southern Africa detected by both instruments, the average underestimation by SEVIRI (which is less sensitive to pixels with low FRP) is 5%. Similarly, Wooster et al. (2003) indicate that MODIS-derived FRE differed by ~15–45% from FRE derived from the Bi-spectral InfraRed Detection (BIRD) satellite for fires detected by both instruments, with an average underestimation by MODIS of ~15% for all individually compared fires. Since the BIRD measurements are higher spatial resolution and expected to observe fires more accurately, this suggests an average underestimation of FRP of no more 15–30% in the MODIS product.

There is other evidence for underestimation of total regional FRP based on the MODIS retrieval. Some biomass burned and fire emission inventories have been developed using FRP (e.g. Ellicott et al., 2009; Vermote et al., 2009) and these generally indicate that biomass burned derived from MODIS FRP are lower than estimates of biomass burned using GFEDv2, possibly by up to a factor of 3. Other studies indicate that biomass burned from GFEDv2 could be underestimated itself (e.g. Kopacz et al., 2010; Liousse et al., 2010), indicating a possible underestimation in MODIS estimates of total regional FRP that could be significant. However, it is likely that these discrepancies are largely due to omission of small fires that are either completely obscured by clouds or not detected by the MODIS algorithm which has limited sensitivity to pixels with low FRP. This effect was observed in the aforementioned studies: Roberts et al. (2005) noted a much larger underestimation in FRP of 38% by SEVIRI (which is not as sensitive as MODIS to fires with FRP<100MW) relative to MODIS when comparing total regional FRP measurements. Wooster et al. (2003) also observed that total regional MODIS FRP was only ~60% of total regional BIRD FRP, despite 15% average differences for individual fire comparisons. Our analysis evaluates emissions of individual detected fires to derive ECs; consequently, our conclusions are insensitive to fires that are too small to be detected and uncertainties specific to total regional FRP do not affect our results. However, the application of these ECs to predict total emissions in a region (as opposed to emission from a specific fire) will require evaluation of the contribution of fires that are undetected by MODIS to the total emissions.

It is also possible that since our observations occur close to the peak in fire activity, the fires we observe may be more heavily weighted towards flaming emissions than an average wildfire,

and thus are biased high. This uncertainty is difficult to quantify, since precise measurements of diurnal patterns in NO_x emission factors have not yet been performed. In addition, the diurnal pattern in wildfire flaming to smoldering fraction is not established, and while NOx emissions are correlated with flaming combustion and higher modified combustion efficiency (MCE), this correlation is small – R^2 = 0.11 in Battye and Battye (2002) – and the slope of the line very uncertain. However, MCE for most fires ranges between 0.80 and 1.0 (McMeeking et al., 2009; Yokelson et al., 2008; Battye and Battye, 2002) and thus any diurnal change in average MCE would likely be well within this range. Using the Battye and Battye (2002) fit despite the weak correlation, we determine that for changes in average MCE from 0.95 to 0.90, there is a 30% decrease in NO_x EF; for changes in average MCE from 0.90 to 0.85, there is a 40% decrease in NO_x EF. This is consistent when compared to seasonal variations in NO_x emission ratios presented by Lapina et al. (2008), who attribute the observed seasonal change in emission ratio of NO_y to CO for boreal forests, from 7.3 mol mol^{-1} to 2.8 mol mol^{-1}, to higher smoldering fraction in the late-season fires. In order to translate these values to differences in NO_x EFs, the increase in CO emissions with increasing smoldering fraction must be accounted for. Unfortunately, Lapina et al. (2008) do not report MCE for the fires, but using equations presented in Battye and Battye (2002), a decrease in MCE from 0.95 to 0.90 results in a factor of ~2.3 increase in the CO emission factor (from 45.6 g kg^{-1} to 103 g kg^{-1}); a decrease from 0.90 to 0.85 results in a factor of ~1.5 increase. If these CO emission factors are used with the NO_y emission ratios from Lapina et al. (2008) to calculate NO_x EFs, then the seasonal decrease in NO_x EF inferred from the reported data would be 15–40%. Thus, while it is currently impossible to accurately quantify the potential bias induced by this diurnal variation in NO_x EF, we suggest that the bias is at most 40%.

A summary of all quantified potential biases is presented in Table 2.2, in the first seven rows. Summing these biases suggests that our values are nearly equally likely to be biased high or low (likely bias ranging from approximately 55% low to 55% high). In addition, these potential biases cannot entirely account for the discrepancy between our emission coefficients and prior estimates.

We might interpret these results to indicate that there is a bias in the OMI retrieval process over wildfires. The NO_2 tropospheric column retrieval does not account for specific temporal differences in NO_2 vertical profile and aerosol loading associated with wildfire conditions, nor does it explicitly account for effects of aerosol loading due to fires, both of which can act to systematically bias NO_2 columns over wildfires. Most analyses suggest the bias due to aerosol is relatively minor (<20 %), as aerosol is treated implicitly as part of the cloud correction (Boersma et al., 2004). Uncertainty due to profile shape is more difficult to constrain, as NO_2 profile data is sparse; Lamsal et al. (2010) indicate that biases between the OMI standard product and ground based measurements range from −5.6% to 71%, and they attribute much of this difference to profile error. Unfortunately, any bias in this work cannot be assessed using data from another NO_2 remote sensing platform e.g. SCIAMACHY, due to differences in overpass times and spatial coverage, lower spatial resolution, or the fact that these instruments generally use a similar retrieval process and so may be subject to similar biases. Simultaneous in situ and satellite observation of NO_2 in plumes would be extremely useful as a constraint. Despite our inability to quantify the contributions to the values presented in this work, we include a bias in the OMI retrieval in Table 2.2.

Another possibility is that emissions from wildfires in California are lower than emissions used to derive prior estimates. However, this is not observed in previous measurements of emissions (e.g. Battye and Battye, 2002). Our own preliminary analysis of global measurements using the methods outlined in this work also provides no evidence that CA/NV fires are uniquely different from fires in other geographic locations. Nonetheless, we include this in Table 2.2 as a potential source of bias to be thorough.

A third possible explanation for the difference is that previous in situ and laboratory studies overestimate NO_x emissions from wildfires, due to oversampling of flaming emissions in the laboratory or from airborne platforms. There is evidence that laboratory and airborne emission measurements sample plumes with higher MCE and greater NO_x emissions than ground stations (e.g. Yokelson et al., 2008). These low-level smoldering emissions have been suggested to contribute only very minimally to total fire emissions (Andreae and Merlet, 2001); however, if smoldering combustion contributes more significantly to overall emissions than previously suggested, that would result in an overestimation of EFs of species associated with flaming combustion (e.g. NO_x) when these EFs are measured via airborne platforms and then applied to large-scale fires. We note that results from other studies producing ECs for aerosol using satellite data are consistent with this hypothesis (Ichoku and Kaufman, 2005; Vermote et al., 2009); aerosol is more strongly emitted during smoldering combustion, and both of the aforementioned studies measure higher aerosol emissions than are represented by currently accepted aerosol EFs. Kopacz et al. (2010) constrain CO emission sources using data from several satellite platforms, and find that wildfire emissions as a source of CO are underestimated using GFEDv2 emissions. While Kopacz et al. (2010) conclude that GFEDv2 biomass burned is underestimated, other studies suggest that GFEDv2 biomass burned may be overestimated (e.g. Ellicott et al., 2009), and the result in Kopacz et al. (2010) may also be consistent with the hypothesis that current EFs underestimate contributions of smoldering combustion, as emissions of both CO and hydrocarbons that oxidize rapidly to CO are associated with smoldering combustion. The support of this hypothesis across studies that measure different species, emitted during different stages of combustion, and across different satellite platforms is remarkably consistent. We recommend that a more systematic study of smoldering and flaming combustion as they pertain to wildfire emissions be conducted, and conclude that the NO_x ECs and EFs presented here are a useful lower bound on NO_x emissions and, if the contribution of smoldering combustion to total wildfire emissions is indeed underestimated, may provide a more accurate characterization of fire emissions than currently used values.

2.5 Conclusions

We derive NO_2 ECs (in g MJ^{-1} NO_2) for wildfires in California and Nevada using satellite measurements of NO_2 column densities and fire radiative energy. ECs for forest, grass and shrub fuels were found to be 0.279±0.077, 0.342±0.053, and 0.696±0.088 g MJ^{-1} NO_2, respectively, with reported uncertainties equal to the standard deviation in the measurement. The variation of these ECs with land type reproduces ratios seen in previous work; however, these ECs are significantly lower than previously reported emissions estimates. Systematic biases in assumptions within the analysis and in FRP measurement cannot fully account for these differences. We conclude that there may be a large (50–100 %) negative bias in the OMI

retrieval of NO_2 columns over wildfire plumes, presumably due to errors in assumed profile shape. However, comparison of our results with those of Ichoku and Kaufman (2005), Vermote et al. (2009), and Kopacz et al. (2010) also indicates that previously reported NO_x EFs are likely overestimated, due to oversampling of flaming combustion by laboratory and airborne measurements. Regardless of the contributions of these factors, the parameters derived here are unambiguously a lower bound on fire NO_x emissions.

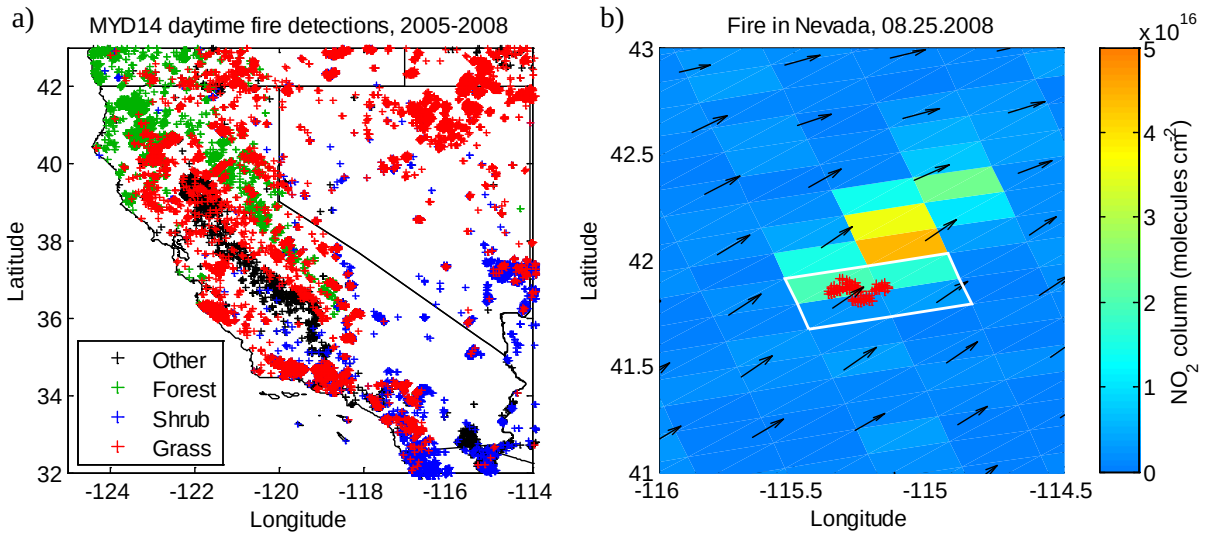

Figure 2.1. (a) MODIS fire detections (totaling ~2.8×10^4 1 km pixels) from the daytime EOS-Aqua overpass over California and Nevada, for 2005–2008, colored by land type. (b) OMI tropospheric NO_2 column densities (molecules cm^{-2}), overlayed with MODIS fire detections (red) and NARR wind vectors (black arrows) for a fire detected in Nevada on 25 August 2008; OMI pixels analyzed for this fire are outlined in white. Average wind speed shown is 8.23 m s^{-1}.

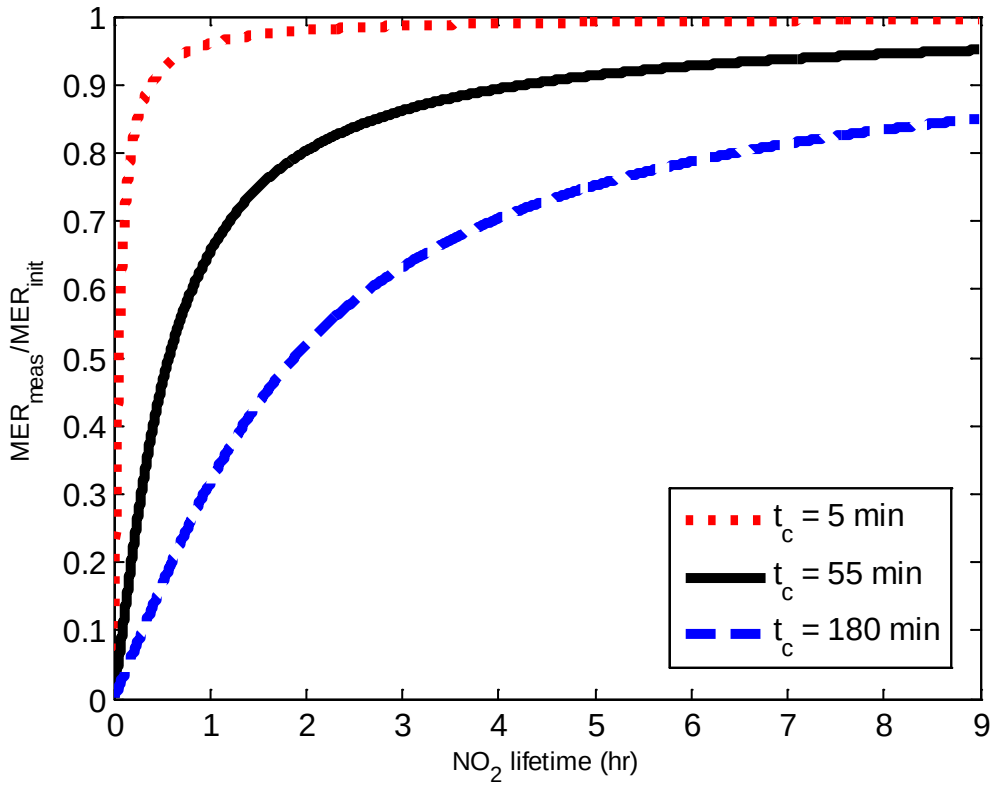

Figure 2.2. The NO_2 mass emission rate (MER) measured in this analysis (as a fraction of the initial MER from the fire) vs. NO_x lifetime in the plume (Eq. 10) for three sample clear times in our analysis: the shortest (5 min), average (55 min) and longest (180 min).

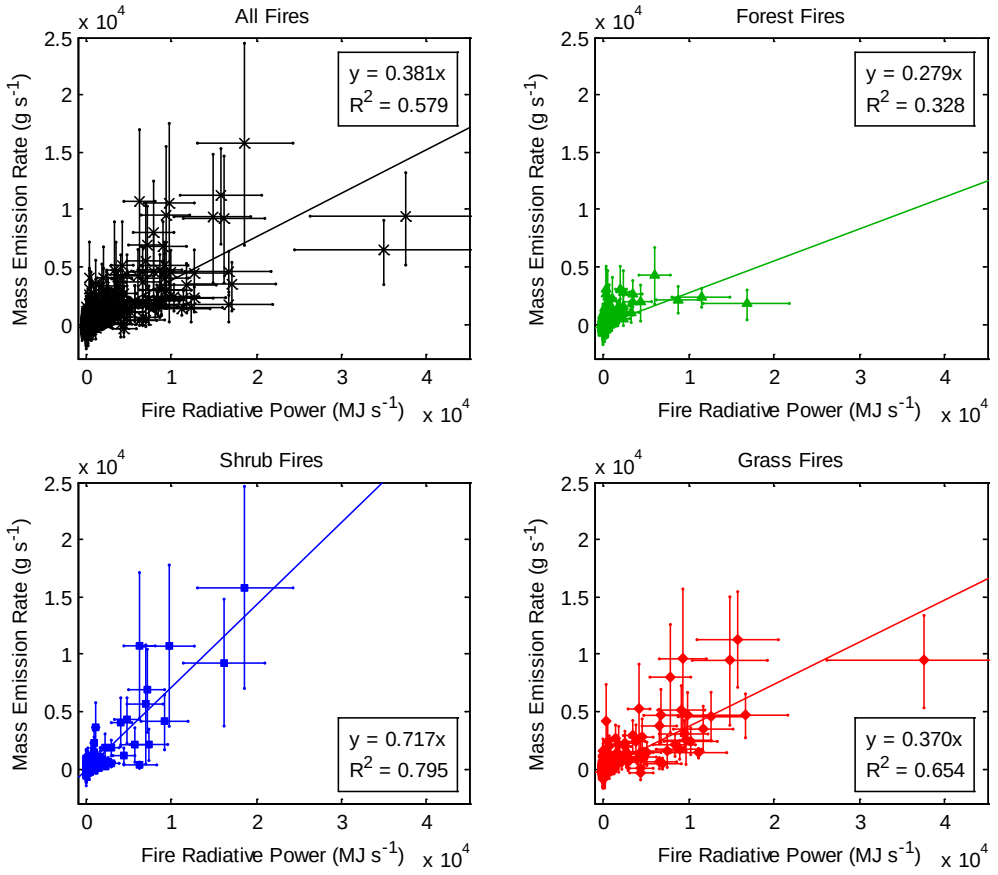

Figure 2.3. Plots of fire radiative power (FRP) vs. NO_2 mass emission rate (MER) for fires grouped by land type: all (a), forests (b), shrubs (c), and grasses (d), with lines of best fit and R^2 values. Error bars are one standard deviation for MER and range for FRP as reported in the text.

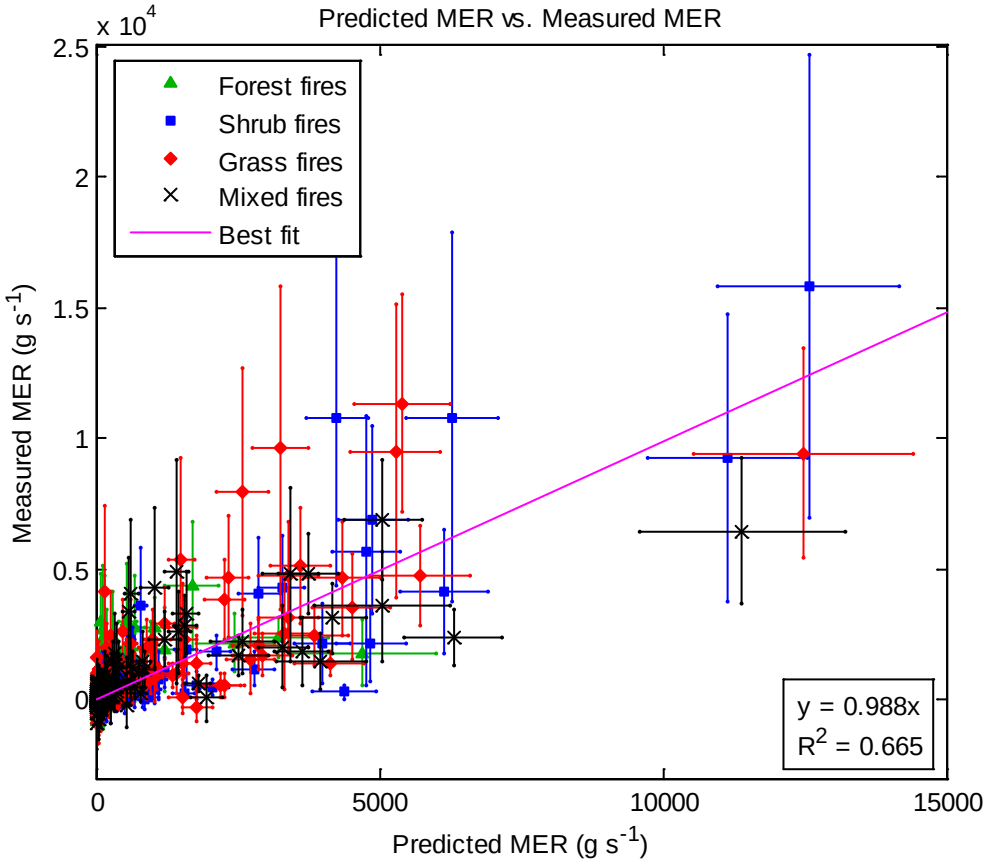

Figure 2.4. Predicted NO_2 mass emission rate (MER), calculated using fire radiative power and the multiple regression coefficients, vs. MER measured in the analysis. Error bars in measured MER are one standard deviation, calculated as reported; error bars in predicted MER are calculated using one standard deviation of each calculated emission coefficient.

Land Type	NO_2 EC (g MJ^{-1})	NO_x EF (g kg^{-1}) [a,b]	NO_x EC (g MJ^{-1}) [a]
Forest	0.279 ± 0.077	0.59 ± 0.16	0.243 ± 0.067
Grass	0.342 ± 0.053	0.73 ± 0.11	0.297 ± 0.046
Shrub	0.696 ± 0.088	1.48 ± 0.19	0.605 ± 0.077

Table 2.1. NO_2 and NO_x ECs and NO_x EFs by fuel type.
Reported uncertainties are 1σ, calculated via nonparametric bootstrap resampling.
[a] assumes NO_2/NO_x of 0.75. Total NO_x mass expressed as NO.
[b] assumes $K = 0.41$ kg MJ^{-1}.

Possible biases	Bias range (%)	Bias direction
Assumed NO_x lifetime	0-20	Indeterminate
NO_2:NO_x ratio	0-20	Indeterminate
Value for K	0-15	Indeterminate
FRP overestimation due to diurnal fire cycle	15-20	Negative
FRP underestimation due to clouds/smoke/canopy	15-30	Positive
Increased flaming sampling due to diurnal fire cycle	10-20	Positive
Emissions from CA/NV are lower than global average	Indeterminate	Indeterminate
Bias in OMI retrieval	Indeterminate	Indeterminate

Table 2.2. Possible biases in this analysis.

Chapter 3

Space-based observations of fire NO_x emission coefficients: a global biome-scale comparison

This chapter has been adapted from the following publication: A. K. Mebust and R. C. Cohen, Space-based observations of fire NO_x emission coefficients: a global biome-scale comparison, Atmos. Chem. Phys. Disc., 13, 21665-21702, 2013.

3.1 Introduction

Biomass burning emissions induce a variety of effects to climate and air quality. They impact the global radiative budget directly by absorbing or reflecting incoming radiation, e.g. CO_2 and aerosols, and/or indirectly by influencing the chemistry of climate forcers, e.g. nitrogen oxides (NO_x = NO + NO_2) and CO acting as ozone (O_3) precursors (Bowman et al., 2009; Fiore et al., 2012; Jaffe and Wigder, 2012). NO_x, O_3 and aerosols also have negative health impacts, especially at high concentrations. Understanding, quantifying and mitigating these effects requires an understanding of both the magnitude of the emissions, and their variability across a range of spatial and temporal scales.

Current models of fire emissions rely on a biomass-burned approach: to estimate the mass of a compound emitted, an empirically measured emission factor (EF) is multiplied by an estimate of the total biomass burned, often calculated as the product of other factors (e.g. burn area, fuel loading, combustion completeness) that are simpler to measure or estimate (Andreae and Merlet, 2001; Wiedinmyer et al., 2006; van der Werf et al., 2010). This strategy has weaknesses, as the uncertainty in biomass burned for a particular fire is high, and even aggregate estimates at lower spatial and temporal resolution can have significant biases (van der Werf et al., 2010; Granier et al., 2011). Additionally, measured EFs vary greatly between individual fires due to differences in fire conditions, e.g. fuel type, structure, moisture, etc. (Andreae and Merlet, 2001; Korontzi et al., 2003; van Leeuwen and van der Werf, 2011; van Leeuwen et al., 2013). In this work, we focus on emissions of NO_x, which are produced in wildfires as the result of oxidative combustion of nitrogen (N) contained in the biomass (Andreae and Merlet, 2001). Measured NO_x EFs for fires are generally considered to be positively correlated with modified combustion efficiency (MCE) and fuel N content (e.g. Lacaux et al., 1996; Battye and Battye, 2002). A high MCE indicates a greater contribution of higher-temperature flaming combustion which is thought to oxidize the N more effectively, while high fuel N provides a larger source of N to ultimately be oxidized to NO_x (Andreae and Merlet, 2001). However, observational evidence confirming these effects is limited. Observed correlations between NO_x EFs and MCE are typically poor (e.g. Battye and Battye, 2002; Yokelson et al., 2011), and fuel nitrogen content is rarely quantified. Models of fire NO_x emissions typically use EFs for a few (3-7) fuel types, based on averages of EFs measured for fires of each particular fuel type (e.g. Andreae and Merlet, 2001; Hoelzemann

et al., 2004; van der Werf et al., 2010; Akagi et al., 2011). The number of fires from which each EF is derived ranges from a handful (3-5) to tens or perhaps even hundreds, depending on the fuel type and the emitted species in question. However, even when EFs are derived from large numbers of fires, these observations come from only a few targeted measurement campaigns that sample many fires with fuels comprised of a relatively small range of plant species and over a short temporal span (e.g. Akagi et al., 2011). This raises the question of whether the observations are representative of variations in emissions that would be observed under a more spatially and temporally comprehensive sampling strategy that incorporates spatially distinct fire regimes with the same fuel type and covers seasonal and interannual variations in rainfall, wind speed and other climatic conditions.

Several satellite instruments measure fire-related properties, providing data that span the globe, have full annual coverage, and sample many fires in each region, allowing for statistical evaluation of variance in emissions and reducing the potential for bias due to an unrepresentative sample. Deriving an EF from satellite observations, however, is challenging due to the difficulty in estimating biomass burned in the fire and connecting that information to instantaneous measurements of atmospheric composition. Instead, methods for estimating the mass of a pollutant emitted per unit radiative energy released from the fire—a value we define as the emission coefficient (EC) to distinguish it from the EF—have been developed (Ichoku and Kaufman, 2005; Jordan et al., 2008; Vermote et al., 2009; Mebust et al., 2011; Mebust and Cohen, 2013). The idea for an EC was born out of laboratory work that established a linear relationship between the amount of energy released by a fire and the total biomass burned, suggesting that (a) an energy-based parameterization is a logical alternative to a mass-based one, and (b) measured ECs should be proportional to EFs (Wooster, 2002; Wooster et al., 2005; Freeborn et al., 2008). ECs provide a straightforward way to estimate EFs from satellite observations because measurements of fire radiative power (FRP) are made daily with near-global coverage from the two Moderate Resolution Imaging Spectroradiometer (MODIS) instruments, allowing for simultaneous estimation of energy and pollutant emissions for any species measured from space near the MODIS overpass times.

In two previous papers, we developed a method to combine global observations of FRP from MODIS with NO_2 tropospheric column density measurements from the Ozone Monitoring Instrument (OMI) to calculate ECs for NO_x and assessed the method as applied to fires in California and Nevada, and also examined seasonal variability in ECs in African savannas (Mebust et al., 2011; Mebust and Cohen, 2013). Here we adapt this method to provide a global picture of variations in NO_x emissions. We calculate ECs for several global biomes and for different ecoregions within these biomes, and describe how these ECs compare to each other and to EFs reported in previous studies.

3.2 Datasets

This analysis incorporates information from OMI, MODIS, a climate classification system, and the Climate Forecast System Reanalysis (CFSR) and Version 2 Reforecast (CFSv2). We use global observations from years 2005-2011.

3.2.1 OMI

OMI is a nadir-viewing spectrometer onboard the polar-orbiting EOS-Aura satellite, with an equatorial overpass time of ~1:45pm (local time). OMI measures the solar irradiance and backscatter radiance from earth at UV and visible wavelengths (270-500 nm with 0.5 nm resolution) to derive column densities for several trace gases. We use tropospheric vertical NO_2 column densities obtained from the OMI NO_2 standard product (OMNO2, Level 2, Version 2.1, Collection 3). The retrieval process for these columns is described in detail elsewhere (Bucsela et al., 2013); briefly, slant NO_2 columns are derived using differential optical absorption spectroscopy (DOAS), separated into stratospheric and tropospheric components, and converted to vertical column densities using an air mass factor, which is derived from several parameters including terrain reflectivity and height and an estimated NO_2 vertical profile. The spatial footprint is 13 × 24 km^2 at nadir. We use data from the inner 40 (of 60) across-track pixels, omitting the low spatial resolution observations at the edge of the swath. We also limit observations to those with a cloud fraction of less than 20%, as pixels with a high cloud fraction have reduced sensitivity to NO_2 below the clouds (Boersma et al., 2002), and we reject all pixels affected by the row anomaly.

It is plausible that the *a priori* NO_2 vertical profile shapes used in the retrieval process might lead to a bias in measured NO_2 columns over smoke plumes. The OMNO2 standard product v2.1 uses GMI CTM monthly mean modeled NO_2 vertical profile shapes at 2° × 2.5° (Bucsela et al., 2013). Previous work has identified a negative bias over persistent features smaller than this model resolution that results from the low spatial resolution of the estimated NO_2 profile. Specifically, Russell et al. (2011) developed a regional OMI NO_2 retrieval and found that urban NO_2 columns increased by 8%, and this increase was primarily attributed to using WRF-Chem profiles at 4 km × 4 km resolution as opposed to the lower resolution profiles in the NASA standard product v1.0. This is consistent with the observation by Boersma et al. (2011) that when near-surface NO_2 gradients were less strong, it resulted in a decrease in measured NO_2 for a different retrieval of OMI, because a larger fraction of NO_2 was distributed relatively higher in the atmosphere where the OMI instrument sensitivity is higher. Given that fires are episodic, heavy-emitting point sources in regions that are typically remote with few NO_x emission sources, the assumed NO_2 vertical profile will have very little NO_2 distributed in the lowest layer as compared to the "true" NO_2 vertical profile over most fires. This difference will be much more pronounced than in an urban area where the assumed profile, while diluted over a large spatial scale, still represents some of the vertical gradient over a NO_x source, and thus we expect a much larger bias. The impact of high aerosol loading may also have an effect, as one study considered the effects of mixed and/or layered aerosol and NO_2 on the NO_2 retrieval and found that effects are theoretically small when NO_2 and aerosol are collocated but much larger of the aerosol is above or below the plume (Leitao et al., 2010). However, the importance of this effect to our work is uncertain, as it is expected that fresh smoke plumes will generally contain well-mixed NO_2 and aerosol. Regardless, there is a theoretical basis for a low bias in OMI NO_2 measurements over smoke plumes.

In Mebust et al. (2011) we found that EFs derived from measurements of MODIS FRP and OMI NO_2 were lower than reference EFs by a factor of approximately 2-5 (depending on the reference EF). The source of that discrepancy is not understood, although it potentially stems in part from the aforementioned low bias in OMI NO_2 over fires. However, we do not believe it

varies in a statistically representative ensemble of fires, and thus relative differences in ECs are believed to be reliable.

3.2.2 MODIS

MODIS instruments operate on NASA's Aqua and Terra satellites. MODIS measures spectral radiance in 36 bands which cover visible and IR wavelengths. We use the Thermal Anomalies product (MYD14, Level 2, Collection 5) and the Land Cover product (MCD12Q1, Level 3, Collection 5.1). We only include fires detected by the Aqua MODIS instrument during daytime, as this allows near-coincident measurement of fires and NO_2 column densities. Fires are detected using the 4 μm and 11 μm bands; pixels with elevated radiance in these bands as compared to surrounding pixels are labeled as containing fire. The spatial resolution of the bands is 1×1 km^2, but the algorithm is sensitive enough to detect fires as small as 100 m^2. An estimate of pixel FRP is derived from the 4 μm brightness temperature. Further details on the fire detection and FRP estimation algorithms are discussed elsewhere (Kaufman et al., 1998; Justice et al., 2002; Giglio et al., 2003).

It has been suggested that there exists a low bias in MODIS FRP resulting from reduced sensitivity to radiance under conditions where fires are too small to be detected, obscured by clouds or canopy cover, or burning below ground (e.g. Wooster et al., 2003; Boschetti and Roy, 2009; Vermote et al., 2009; Freeborn et al., 2011). In this analysis we minimize most of these biases because we use only detected fires and compare with NO_2 columns directly over the source. In most of these cases, the percentage of undetected FRP due to undetected or cloud-obscured actively burning locations is likely small. Nevertheless, our analysis may be sensitive to canopy effects or underground burning, particularly because we consider relative differences in ECs between different biomes where this effect may vary in magnitude. A low bias in FRP in particular biomes would elevate reported EC values in those biomes.

Land cover classifications are assigned to 500×500 m^2 pixels using the International Geosphere-Biosphere Programme (IGBP) classification (Friedl et al., 2010). We assume that land cover in 2011 is the same as in 2010 because at the time of this analysis, the land cover product was only available for years 2005-2010. The IGBP classification scheme provides 17 different categorizations of land type; we assign many of these categories to biome categories as shown in Table 3.1, but occasionally use the direct IGBP classifications.

3.2.3 Köppen-Geiger climate classification

Common EF schemes distinguish between tropical, temperate, and boreal forests; to identify these distinct forest types we use the Köppen-Geiger global climate classification system at $0.5° \times 0.5°$ resolution (Kottek et al., 2006). This dataset classifies climate as one of five main climate types ("equatorial," "arid," "warm temperature," "snow," "polar"), with additional sub-classifications related to precipitation and temperature. We classify forests as "tropical" if they are found in "equatorial" climates, "temperate" if they are found in "arid" or "warm temperate" climates, and "boreal" if they are found in "snow" or "polar" climates. We also use sub-classifications of the "equatorial" regime ("fully humid", "monsoonal" and "winter-dry") to separately examine differences in tropical evergreen vs. tropical dry deforestation.

3.2.4 CFSR, CFSv2

The CFSR is a global reanalysis and forecast for years from 1979 through 2010; CFSR was extended starting in 2011 using CFSv2 and continues as an operational real-time product (Saha et al., 2010; Saha et al., submitted 2013). Wind fields used in this work are from the 850 hPa vertical level (corresponding to approximately 1.5 km altitude) and are available at 0.5° × 0.5° resolution hourly. The reanalysis is performed with 6 hr time steps and this is coupled with forecasts to provide output for every hour.

3.3 Methodology

We build on the methodology described in Mebust et al. (2011), which was adapted from Ichoku and Kaufman (2005). All fire pixels detected by the Aqua MODIS instrument daytime overpasses during 2005-2011 are assigned a land type using the MODIS land cover product for the appropriate year (or 2010 for fire pixels detected in 2011) and matched with OMI pixels coincident in time and space. OMI pixels that contain fire pixels with FRP above 250 MW are aggregated using a sorting algorithm such that adjacent OMI pixels are analyzed as a single fire "event". We note that Mebust et al. (2011) included OMI pixels containing less than 250 MW of FRP. Globally, we observed that there are many regions where fires occur more densely than in California and Nevada. Here, we chose the 250 MW criterion because we determined through testing that it was the minimum possible cutoff at which most pixels in these fire-dense regions did not aggregate into extremely large groups; we also calculated that under standard conditions of wind speed and predicted emission rates, the change in column density of NO_2 over an individual fire with FRP equal to 250 MW would generally be below the detection limit of OMI. To further ensure removal of data that cannot be attributed to an individual fire, we did not analyze any fire events that were greater in size than 3 OMI pixels in the along-track dimension or 2 OMI pixels in the across-track direction.

The total mass of NO_2 emitted by each fire was calculated using the total area of OMI pixels in the event and the column density of NO_2 over the fire after subtracting a background column density, calculated using fire-free OMI observations in the same location covering a period of 60 days before and 60 days after the fire. Events for which there were less than 10 valid background observations were considered to have a poorly characterized background column and were not analyzed further. Tests in Mebust and Cohen (2013) established that deriving the background from a smaller range of observations (e.g. 30 days before and 30 days after) reduced the observational sample size but did not otherwise affect the results. The time over which the observed NO_2 was emitted, the "clear time", was then calculated using the wind speed and direction near the fire, the OMI pixel edges, and the center of the fire, calculated as the mean of fire pixel locations weighted by pixel FRP. Dividing the mass of NO_2 emitted by the clear time yields the mass emission rate (MER), or rate at which the fire is emitting NO_2 as observed by the satellite. This is not, however, the direct NO_2 EC from the fire, since the NO_2 observed by satellite is at photostationary state. We assume that at photostationary state, 75% of NO_x is present as NO_2 to obtain the EC for NO_x. This assumption is consistent with previous *in situ* measurements which typically find that NO_2 constitutes 50-100% of NO_x. Since we are concerned with relative comparisons of EFs, it is important to establish that this fraction will not

vary significantly as a result of background ozone concentration. We estimate that the impact from this effect is small because our ECs scale by $(NO+NO_2):NO_2$ rather than the direct ratio $NO:NO_2$, and calculate that factor-of-two differences in background ozone will result in <20% change to $(NO+NO_2):NO_2$. In Mebust and Cohen (2013) we presented evidence that seasonal variations in NO_x ECs in African savannas were not primarily driven by changes in background ozone.

Satellite observations of fire plumes inevitably contain a mix of fresh (immediately over the source) and aged (downwind) emissions. Although the OMI spatial resolution is relatively high, NO_x loss is fast enough (lifetime on the scale of hours) that significant loss of NO_x can occur by the time the plume reaches the edge of the OMI pixel. We correct for this effect using a 1D model and 2 hr lifetime assumption as described in Mebust et al. (2011). All data subsequently presented in this paper has been adjusted using this model and assumed lifetime.

To ensure the data is representative of emissions from fires, we remove points with high background column density (3.5×10^{15} molecules cm^{-2}), or either long (>3 hr) or short (<15 min) clear times. Observations with a high background tend to yield higher uncertainty in calculated mass of NO_2 emitted by the fire; long clear times increase the likelihood that the fire violates the assumption that the fire properties have not changed significantly over the time of observation; and short clear times can result in an anomalously high (or negative) MER as the clear time appears in the denominator of the MER, amplifying uncertainty in the difference between the observed NO_2 column density over the fire and the background NO_2 column density. Approximately 30% of observations are removed by these filters.

We present results for all fires of a particular fuel type across the globe (i.e. a "biome-scale" EC) and for spatially distinct clusters of fires of similar fuel types (i.e. an "ecoregion-scale" EC). Fire biomes are identified using primary land cover type (for all fires) and climate classifications (for forests). To be classified as a particular biome type, 75% of FRP from a fire must come from fire pixels identified as that biome type. We use a spatial clustering method to further classify fires into ecoregions; fires of an individual fuel type (e.g forests) that occur within 250 km (100 km for grasses) of each other are grouped and each group is considered an ecoregion for the purpose of this analysis. ECs for both biomes and ecoregions are derived via linear regression with nonparametric bootstrap resampling (5000 resamples). The intercept is not forced through zero to account for any possible small bias in emission estimates from low-energy fires. Typically we require at least 100 observations to consider an EC adequately constrained. We also remove extreme high-weight points by removing all points that affect the fit by 100% or more. There are only two ecoregions (and no biomes) that contain points that fall into this category; one ecoregion contained one such point and the other contained two. For all ECs and EFs described in this work, the mass of NO_x is calculated as NO, a common practice for fire NO_x emissions.

3.4 Results

3.4.1 Biome-scale ECs

Figure 3.1 shows a map of all fires used to derive ECs. Fires are labeled as "other" if at least 75% of FRP came from fire pixels not assigned to a biome type (see Table 3.1), or as "mixed" if they fail to meet the 75% criteria for any individual biome type. We derive ECs for seven different biomes, keeping in mind that similar classifications are used in most fire emission modeling frameworks (e.g. GFED). The results are presented in Table 3.2, along with an estimate for conversion to an EF, the number of fires (N), and R^2. Calculated ECs fall between 0.250-0.362 g NO MJ^{-1}; the lowest calculated EC (boreal forest) is ~70% of the highest calculated EC (grasslands).

In the process of deriving ECs, we must distinguish between variance and uncertainty. Consider a linear regression between FRP and MER. Variance describes the distribution of observations with respect to the line of best fit. This distribution can result from uncertainty in individual measurements, and also from the natural variability of the system. In situations where the natural variability is comparable or large compared to the measurement uncertainty, it will be at least partially reflected in the variance. However, the variance does not by itself describe the uncertainty in the parameters of the best fit. That is best described by the standard error of the fit, which partly derives from the variance but also from the number of observations included in the fit—as the number of observations increases, the variance does not change, but the standard error of the fit decreases. This is because the standard error of the fit does not estimate the distribution of the observations, but rather estimates the distribution of values that would be measured for the parameters if the experiment was repeated with the same number of observations. As this number increases, the parameters are less likely to be anomalously high or low, and so the standard error decreases.

We demonstrate the natural variability (with contributions from individual measurement uncertainty) by calculating ECs directly (dividing MER by FRP) for fires of all fuel types with high FRP (>5000 MJ s^{-1}); we note that the standard deviation is the square root of the variance. The distribution, with both arithmetic and geometric mean and standard deviation, of the directly-calculated ECs is shown in Fig. 3.2. The arithmetic standard deviation of ECs is 72% of the arithmetic mean. However, the distribution is not normal, limiting the value of arithmetic statistics. A log-normal distribution and geometric statistics offer a better description of the observations. The geometric mean for a log-normal distribution is equal to the median; the geometric standard deviation is a multiplicative factor rather than an additive one. In this case, a geometric standard deviation of ~2 indicates that approximately 68% of observations are contained between one-half and twice the geometric mean. Another way to highlight the natural variability of ECs between individual fires is to consider the R^2 value, which is also the fraction of explained variance. An R^2 of ~0.3 (as observed in the case of most of our biome-scale ECs) indicates that about 70% of the variance is unexplained by a linear relationship between FRP and MER.

Despite the large variance, however, most of our ECs have a relatively low standard error (15% or lower). This is because of the large number of observations that factor into each EC. Uncertainty in the best fit (i.e. the EC) is given by the standard error, which is the estimated standard deviation of the best fit parameter (i.e. the slope) as the experiment is repeated with the same number of observations. In our case, we use nonparametric bootstrap resampling to

calculate the EC. One advantage of the bootstrap is that it provides a direct estimate of this distribution of variability in the best fit parameter via the distribution of bootstrap resamples. Therefore we can estimate the standard error in our ECs by calculating the standard deviation of the bootstrap resamples. We use this method to provide the standard error of all ECs presented in this work. The bootstrap resamples are generally normally distributed, so we provide arithmetic standard deviations as our estimate of the standard error.

3.4.2 Spatial variability within biomes

Within each biome there are several spatially distinct ecoregions. We calculate 45 ECs for 42 separate ecoregions; forests are not separated by climate classification for the purposes of determining ecoregions, but for the three forest ecoregions with sufficient sampling of multiple forest biomes, we include multiple ECs. Maps of ecoregions and corresponding ECs are shown in Figures 3.3-3.6; ECs, R^2 and N for each ecoregion are available in Tables 3.3-3.6. We also calculate p values for statistical testing directly using bootstrap distributions of the difference between each ecoregion EC and the mean EC for that biome. We find that most (34 out of 45, or approximately ~75%) ecoregion ECs are not statistically significantly different than the mean biome EC at the 0.05 level. However, there are ecoregions with statically significantly different ECs in all biomes. We include the p value in Tables 3.3-3.6 for these cases. When differences between ecoregion and mean biome ECs are statistically significant, they tend to be large, with most differences ranging from 50% to more than a factor of 2.

3.4.2.1 Forests

Figure 3.3 shows a map of all forest ecoregions containing more than 100 separate observations and ECs for those ecoregions. Fires from clusters with fewer than 100 observations are shown in black. ECs are calculated separately for each biome category (e.g. tropical vs. temperate forest) and biomes are indicated by marker shape. The range of mean biome ECs for all biomes is indicated in grey. We find that one of six tropical forest ecoregion ECs is significantly different from the mean tropical forest EC (Region B); similarly, one of six temperate forest ecoregion ECs is significantly different from the mean temperate forest EC (Region G). One of two boreal forest ecoregion ECs is different from the mean boreal forest EC (Region K). Correlation coefficients (R^2) for each ecoregion range between 0.1 and 0.5 (see supplementary material).

3.4.2.2 Grasses

Results for grass fire ecoregions are found in Fig. 3.4. These ecoregion ECs are the most variable of all the biomes; six of the seventeen ecoregions have ECs that are significantly different from the mean grassland EC (Regions L, P, R, X, Y, and Z). In these ecoregions, ECs range from as large as 0.95 to as small as 0.187 g NO MJ^{-1}. However, ECs in the remaining ecoregions are all within 30% of the mean grassland EC. Correlation coefficients (R^2) for each ecoregion range from 0.1 to 0.7; seven of the seventeen ecoregions have R^2 greater than 0.4. Three of those have ECs that differ significantly from the mean (Regions X, Y and Z).

3.4.2.3 Shrubs

The shrubland biome is not considered in most global treatments of fire NO_x emissions, likely because there are few measurements of shrub EFs and shrub fires generally do not make up a large portion of the global biomass consumed by fire. These fires are (presumably) partitioned into other biome categories. Our mean biome EC for shrubs falls within the range of other mean biome ECs, suggesting that treating shrub fires as grass or forest fires would not cause a large bias in global total fire emissions. Results from our shrub ecoregion analysis are presented in Fig. 3.5. The range of variation is smaller than in other biomes, although one of five ecoregions is statistically significantly different from the mean shrub EC (Region DD). Correlation coefficients for these ecoregions are generally much higher than for ecoregions in other biomes, ranging from 0.3 to 0.7 with four of five regions having R^2 ~0.4 or above. This may be due to better consistency in emission conditions as a result to the smaller size of the shrub regions vs. grass or forest regions and/or to the greater number of highly energetic fires as a percent of observations (>10% of observations have FRP above 2000 MJ s^{-1} for shrub fires, as opposed to less than 10% for grass and forest fires).

3.4.2.4 Agriculture

Results for agricultural fires are presented in Fig. 3.6. Fire emissions of NO_x from this biome are perhaps the hardest to characterize, because these controlled fires are usually small. This is reflected in the relatively larger uncertainties (see Fig. 3.6b) and also in much lower correlation coefficients; R^2 is below 0.15 for all but one of the 9 crop regions shown below. Only one of the nine ecoregion ECs is statistically significantly different from the mean agricultural EC (Region NN); however, that may partly be due to the higher uncertainties in ECs for this crop type. Using a harvested crop area dataset (Monfreda et al., 2008), we identify the main crop type for most regions to be wheat, except region HH (sorghum) and regions KK and LL (soybeans). There is no obvious relationship between crop type and EC.

3.5 Discussion

3.5.1 Biome- and ecoregion-scale similarities and differences

Broadly, the ECs presented here suggest that mean fire behavior is similar regardless of biome or ecoregion. We find that 75% of ecoregion ECs are not significantly different from the corresponding biome-scale EC. These ECs fall within 32% of the mean biome EC for all biomes except agriculture, and for individual biomes the range can be as low as a few percent. Differences in the agricultural biome are larger partly because of larger uncertainties in the derived ECs. As previously noted, biome-scale ECs themselves cover a relatively narrow range (the lowest value is ~70% of the highest value). We find that almost half of the ecoregion-scale ECs (21 out of 45) fall directly into this range, and 9 more overlap the range within the standard error of the EC. However, there are several ecoregion-scale ECs that do not overlap this range within standard error or even twice the standard error. These ECs are generally substantially different (i.e. by 50% or more) from the biome scale ECs. These differences suggest that emissions differ more with location than with fuel type, challenging the traditional model of emissions as fuel type-specific.

Ecoregions observed to deviate from mean ECs contain a moderate number of observations rather than a small number, suggesting that the differences are robust. The large differences in these ECs as compared to the mean biome EC will result in significant biases in emission estimates for these specific regions. The most notable of these is for boreal forest in Asia (Region K). Most conventional estimates of boreal forest NO_x EFs are derived from measurements of fires in North America; however, we find that ECs in boreal forest in Asia are fully twice those in North America (Region J). This is particularly important because emissions from boreal forest fires lay an especially important role in global atmospheric composition and chemistry (Jacob et al., 2010; Simpson et al., 2011).

We do not fully understand causes of the observed ecoregion-scale differences. It is possible that differences in fuel N content and/or fire MCE are responsible, but evaluating these factors on the scale of an ecoregion requires an in-depth understanding of local fire behavior as well as observations of these factors that currently do not exist on the spatial or temporal scale of this analysis. Rather than speculating on specific causes here, we instead hope that identification of clear differences in different ecoregions guides future efforts to reveal and assess processes that govern fire emissions.

3.5.2 Comparison to previous work

We compare both to our previous work quantifying fire emissions from space, and to global biome EFs from conventional fire emission schemes.

3.5.2.1 California and Nevada revisited

In Mebust et al. (2011) we applied the same basic methodology with minor differences to fires over California and Nevada (126-113°W, 31-44°N) and found that our calculated MER was correlated with FRP with R^2 ranging from 0.3 to 0.8, that relative differences in emissions between fuel types previously obtained by in situ measurements were reproduced by our analysis, and that the absolute values of the EC and EFs we measured were several times smaller than previously obtained EF and EC measurements. In this work we update our analysis to incorporate a more recent version of the OMI NO_2 retrieval (Standard Product v2.1 vs. v1.0), a different wind dataset (CFSR winds at 850 hPa and 0.5° × 0.5° resolution vs. NARR winds at 900 hPa and 32 km resolution), additional years of observations (2009-2011), removal of OMI pixels containing less than 250 MW of total FRP from further analysis, and adjustments to how observations were selected for removal with respect to e.g. background, clear time, etc. Here we include a comparison to those previous results.

Figure 3.7 shows MER vs. FRP for (a) all fires, (b) forest fires, (c) shrub fires and (d) grass fires in the California/Nevada region indicated above. In most cases, the R^2 for each category is slightly higher than observed in Mebust et al. (2011), possibly due to improvements in methodology, improvements to the NO_2 retrieval in the Standard Product v2.1 vs. v1.0, and/or a reduction in the number of points scattered around zero. We also perform a multiple regression as in Mebust et al. (2011), and derive ECs of 0.203 ± 0.042, 0.290 ± 0.040, and 0.195 ± 0.022 g NO_x MJ^{-1} (as NO) for forest, shrub, and grass fires, respectively. In an absolute sense, these values are lower than those derived in Mebust et al. (2011) by 52% for shrubs, 34% for grasses, and 16% for forests. Much of the decrease is due to generally lower values of tropospheric NO_2

columns in version 2.1 of the NASA OMNO2 standard product relative to version 1.0. Further reduction in the case of shrub fires is due to inclusion of the years 2009-2011 which had generally lower ECs (~26% below the mean EC for all years).

In Mebust et al. (2011) we found that the relative differences between grass, shrub and forest fire ECs derived from OMI and MODIS data reproduced similar relative differences in EFs measured for primarily North American fires *in situ*. In this analysis, we find that the relative differences in ECs and EFs remain within one standard deviation of one another, though the agreement in the ratio is slightly worse. For example, the ratio of grass to forest fire EFs obtained in Battye and Battye (2002) is 1.4 ± 0.8; the ratio of ECs for the same fuels as reported in Mebust et al. (2011) is 1.2 ± 0.4 and in this work is 1.0 ± 0.2. The ratio between shrub and forest fire ECs in both studies is similarly within one standard deviation of the ratio of shrub and forest fire EFs. As in both Battye and Battye (2002) and Mebust et al. (2011), we find that shrub fires in this region emit more NO_x per unit energy (or mass) than either grass or forest fires. In both this work and Mebust et al. (2011), we find that forest ECs are higher (relative to grass and shrub fires) than EFs presented in Battye and Battye (2002).

3.5.2.2 Comparison with global EF summaries

There exist several previously published EFs intended for use in global models: an initial comprehensive summary of EFs for many species and fuel types presented by Andreae and Merlet (2001); two updates to that work (Hoelzemann et al., 2004; van der Werf et al., 2010); and a recent summary using a more selective set of observations (Akagi et al., 2011). EFs from each of these references, along with ECs from this work, are shown in Fig. 3.8 (on different y-axes). Values for temperate forest, extratropical forest and chaparral from Akagi et al. (2011) are updated to include observations that were published after the summary (Akagi et al., 2013; Yokelson et al., 2013); these updates are available at http://bai.acd.ucar.edu/Data/fire/. We note that EFs in previous studies are derived as the mean of several measurements, and the associated "error" bars shown in Fig. 3.8 are one standard deviation of the measurements. As we previously discussed, this means they reflect some of the natural variability in individual fire emissions, and are not an estimate of the uncertainty in the mean EF. This uncertainty could be estimated using the number of fires from which the EFs are derived, but this information is not easily and uniformly accessible and so we do not attempt it. The error bars for our work in Fig. 3.8 are estimates of the uncertainty in the EC, not the variance in individual measurements, and so they estimate a different quantity than the "error" bars from the other studies and should not be directly compared.

The previously published summaries differ substantially from one another, a reflection of the large variability in measured NO_x EFs for individual fires even within a single global-scale biome, and the relatively small sample size which results in substantial changes to the mean when new measurements are added. We find that our biome-scale ECs fall within a narrower range than all of the previous studies. In a relative sense, our values compare best with those updated from Akagi et al. (2011), although in forested regions they are generally higher (relative to other biomes). This difference may reflect the improvements in sampling coverage in the full satellite record vs. fire emissions measured in situ. However, it is also plausible that this difference results from a low bias in FRP over forested regions. We estimate the plausible magnitude of this bias by assuming that the observed difference results entirely from the bias and

not from sampling differences; in that case, FRP is biased low by ~34%, ~40%, and ~67% for tropical, temperate, and boreal forest fires, respectively. The difference in bias for boreal forest (vs. tropical and temperate forest) could be due to a higher proportion of burning of ground-level or below-ground burning (e.g. peat) in boreal fires. While the differences we observe relative to Akagi et al. (2011) are almost certainly varied in source, this nevertheless provides a rough estimate of one plausible bias. We note that this estimate is specific to the accuracy of FRP as it pertains to actively detected fires, not the accuracy of FRP at e.g. 0.5° × 0.5° scale where canopy cover might e.g. completely obscure fires that would otherwise be detected by the MODIS algorithm.

Detailed information on the EF calculations in Akagi et al. (2011) is available in supplementary material of that paper, and thus we can directly compare regional differences in ECs presented here with the EFs used in Akagi et al. (2011) to examine how consistent our results are beyond broad biome categorizations. Akagi et al. (2011) divide the tropical forest NO_x EF into two EFs: one for tropical evergreen deforestation, and one for tropical dry deforestation that is approximately twice as high. When we calculate ECs separately for forest fires in "monsoonal" and "winter-dry" equatorial regimes, that value is higher (by a factor of 1.89) than the EC calculated for forest fires in the "fully humid" equatorial regime. If these climate classifications provide an adequate proxy for evergreen vs. dry deforestation, this result is consistent with Akagi et al. (2011). We also find that the temperate forest EC from Region J is very slightly below the mean temperate forest EC, and forest fire ECs in the California/Nevada region are even lower than in Region J; this is consistent with results from Akagi et al. (2011) in that measurements of California pine understory EFs made by Burling et al. (2011) are slightly below the mean temperate forest understory EF, and EFs from Oregon wildfires measured by Radke et al. (1991) are below the mean temperate forest EF.

In contrast, in Akagi et al. (2011) EFs reported for tropical forest fires in Mexico (Yokelson et al., 2011) are higher (3-5 g NO_x as NO kg^{-1}) on average than EFs for tropical forest fires in Brazil (1-2 g NO_x as NO kg^{-1}; Ferek et al., 1998; Yokelson et al., 2008), while our analysis suggests that ECs from tropical forests in Mexico and Brazil are similar to each other, with ECs in Mexico slightly lower (see Fig. 3.3, regions D and E). We also find that ECs for the region that encompasses North and South Carolina in our analysis (region G) are much higher than the mean EC for temperate forests, which is inconsistent with the below-mean (Akagi et al., 2013) or slightly above mean (Burling et al., 2011) EFs in the aggregate EF from Akagi et al. (2011) for this biome.

3.6 Conclusions

We present biome- and ecosystem-resolved NO_x ECs, based on satellite measurements of tropospheric NO_2 from OMI and of FRP from MODIS, for several different biome and ecosystem categories. These ECs are obtained via a method that was adapted from Mebust et al. (2011) for application to global fires and is also updated to include subsequent years of observations and an improved version of the OMI NO_2 retrieval. We compare our biome-scale ECs with summaries of EFs based on in situ measurements and find that the range of biome-scale ECs observed here is smaller than for EFs in previous works. Our results are for the most

part consistent with relative differences in EFs from Akagi et al. (2011) although emissions in forest biomes are relatively higher.

We find that the majority of ecoregion-scale ECs are not statistically significantly different from the corresponding mean biome EC, while biome-scale ECs themselves fall into a narrow range with the smallest EC (0.250 g MJ^{-1}) fully 70% of the largest (0.362 g MJ^{-1}) EC. We do, however, observe ecoregion-scale ECs that are both significantly and substantially different from the mean biome EC and/or from the range of biome-scale ECs, demonstrating that there exist regions where mean fire NO_x emission behavior is very different from the global mean. While mean biome and ecoregion ECs are relatively similar, variability in individual fire ECs remains high. Future efforts should focus on elucidating the particular processes that govern this variability; the observed differences in ECs can hopefully guide these efforts by identifying regions where there are important differences in fire NO_x emission behavior.

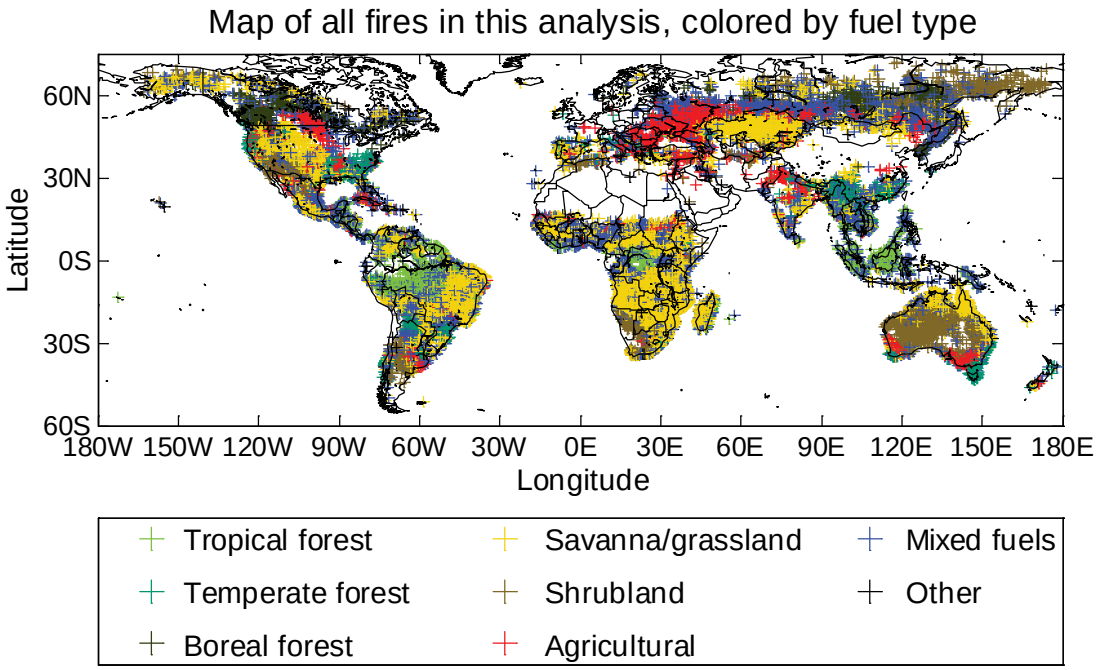

Figure 3.1. Map of fires used in this analysis. Color indicates fuel type as determined using land cover and climatology. Fires were identified as having a particular fuel if greater than 75% of measured FRP for that fire came from fire pixels of a single fuel type; fires not meeting this criterion are designated “mixed fuels”.

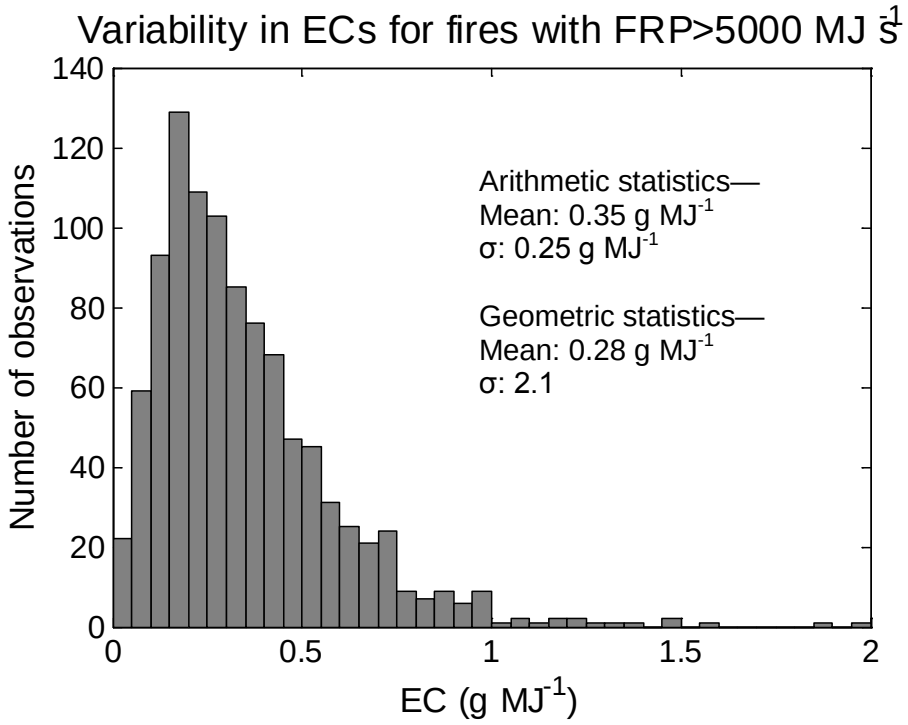

Figure 3.2. Histogram of ECs measured for fires with FRP above 5000 MJ s^{-1}. ECs were calculated by dividing the MER by FRP for individual fires.

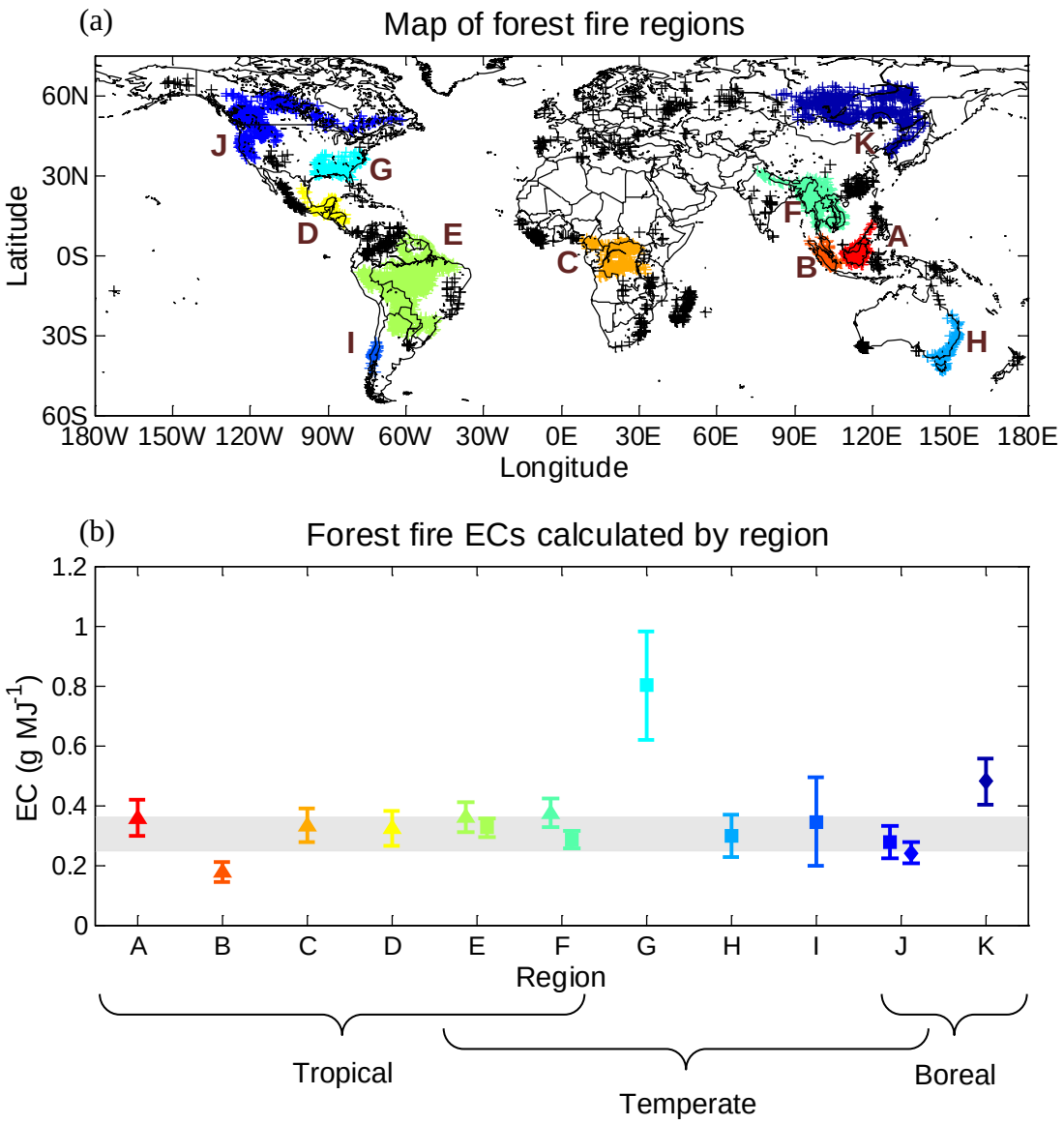

Figure 3.3. A map of forest fire regions determined by a clustering analysis (a) and ECs calculated individually for each region (b). In (a), black markers identify forest fires belonging to clusters with less than 100 observations. In (b), marker shapes are used to identify biomes for each EC, determined via climate classifications: triangles indicate tropical, squares indicate temperate, and diamonds indicate boreal forests. In regions where there is adequate sampling of more than one biome type, ECs are calculated for both biomes (e.g. region E). The range of mean biome ECs (as presented in Table 3.2) is indicated in grey.

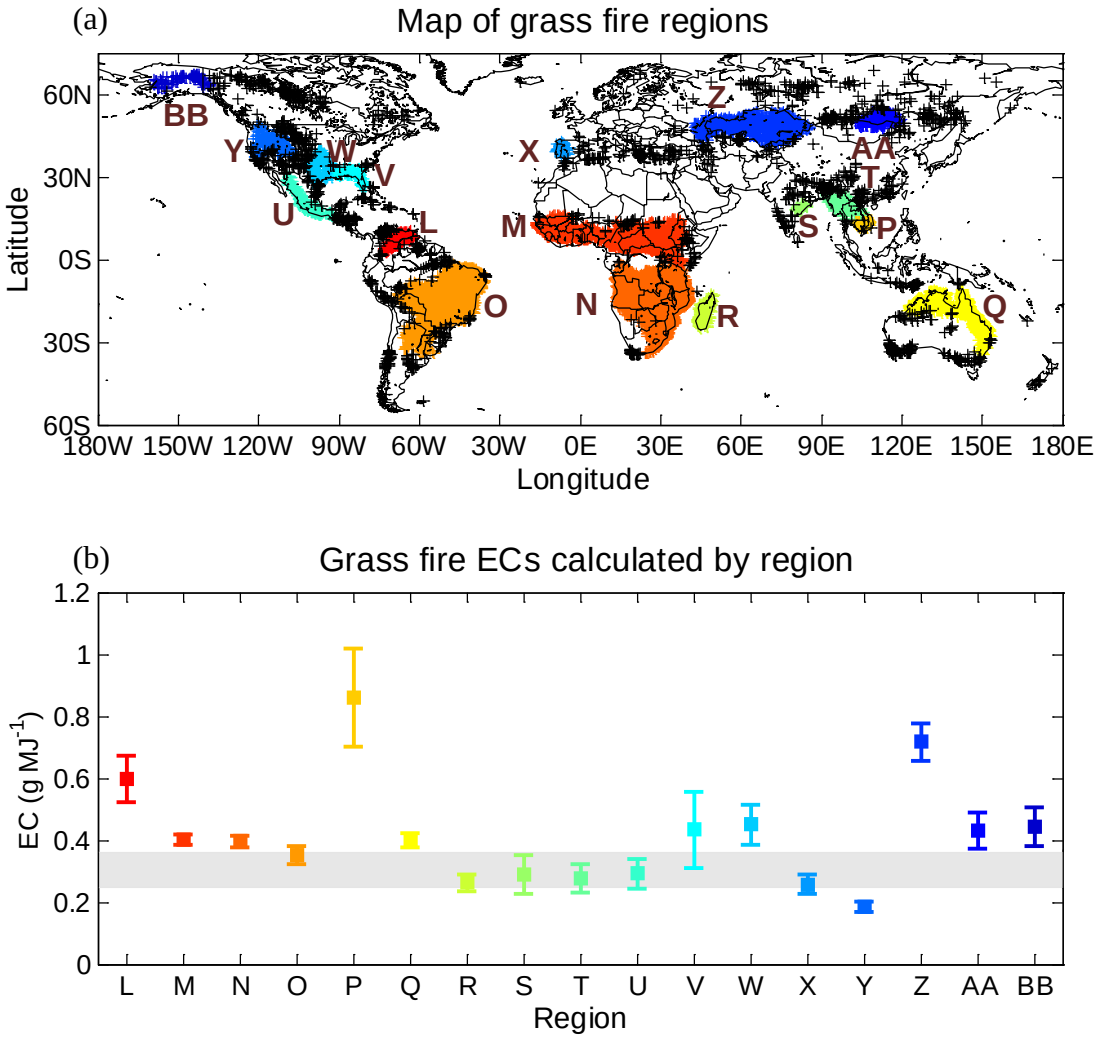

Figure 3.4. A map of grass fire regions determined by a clustering analysis (a) and ECs calculated individually for each region (b). In (a), black markers identify grass fires belonging to clusters with less than 100 observations. In (b), the range of mean biome ECs (as presented in Table 3.2) is indicated in grey.

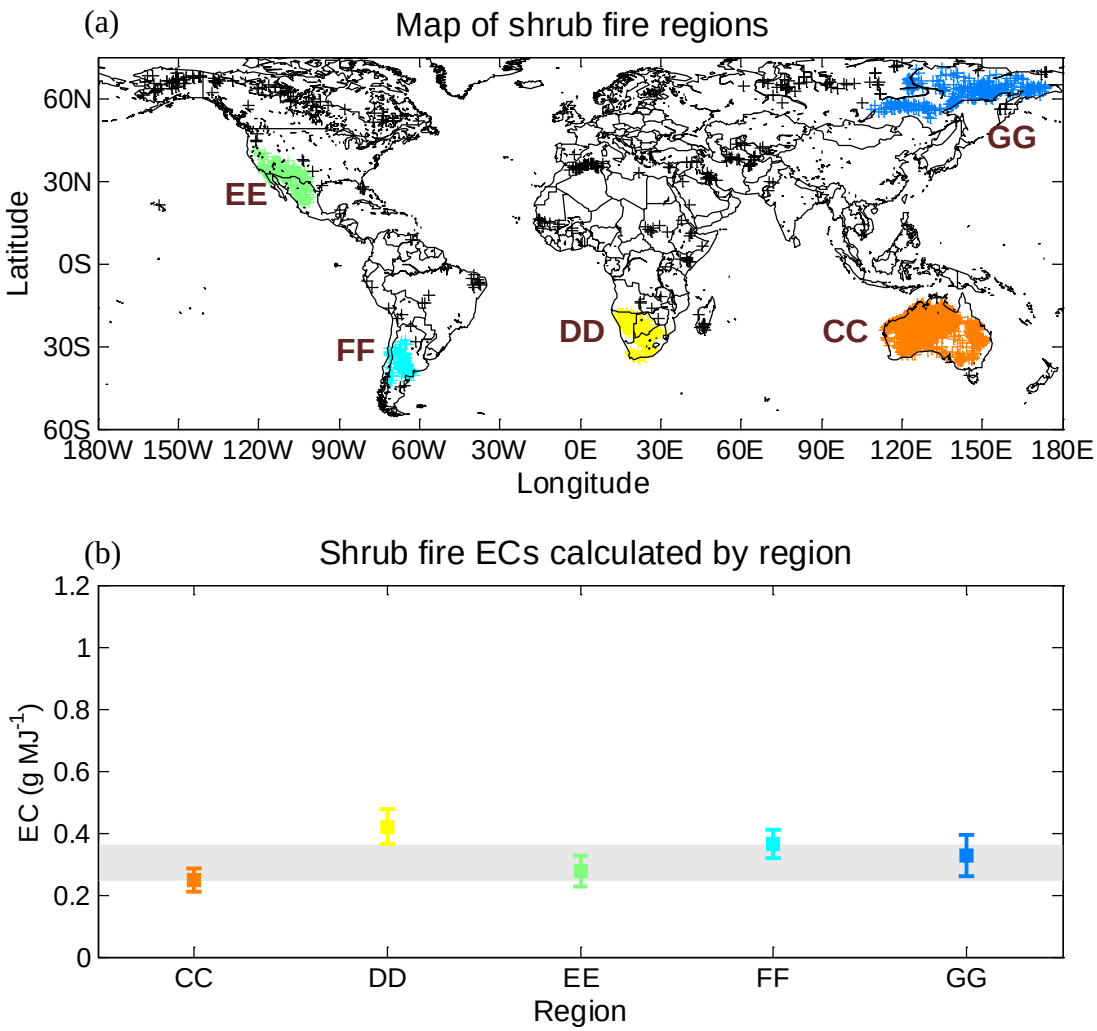

Figure 3.5. A map of shrub fire regions determined by a clustering analysis (a) and ECs calculated individually for each region (b). In (a), black markers identify shrub fires belonging to clusters with less than 100 observations. In (b), the range of mean biome ECs (as presented in Table 3.2) is indicated in grey.

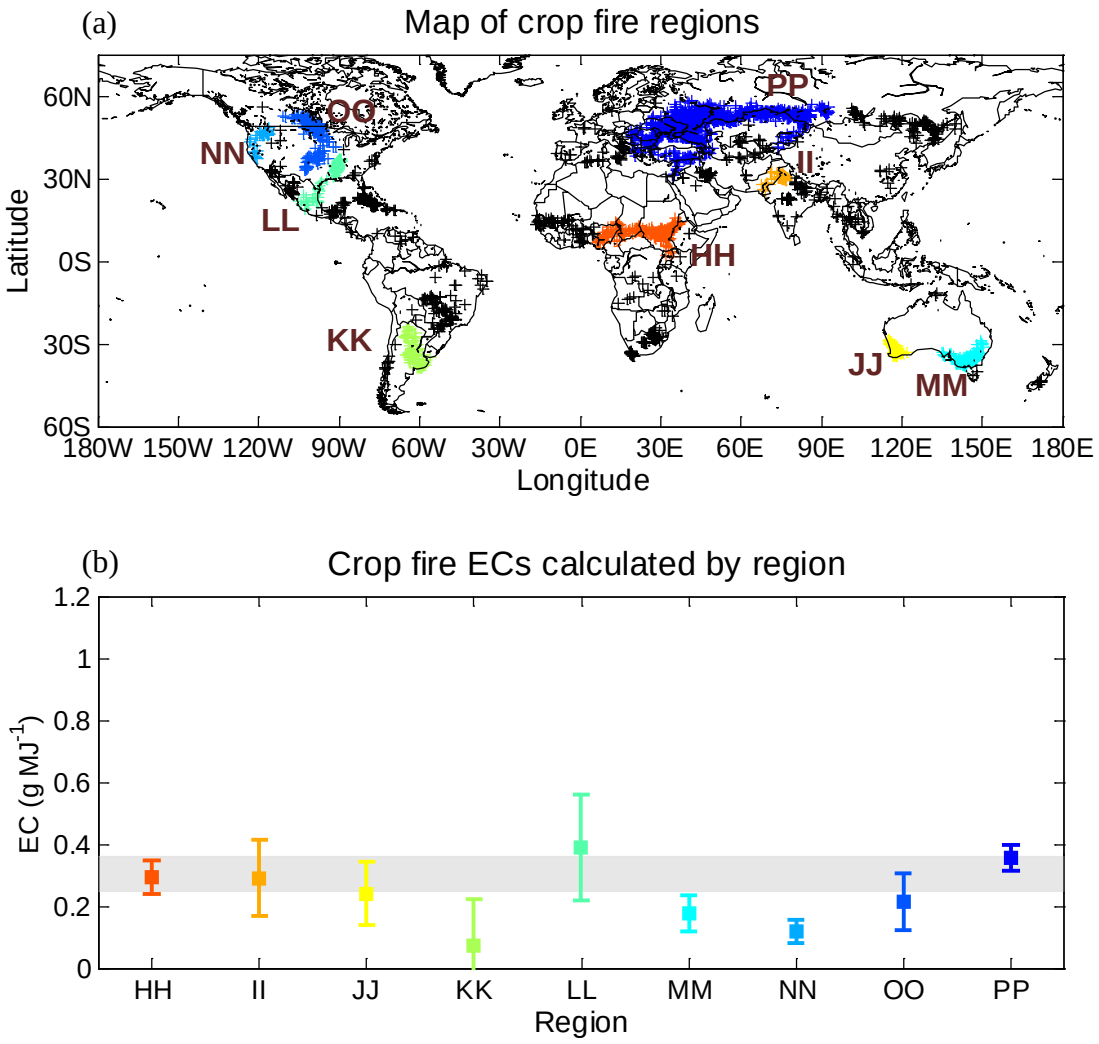

Figure 3.6. A map of agricultural fire regions determined by a clustering analysis (a) and ECs calculated individually for each region (b). In (a), black markers identify agricultural fires belonging to clusters with less than 100 observations. In (b), the range of mean biome ECs (as presented in Table 3.2) is indicated in grey.

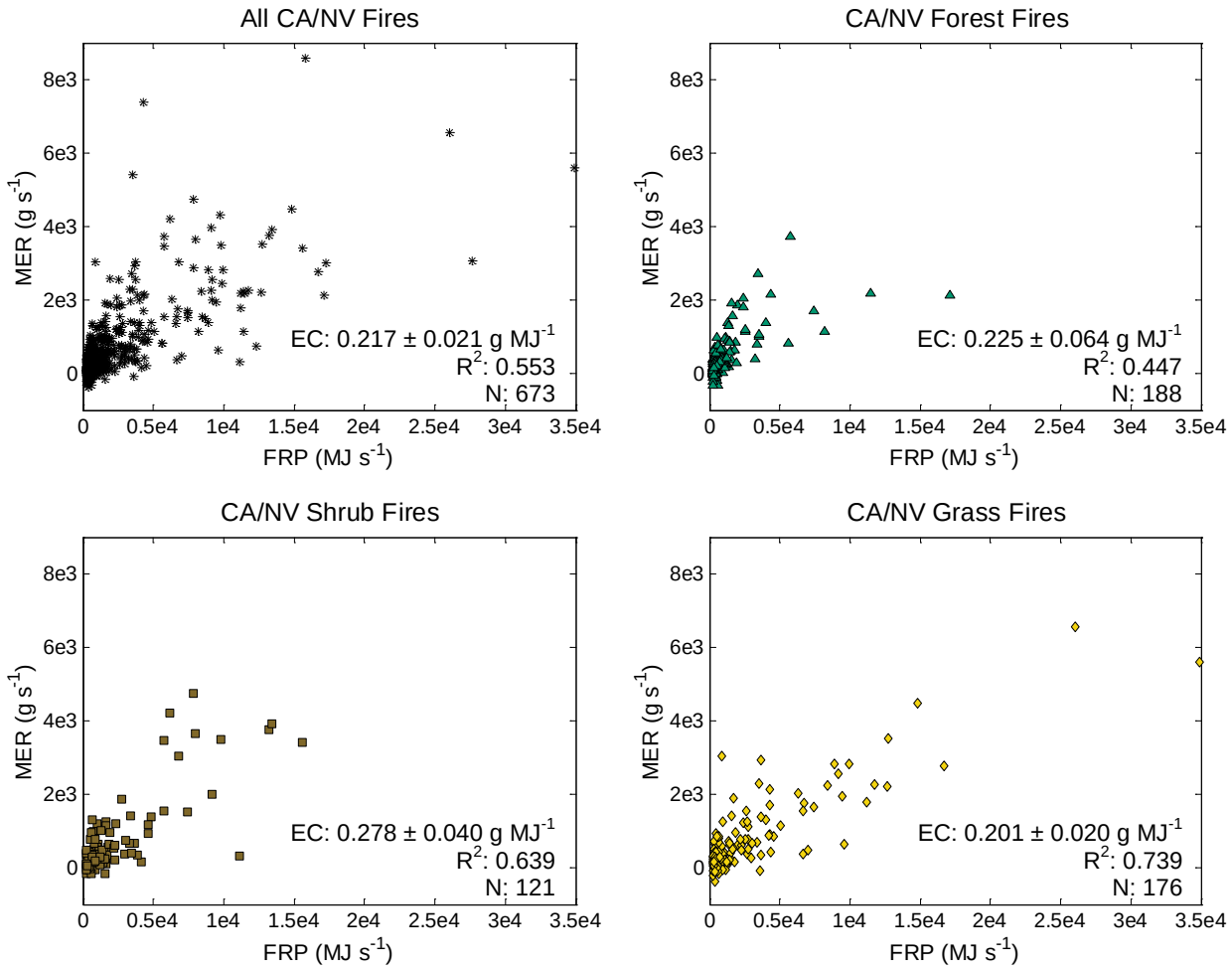

Figure 3.7. Regressions of fire radiative power (FRP) vs. mass emission rate (MER) for (a) all fires, (b) forest fires, (c) shrub fires and (d) grass fires in the California/Nevada region (126-113°W, 31-44°N). Listed on each plot are the calculated EC (i.e. the slope of the best fit line), R^2, and number of points.

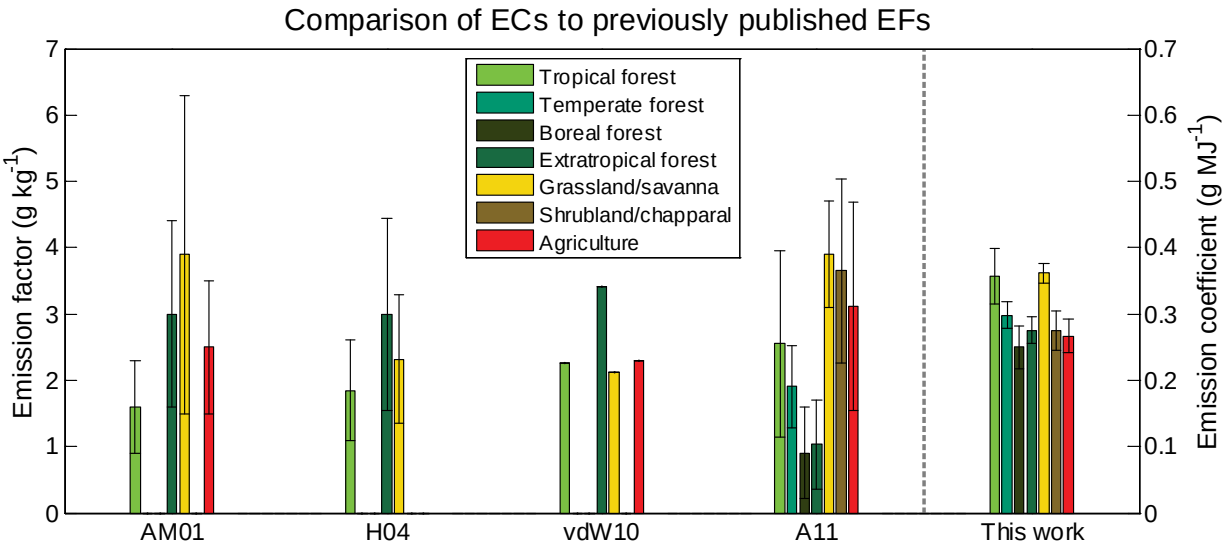

Figure 3.8. Bar graph showing the different EFs (left y-axis) in previous work and ECs (right y-axis) presented here at the global biome scale. EFs from previous studies (from left to right) are: Andreae and Merlet (2001), Hoelzemann et al. (2004), van der Werf et al. (2010), Akagi et al. (2011). In previous work, error bars indicate one standard deviation of the mean; in the case of van der Werf et al. (2010), no standard deviation was reported. Error bars for this work indicate the standard error of the fit.

IGBP class	Biome category
Water	Not assigned
Evergreen needleleaf forest	Forest
Evergreen broadleaf forest	Forest
Deciduous needleleaf forest	Forest
Deciduous broadleaf forest	Forest
Mixed forest	Forest
Closed shrublands	Shrub
Open shrublands	Shrub
Woody savannas	Grass
Savannas	Grass
Grasslands	Grass
Permanent wetlands	Not assigned
Croplands	Agricultural
Urban and built-up	Not assigned
Cropland/natural vegetation mosaic	Not assigned
Snow and ice	Not assigned
Barren/sparsely vegetated	Not assigned

Table 3.1. Classification of IGBP classes to broad biome categories.

Fuel type	NO_x EC (g MJ^{-1})[a]	NO_x EF (g kg^{-1})[a,b]	N	R^2
Tropical forests	0.356 ± 0.044	0.87 ± 0.11	6266	0.307
Temperate forests	0.298 ± 0.019	0.727 ± 0.047	3417	0.293
Boreal forests	0.250 ± 0.033	0.609 ± 0.079	1633	0.308
Extratropical forests[c]	0.275 ± 0.020	0.670 ± 0.049	5050	0.298
Grasslands	0.362 ± 0.015	0.883 ± 0.037	73789	0.290
Shrublands	0.275 ± 0.030	0.671 ± 0.075	4764	0.439
Agriculture	0.266 ± 0.024	0.650 ± 0.061	4732	0.068

Table 3.2. Summary of calculated emission coefficients and emission factors for NO_x as NO. Reported uncertainties are 1σ, calculated via nonparametric bootstrap resampling.
[a] assumes NO_2/NO_x of 0.75. Total NO_x mass expressed as NO.
[b] assumes K = 0.41 kg MJ^{-1}.

Region	Type	EC (g MJ^{-1})	SE (g MJ^{-1})	N	R^2	p<0.05
A	Tropical	0.357	0.058	366	0.193	
B	Tropical	0.179	0.035	351	0.207	=0.0096
C	Tropical	0.333	0.055	653	0.100	
D	Tropical	0.341	0.061	402	0.226	
E	Tropical	0.360	0.051	3493	0.307	
	Temperate	0.326	0.030	778	0.352	
F	Tropical	0.374	0.046	579	0.362	
	Temperate	0.285	0.028	1147	0.214	
G	Temperate	0.80	0.18	320	0.253	<0.0004
H	Temperate	0.298	0.072	336	0.358	
I	Temperate	0.34	0.15	129	0.490	
J	Temperate	0.275	0.056	257	0.440	
	Boreal	0.240	0.035	776	0.465	
K	Boreal	0.480	0.078	740	0.221	=0.0028
Biome means:	Tropical	0.356	0.044	6266	0.307	
	Temperate	0.298	0.019	3417	0.293	
	Boreal	0.250	0.033	1633	0.308	

Table 3.3. ECs, standard error, number of observations (N) and R^2 for forest ecoregions.

Note: for Tables 3.3-3.6, the column "p<0.05" provides p values measured for all ecoregions with ECs that are significantly different than the mean biome EC at the p<0.05 level. The p value is estimated using a nonparametric boostrap technique where the ecoregion and mean biome slope are resampled with replacement and the difference is recorded; there are 5000 resamples and p is calculated directly from the distribution of the differences in slope.

Region	EC (g MJ^{-1})	SE (g MJ^{-1})	N	R^2	p<0.05
L	0.597	0.075	633	0.257	=0.0012
M	0.404	0.016	22747	0.271	
N	0.397	0.019	26944	0.260	
O	0.353	0.031	10698	0.286	
P	0.85	0.16	313	0.259	=0.0004
Q	0.401	0.022	5110	0.510	
R	0.263	0.029	814	0.283	=0.014
S	0.291	0.062	176	0.123	
T	0.277	0.045	748	0.215	
U	0.291	0.047	375	0.178	
V	0.43	0.13	175	0.200	
W	0.450	0.065	310	0.452	
X	0.258	0.031	109	0.571	=0.0272
Y	0.187	0.018	280	0.657	<0.0004
Z	0.717	0.060	1884	0.527	<0.0004
AA	0.433	0.059	286	0.417	
BB	0.444	0.064	200	0.404	
Biome mean:	0.362	0.015	73789	0.290	

Table 3.4. ECs, standard error, number of observations (N) and R^2 for grass ecoregions.

Region	EC (g MJ^{-1})	SE (g MJ^{-1})	N	R^2	p<0.05
CC	0.246	0.038	2944	0.390	
DD	0.420	0.056	506	0.557	=0.0088
EE	0.277	0.049	307	0.657	
FF	0.365	0.046	183	0.583	
GG	0.330	0.066	440	0.287	
Biome mean:	0.275	0.030	4764	0.439	

Table 3.5. ECs, standard error, number of observations (N) and R^2 for shrub ecoregions.

Region	EC (g MJ^{-1})	SE (g MJ^{-1})	N	R^2	p<0.05
HH	0.293	0.051	425	0.237	
II	0.29	0.12	224	0.085	
JJ	0.24	0.10	111	0.114	
KK	0.07	0.15	108	0.001	
LL	0.39	0.17	154	0.115	
MM	0.176	0.059	314	0.050	
NN	0.120	0.038	101	0.131	=0.006
OO	0.212	0.095	233	0.065	
PP	0.356	0.042	2214	0.081	
Biome mean:	0.266	0.024	4732	0.068	

Table 3.6. ECs, standard error, number of observations (N) and R^2 for crop ecoregions.

Chapter 4

Observations of a seasonal cycle in NO_x emissions from fires in African woody savannas

This chapter has been adapted from the following peer-reviewed publication: A. K. Mebust and R. C. Cohen, Observations of a seasonal cycle in NO_x emissions from fires in African woody savannas, Geophys. Res. Lett. 40, 7, 1451-1455, 2013.

4.1 Introduction

Wildfire emissions of nitrogen oxides ($NO_x \equiv NO + NO_2$) perturb atmospheric chemistry at a wide range of spatial scales with impacts on air quality and climate (Andreae and Merlet, 2001). NO_x emissions from fires are known to depend on the total biomass burned, the percent nitrogen (N) of the fuel, and the extent of flaming versus smoldering combustion (Andreae and Merlet, 2001). To understand the role of fires in the global atmosphere, numerical models represent emissions as the product of an emissions factor (EF, in g of emitted species per kg of consumed fuel) and an estimate of the mass burned for each fire. EFs for a variety of species/biomes have been previously estimated from laboratory and field observations of wildfires (Andreae and Merlet, 2001; Akagi et al., 2011). However, even for a single species in a single biome, these studies indicate that there can be large variability in estimates of the EF (Andreae and Merlet, 2001; Freeborn et al., 2008; Yokelson et al., 2011; Akagi et al., 2011).

Satellite instruments provide observations of NO_2 at the high spatiotemporal resolution needed to observe wildfire emissions with sufficient statistics to examine variability in fire emissions between distinct biomes and over time within biomes. The highest resolution products currently available allow observation of plumes from individual fires (Mebust et al., 2011). Several recent studies have described strategies for combining satellite observations of fire radiative power (FRP in MJ s^{-1}) with trace gas or aerosol observations to provide emission coefficients (ECs in g emitted species MJ^{-1}) for fires (Ichoku and Kaufman, 2005; Mebust et al., 2011; Vermote et al., 2009). Laboratory studies indicate that total fire radiative energy (FRE, or time-integrated FRP) is proportional to the total biomass burned in a fire, implying ECs and EFs are proportional to one another (Freeborn et al., 2008; Wooster et al., 2005). In a study of California and Nevada fires, we found that satellite-observed NO_x ECs depended on fuel type (forest, grassland, etc.) and that, despite differences in absolute emissions per unit mass measured in that study and in previous work, the ratios of the derived ECs for different biomes were consistent with estimates of emissions per unit mass burned based on in situ and laboratory observations, implying that satellite-derived ECs capture relative differences in emissions (Mebust et al., 2011). Here we extend the methods used in that prior work to infer seasonal variation in ECs for fires in Africa, using NO_2 observations from the Ozone Monitoring Instrument (OMI) and fires detected by the Moderate Resolution Imaging Spectroradiometer

(MODIS), as well as wind and land cover data. At the scale resolved by OMI, NO_2 and NO in the fire plume are in photostationary state, allowing us to infer differences in NO_x emissions from NO_2 columns.

4.2 Methods

Satellite and reanalysis data used in this analysis include the Dutch OMI NO_2 (DOMINO) data product (Version 2.0) (Boersma et al., 2011); the MODIS Aqua Thermal Anomalies (MYD14, Level 2, Collection 5) data product (Giglio et al., 2003); the MODIS Aqua+Terra Land Cover (MCD12Q1, Level 3, Collection 5) data product (Friedl et al., 2010); and wind fields from the National Centers for Environmental Prediction (NCEP) Climate Forecast System Reanalysis (CFSR) at 850 hPa and 0.5°×0.5° resolution (Saha et al., 2010).

The method used to derive ECs is described in detail in Mebust et al. (2011); here we outline the general strategy and discuss changes that have been made to the original method. We analyze Aqua MODIS fire detections (1 km^2 pixel resolution at nadir) collected from 2005-2008 over Africa (35°S-30°N, 20°W-60°E). All OMI pixels (13×24 km^2 at nadir) containing fire pixels from the corresponding MODIS Aqua daytime overpass were identified and grouped together into single fire events using a sorting algorithm as described in Mebust et al. (2011); here, however, OMI pixels containing fire pixels with FRP totaling less than 250 MW were not included in the sorting algorithm to avoid aggregating close small fires into single large events. Also, in this analysis we use the DOMINO retrieval whereas Mebust et al. (2011) used the OMI standard product (SP; Level 2, Version 1.0.5, Collection 3) (Bucsela et al., 2006); we focus on results from DOMINO here since the version of the SP retrieval used in Mebust et al. (2011) is known to be seasonally biased due to the yearly averaged NO_2 profiles employed in the retrieval (Lamsal et al., 2010), whereas the version of DOMINO used here employs daily output (Boersma et al., 2011). However, we note that similar results were found using the SP retrieval. As in Mebust et al. (2011), only OMI pixels with <20% cloud fraction are used, and only the inner 40 pixels (of 60 across-track pixels) are used to avoid the significant decrease in resolution in the outer pixels. Because we use MODIS Aqua daytime fire detections only, measurements of FRP and NO_2 column density are coincident in time (within 15 minutes).

Once each fire event is defined, the analysis proceeds as outlined in Mebust et al. (2011). Briefly, the total mass of NO_2 within each region emitted by fire is calculated using OMI observations of tropospheric column density of NO_2 on the day of the fire and subtracting a background value for NO_2 column density calculated using observations over the same region in the 60 days before and after the fire. Using wind fields as well as fire pixel locations and OMI pixel geometry, the "clear time" or time over which the observed mass of NO_2 was emitted is obtained. We note that in Mebust et al. (2011), wind fields were obtained from the North American Regional Reanalysis (NARR) at 900 hPa; in this work, to enable analysis of emissions over Africa, we use the CFSR wind fields previously mentioned. We then use a 1D model to correct the measured mass of NO_2 for chemical loss and deposition over the clear time. Dividing the corrected measured mass of emitted NO_2 by the clear time yields the fire mass emission rate (MER in g s^{-1}); the total FRP in each region is also calculated as a sum of FRP over all individual fire pixels contained in the region. For any collection of fires, a linear regression of FRP vs. MER yields the EC as the slope. We note that in this study, we produce NO_2 ECs because the

satellite observes only NO_2 (not NO_x); however, these are not direct NO_2 emissions from the fire, but rather represent NO_2 at photostationary state and are proportional to the NO_x EC via the NO_2:NO_x ratio. Thus any percent change in NO_2 EC should be equal to the percent change in NO_x EC assuming there is no change in the NO_2:NO_x ratio. We use nonparametric bootstrap resampling as a method to minimize the impact of outliers on the calculated slope and standard deviation; points were sampled randomly with replacement, and 1000 bootstrap samples were used for each calculation. When the percent error is >100% the slope is considered poorly constrained and is not presented. An extensive assessment of the sources of error in deriving these values can be found in the appendix.

Some data was filtered out to maintain data quality as in Mebust et al. (2011); however, the methods used to filter data were slightly different. Simple filters were applied instead of propagating uncertainty and applying an uncertainty filter; the uncertainty-based approach skewed the distribution of points along the y-axis, leading to a statistically-derived bias in the analysis, while simple filters removed most unrealistic points without skewing the distribution of points. We applied a high background column density filter ($>3.5 \times 10^{15}$ molecules cm^{-2}) as it was difficult to distinguish fire emissions from anthropogenic variability in these regions (~5% of data); a long clear time filter (>3 hrs) as the analysis requires that we approximate wind speed and fire radiative power as constant over this time, and this approximation breaks down at long clear times (~4% of data); and a short clear distance filter (<7 km) as the higher percent uncertainty associated with short clear distances can produce unrealistic values for the fire MER (~29% of data). We also removed fires with a region of analysis more than 3 OMI pixels in the along-track dimension, or more than 2 OMI pixels in the across-track dimension (<1% of data). The analysis assumes the fire can be treated as a point source within the region; regions larger than this are likely aggregates of small but close-together fires for which the point source approximation breaks down. Approximately 35% of data was filtered out.

We focus on African savanna fires because the fire season in these locations is well-established and the mass of emissions is globally significant (Giglio et al., 2006). Fires are identified as “savanna” or “woody savanna” fires if at least 75% of the measured FRP comes from the given land type identified using the MODIS Land Cover product (Friedl et al., 2010). Figure 4.1 shows a map of Africa with four distinct fire biomes highlighted: northern vs. southern hemisphere and savanna vs. woody savanna. The borders between each region are generally well-established with very little overlap in location between woody savanna and savanna in each hemisphere.

We also identify some properties of the fire season within the study areas using Aqua MODIS fire pixels from the daytime overpass. The number of fires, total FRP, and mass burned all have an approximately Gaussian distribution in time, peaking in the middle of the fire season in each biome. Within each biome, fires generally move from north to south (independent of hemisphere) throughout the season; thus early season measurements within a biome are more heavily weighted towards fires in the north, while late season measurements are more heavily weighted towards fires in the south. Despite these differences, however, the total length of fire season is spatially consistent throughout each biome, with typical season length ~5 months in the northern hemisphere and ~6 months in the southern hemisphere. Annual rainfall and wet season length increase as distance to the equator decreases in both hemispheres (Nicholson, 2000); however, according to MODIS fire observations, the shorter wet season does not seem to impact

the length of fire season in the northern and southern extremes. Unfortunately, little to no information is available regarding systematic biome-wide variations in mean fuel nitrogen content.

4.3 Results and Discussion

ECs are presented for each month with more than 150 valid observations and <100% percent error. The seasonal variation in ECs, as the percent anomaly from the mean of all monthly ECs, is shown in Fig. 4.2 for all four biome types, with error bars indicating one standard deviation of the value calculated via nonparametric bootstrap resampling. In woody savannas in both the northern (Fig. 4.2a) and southern (Fig. 4.2c) hemispheres, a clear seasonal pattern emerges, with ECs above the mean by 20-40% early in the season and decreasing approximately linearly to 30-40% below the mean by the end of the season. In contrast, no systematic variation is observed in the savanna biomes in either hemisphere. We tested several other possible sources of the observed seasonal cycle, such as aerosol shielding of NO_2 or FRP, or regional-scale seasonal variation in the NO:NO_2 ratio. Our analysis indicates that the impacts of these effects are too small to explain the observed cycle. This is underscored by the lack of a similar seasonal cycle in observations of savanna fires (Fig. 4.2b,d), as well as a lack of a seasonal cycle in crop and forest fire emissions in the same region (not shown).

Few studies have examined the seasonal variability of EFs, even for a single biome. Korontzi et al. (2003) examined early dry season field measurements of modified combustion efficiency (MCE), a measure of the ratio of flaming to smoldering combustion, and EFs for a few trace gases (not including NO_x) from a series of prescribed fires at a savanna site in southern Africa. They concluded that there were significant differences between early dry season EFs (and MCE) and late dry season EFs (and MCE), due to the decrease in fuel moisture across the season. Yokelson et al. (2011) measured EFs for several species in early dry season fires in the savanna biome in Mexico, and found that EFs for NO_x, as well as several products of incomplete combustion (e.g. CO, CH_4, aerosol, etc.) were much higher than late-season measurements from the African savanna. These two studies hint at the potential for significant seasonal variability in fire emissions even in identical ecosystems. Meyer et al. (2012), on the other hand, compared early- and late-season measurements of emission factors of CH_4 and N_2O in Australian savannas and found no significant seasonal difference. No variation in fuel moisture was observed across the season due to rapid drying out of grass; differences in MCE between fires were attributed to differences in fuel structure. None of the studies included sufficient statistics within a single biome to examine a seasonal cycle in emissions in detail.

We consider possible mechanisms for a seasonal variation in the two quantities thought to be the primary factors affecting variability in NO_x emissions from otherwise similar fires:

1) Higher fuel N content yields greater NO_x emissions per unit of biomass burned (Andreae and Merlet, 2001). Temperatures in most wildfires are not high enough to produce significant amounts of NO_x by oxidation of atmospheric N_2; most NO_x originates from N in the fuel (Andreae and Merlet, 2001). Vegetation in African savannas reallocates N to rhizomes and roots during the dry season, with observations of above-ground plant N twice as high during the wet season as during the dry (fire)

season (e.g. Ratnam et al., 2008). While senesced matter likely makes up the majority of the fuel in any fire, a seasonal variation in the contribution of greener vegetation to the fire fuel might result in seasonal changes in emissions per unit energy or biomass.

2) N in the fuel is thought to be more efficiently converted to NO_x during the higher-temperature flaming combustion (high MCE), whereas smoldering combustion (lower MCE) produces more NH_3, amines, and nitriles (Andreae and Merlet, 2001; Battye and Battye, 2002) although correlations between NO_x emissions per unit mass burned and MCE tend to be poor (Battye and Battye, 2002; Yokelson et al., 2011). There has been little systematic investigation of seasonal variability in MCE, which is heavily impacted by fuel moisture (Korontzi et al., 2003; Meyer et al., 2012; Hoffa et al., 1999). For regions that experience a dry season and wet season, like these African savannas, MCE may be lower in the early dry season, implying a higher contribution of smoldering combustion, and increase as the dry season continues and fuels dry out, leading to a greater contribution of flaming combustion (Korontzi et al., 2003). However, this effect was not observed in Australian savannas by Meyer et al. (2012), who instead found that MCE variation between fires was typically due to fire fuel structure.

While no comprehensive set of MCE or fuel nitrogen observations exists over these large regions, given what we know about the processes that govern NO_x emissions from fires we can speculate about some possible causes of the seasonal variation in ECs we observe. We consider only mechanisms that are specific to woody savanna environments. Differences in fuel N or MCE can both potentially play a role in the mechanisms governing this seasonal variation. For example, if aboveground grass biomass has fully senesced by the start of the fire season but trees are still reallocating N, woody savanna fire fuels might experience a decrease in N content across the season consistent with the observed cycle while little or no cycle is observed in savannas. Increasing leaf litter in woody savannas across the season might also decrease fire MCE and thus impact NO_x emissions in a manner consistent with the observed cycle. In both cases, however, competing effects occur; for example, greener material will contain more N yet burn with a lower MCE, while leaves generally contain more nitrogen than savanna grasses. Regardless, variability due to MCE remains of particular interest since EFs of several other compounds (e.g. CO, CH_4, aerosols, etc.) are highly correlated with MCE (Yokelson et al., 2011) and we recommend further research on seasonal cycles of emissions of these other chemicals, as well as a more detailed mechanistic assessment of the changes observed here.

The results presented here have important implications for numerical representations of fire emissions and tropospheric chemistry. Current models do not include seasonal variability in EFs for any species; furthermore, depending on the timing of the measurements from which the EFs were derived, they may not be representative of the mean or median of emissions over the full fire season. Scaling monthly woody savanna NO_x emissions according to the observed cycle does not change the month of peak NO_x emissions, but it skews the emissions distribution towards the early season. We estimate that incorporation of seasonally varying fire NO_x emissions alters monthly surface ozone by up to 6%—small but significant changes.

4.4 Conclusions

Here we present space-based observations of a seasonal cycle in NO_x emissions per unit mass burned for fires in African woody savannas. The cycle shown here has never before been observed due to the lack of spatiotemporal resolution in previous *in situ* studies. Emission coefficients for woody savannas are 20-50% higher than the seasonal mean emission coefficient at the beginning of the fire season and decrease roughly linearly to 30-50% below the seasonal mean by the end of the season, whereas (non-woody) savanna biomes show no systematic seasonal variation. Possible mechanisms include seasonal variation in fuel nitrogen content or modified combustion efficiency in woody savannas, but further research is recommended to explicitly identify the source of this variability.

4.5 Appendix: uncertainty analysis

We note that sources of uncertainty in the derivation of an EC are described in detail in Mebust et al. (2011). The total uncertainty we derive is based on the measurement uncertainties e.g. the uncertainty associated with the retrieved OMI NO_2 column densities; the methodological uncertainties in deriving emissions for individual fires; and the uncertainty in the derivation of the ECs.

4.5.1 Uncertainties in measurements

Tropospheric NO_2 column densities derived from OMI are subject to primary errors due to measurement (i.e. the uncertainty of the fit of measured radiances to reference spectra) as well as derived errors from the retrieval process used to convert the spectra to columns (Boersma et al., 2004). Errors can result from the subtraction of the stratospheric NO_2 column from the total column, and from parameters (cloud fraction, cloud pressure level, surface albedo and NO_2 profile shape) used to calculate the air mass factor, which is used to convert the slant column density to a vertical column density. The presence of aerosols can also induce errors in the retrieval, although in the case of OMI, this is at least partially corrected for by the cloud retrieval algorithm which is somewhat sensitive to the presence of aerosols and interprets them as clouds (Boersma et al., 2004; Boersma et al., 2011). These sources of error and their estimation are described in detail elsewhere (Boersma et al., 2004; Boersma et al., 2007; Boersma et al., 2011). An estimate of the standard error is reported with OMI tropospheric NO_2 columns, calculated separately for each pixel. For the observations used here, the median percent standard error is 54.7%; approximately 93% of observations reported a standard error of less than 100% of the measured value. These uncertainties are largely systematic, as shown for example in Russell et al. (2012). However, we note that in the case of fires, a large systematic bias, not accounted for by the estimated standard error, may arise due to inaccuracies associated with the assumed NO_2 profile shape and with the presence of aerosols. Evidence for this is presented by Mebust et al. (2011) who suggest that the OMI NO_2 Standard Product retrieval underestimates NO_2 columns over fires by as much as a factor of 2. A similar bias should affect the DOMINO retrieval used in this paper as it similarly does not use any special treatment for fire containing pixels. As a result, an absolute measurement of fire ECs is likely to be biased low by a factor of ~2. However, Mebust et al. (2011) found that relative differences in NO_x ECs measured by OMI between different fuel types reproduced differences in measured EFs for the same fuel types; this suggests that any systematic bias in OMI NO_2 retrievals is proportional across a large column density

range, implying that relative differences between ECs (like those presented here) is not impacted by the biases.

Estimations of FRP from MODIS are based on an empirical relationship with radiance in the 4 μm band; this relationship was established by a fit using several theoretical fires containing a mix of flaming and smoldering combustion at different temperatures. The average standard error between this empirical relationship and the theoretical fires is ±16% (Kaufman et al., 1998). However, validation of MODIS FRP has been extremely limited. A comparison with the Bi-spectral InfraRed Detection satellite instrument indicated that MODIS FRP was within 15% of BIRD FRP for several fires but that in a few cases MODIS FRP underestimated BIRD FRP by up to 46% (Wooster et al., 2003). This is likely because the MODIS detection algorithm may miss some fire pixels that are less intensely radiating. MODIS FRP may be further underestimated as the detection algorithm may not identify fires (or energy) obscured by clouds, smoke, or canopy cover. Fires that are entirely obscured are not included in the analysis, i.e. the effect only matters to the extent that small parts of larger fires are obscured. Regardless, while a bias in MODIS FRP may affect the absolute value of an EC or EF, it is unlikely to impact the relative values we express here, for the same reasons given for a bias in OMI NO_2 columns. We also note that fire radiative power as measured by the satellite is not expected to be correlated with the extent of flaming combustion or modified combustion efficiency (MCE), which might induce some non-linearity in the relationship between NO_x emission rate and fire radiative power. While higher intensity fires are likely to have a higher MCE and thus may have a higher NO_x emission rate, MODIS pixels do not contain an estimate of fire size; thus, measured fire radiative power is equally indicative of a small, high-intensity fire and a large, low-intensity fire.

Estimates of uncertainty in CFSR wind speed and direction are not available as part of the data product. However, there are uncertainties associated both with the model and assimilated data, as well as with scaling the hourly-resolved data at 0.5°×0.5° spatial resolution down to the time and location of each fire. We consider systematic errors here and discuss random ones below. The mean impact of wind speeds on this analysis was investigated thoroughly and is described in Mebust et al. (2011); there we found that the choice of dataset and of wind pressure level close to 1km resulted in small differences in calculated ECs (<15%). A similar check on the results in this manuscript produced similar results. The choice of wind pressure level near 1km for all fires may, however, bias ECs systematically low, as some large fires can inject emissions much higher into the atmosphere; however, the majority of fire emissions are typically in the boundary layer (Martin et al., 2010).

4.5.2 Uncertainties in individual fire emissions

Mebust et al. (2011) address uncertainty in individual fire emissions in detail, including assumptions that fire conditions are constant over the period of measurement, that the NO_2/NO ratio does not vary greatly between fires, that NO_x loss can be approximated as a first-order exponential loss, that the lifetime of NO_x is similar across most fires, and that ECs do not vary diurnally—or rather that ECs are not particularly higher or lower as a result of being measured at the OMI/MODIS overpass time. We note that for these assumptions to bias the relative relationships demonstrated in this work, the accuracy of these assumptions would have to be seasonally varying. We have no evidence for such an effect or a hypothesis for one at this time.

Wind speed or direction is a possible source of systematic error that could potentially influence the observed seasonal cycle, manifested as a seasonal cycle in wind speed or direction in the CFSR data. However, polar histograms of wind direction show that the distribution of wind direction within each category is nearly identical across the fire season. Monthly means of wind speeds used in this analysis for each category also show no relationship with the monthly measured ECs, as regressions of mean wind speed and measured EC in each category have very low R^2 values and extremely different slopes (varying from negative to positive).

The method of estimating background could also potentially impact the seasonal cycle. Background columns are estimated using observations in the same location as the fire on 60 days before and 60 days after the fire. At least 10 observations are required and the column is estimated as the average of all observations. This method was selected over a more traditional approach (i.e. using observations directly upwind of the fire) because of the uncertainties in wind direction and the size of the pixels which both make it difficult to be sure that the column "upwind" of the fire according to the data is indeed clean. Another strategy could be to select the minimum column density in the pixels surrounding the fire as the background column; however, our experience showed that this strategy resulted in a low bias to the background. Because the method used here calculates the background as an average over roughly a 4-month period, it is plausible that the method decreases or removes natural seasonal variation in background column and thus potentially biases the data. On the other hand, the background column tends to be only a small percentage of the total column measured over the fire, so small changes to the background column are unlikely to significantly impact the estimated emissions. We compared the original analysis results to an analysis using backgrounds of 30 days before and after the fire (corresponding to an average calculated over roughly 2 months). Using a 2-month average resulted in a 50% decrease in the number of observations because they did not make the minimum 10 observation cutoff. When this cutoff was decreased to 5 observations, the collection of data was still 25% smaller than when using a 4-month average. The smaller number of observations resulted in slightly higher reported uncertainties for most months but no change in the inferred seasonal cycle.

4.5.3 The bootstrap method and associated uncertainties

Given the large data set and the predominance of systematic errors (some of which are poorly characterized), we compare relative values rather than absolute ones. Here we describe the statistics of our observations and results and assess uncertainty in the context of the bootstrap method.

As described in the text, ECs are calculated using observations from each category and month separately, and each EC must be derived from a minimum of 150 observations. ECs for months near the beginning and end of the season are calculated from a smaller number of observations (a few hundred) while sample sizes for the peak of the season are closer to 2,000-3,000. Because of the high variability in emissions from fire to fire coupled with the sources of random error (e.g. winds), correlation coefficients from a linear regression are low to moderate (R^2 ranging from 0.21 – 0.66 and typically ~0.4) indicating that a linear relationship only partially describes the observed variability. However, the nonparametric bootstrap resampling method used to calculate the ECs and the large sample size ensures that we capture the mean behavior. The purpose of the bootstrap is to generate an estimate of the mean and standard

deviation that are independent of the assumptions required by most linear regression strategies, such as normality of the distribution, homoscedasticity and that the x values are free of error. These assumptions, when not met, generally lead to underestimation of the error associated with the estimated slope, an effect especially prevalent for large datasets. The bootstrap, in this case, can provide a more robust estimate of the uncertainty, as well as reducing the impact of outliers on the calculated slope.

Figure 4.3 demonstrates several of these issues. Here we have plotted mass emission rate vs. fire radiative power measured in woody savanna in northern Africa over the months of November (early season, A1a) and April (late season, A1b). While there is some scatter and the R^2 values are low, the difference in slope between the two months is still visible. Also plotted are the bootstrap fit and 95% CI. A Welch's *t*-test between the slopes for the two months indicates that they are significantly different ($p<0.000001$), and this is true whether the OLS or bootstrap slopes and standard errors are used. Thus the difference between the early season and late season ECs is, in fact, highly statistically significant. This is similarly true for the seasonal change observed in woody savanna in northern Africa.

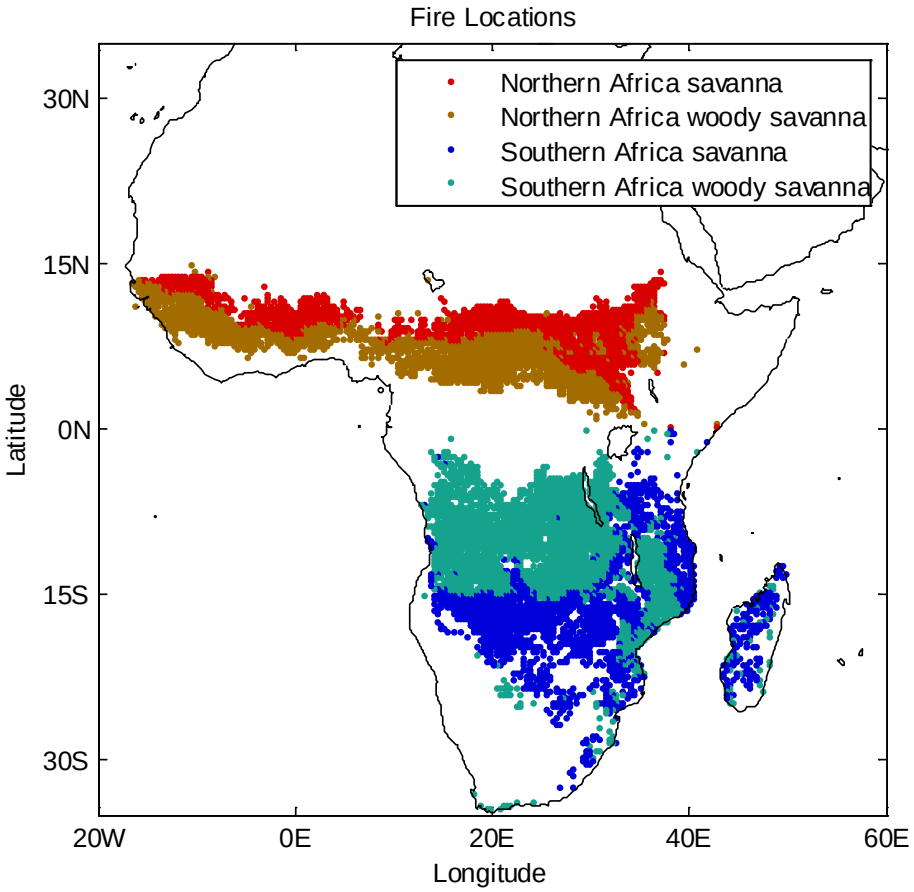

Figure 4.1. A map of the dominant fire type (savanna vs. woody savanna) at 0.33° × 0.33° spatial resolution. Fires in northern and southern hemispheres are indicated separately.

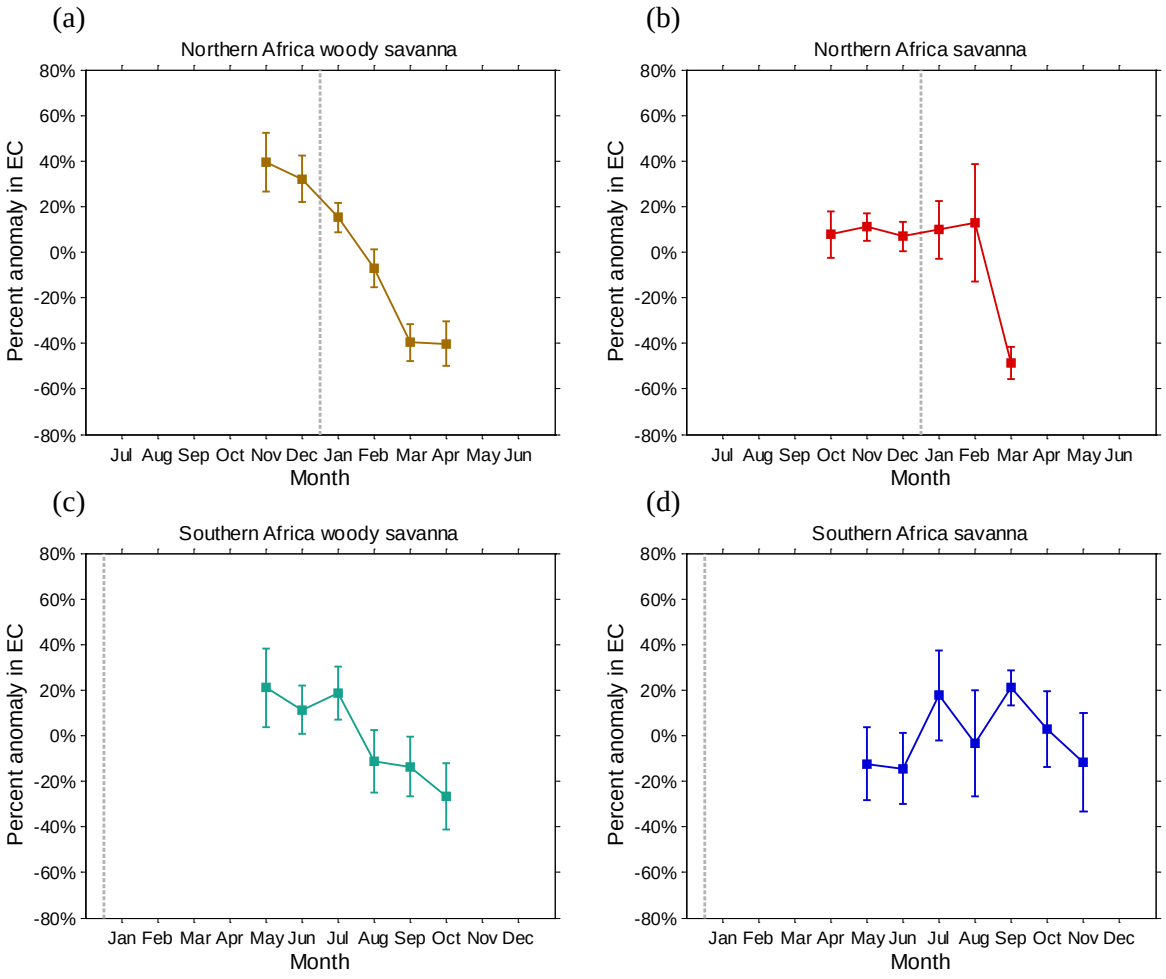

Figure 4.2. Monthly anomaly in EC as a percentage of the mean for north African woody savanna (a) and savanna (b), and south African woody savanna (c) and savanna (d). Months are indicated on the x-axis and begin in July for northern Africa (a, b) and January for southern Africa (c, d). January 1st is indicated by the grey vertical dotted line. Error bars indicate one standard deviation of the value.

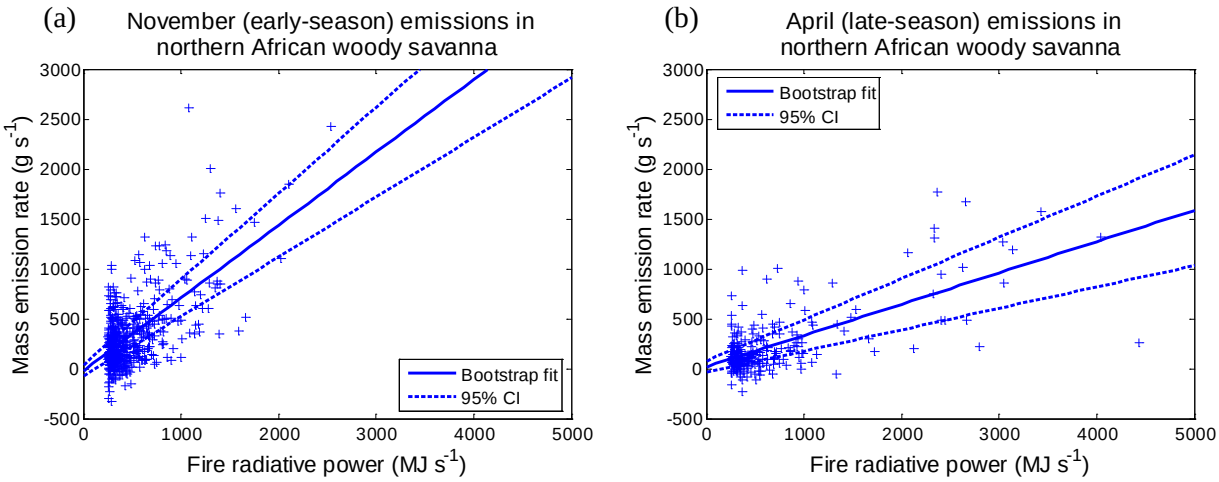

Figure 4.3. Scatter plots of fire radiative power vs. mass emission rate of NO_2 for woody savannas in northern Africa, in the early season (November, a) and late season (April, b). Solid lines show the best fit, calculated using nonparametric bootstrap resampling, and the dotted lines show the 95% confidence interval.

Chapter 5

Observations of variability in wildfire NO_x emission coefficients: seasonal variability and wind speed dependence

5.1 Introduction

Combustion of biomass, like other forms of incomplete combustion, produces substantial quantities of CO, CH_4, aerosols, volatile and semi-volatile organics, and a variety of nitrogen (N) containing species including nitrogen oxides ($NO_x \equiv NO + NO_2$) as well as NH_3 and HCN (Andreae and Merlet, 2001). These species go on to play pivotal roles in the local, regional and global atmosphere, impacting local air quality and influencing radiative forcing (Fiore et al., 2012). To fully understand the net impacts of these emissions and assess how they will respond to geophysical forcings, it is critical that the processes governing the emissions are elucidated.

Many recent efforts to quantitatively describe emissions have aimed to parameterize emissions as a function of fire radiative energy (FRE), yielding a value known as an emission coefficient or EC in g of pollutant emitted per MJ (Ichoku and Kaufman, 2005; Freeborn et al., 2008; Jordan et al., 2008; Vermote et al., 2009; Mebust et al., 2011; Mebust and Cohen, 2013). Estimates of FRE and fire radiative power (FRP or rate of FRE release) are available via satellite observations, enabling high temporal resolution modeling of fire emissions as compared to traditional mass-based methods. ECs are typically derived for specific fuel types but are otherwise considered to be unvarying; however, observations suggest that at the individual fire scale, ECs (and related emission factors or EFs expressing the mass of pollutant emission per unit mass burned) are highly variable from fire to fire (Andreae and Merlet, 2001; Akagi et al., 2011; Mebust and Cohen, submitted 2013). Different combustion stages and/or temperatures can result in a different degree of oxidation of organic material; emissions of highly oxidized species like CO_2 and NO_x are associated with flaming combustion, while less-oxidized species like CO, CH_4, organic molecules, etc. are associated with smoldering combustion (Andreae and Merlet, 2001). Emissions of NO_x also depend on the amount of available N as they are produced via combustion of N-containing fuel (Andreae and Merlet, 2001).

Assessments of fire emissions have, for the most part, neglected this inherent natural variability in ECs and EFs between individual fires in an attempt to characterize mean behavior (e.g. van der Werf et al., 2010). To achieve this, parameters are derived from observations of fires that are assumed to be typical of a particular biome and then applied uniformly to all fires within that biome, regardless of local fire conditions (Andreae and Merlet, 2001; Hoelzemann et al., 2004; van der Werf et al., 2010; Akagi et al., 2011). The assumption of an unvarying EC or EF is supported neither by theory nor by observation, but has been necessary because in situ

observations have lacked the temporal and spatial coverage to provide information on systematic variation in fire emissions, while theoretical variability is neither validated nor quantified.

Satellite measurements of fire emissions offer the opportunity to fill some of the gaps in our knowledge of spatial and temporal variability of fire emissions. Observations of FRP and associated pollutants can be used to derive ECs directly for individual fires, and the greatly expanded spatiotemporal coverage (where measurements are made throughout the fire season and across the globe) provides sufficient statistics to distinguish spatial and temporal differences in emissions that have escaped characterization by in situ measurements (Mebust and Cohen, 2013). By examining differences between ECs at different spatial and/or temporal resolution, or as a function of biogeophysical or meteorological characteristics (e.g. wind speed), we can identify some sources of the observed variability. Conveniently, conclusions about variability in ECs are also generally extendable to EFs because laboratory studies have shown the two values are proportional to one another (Wooster et al., 2005; Freeborn et al., 2008), so understanding variability in ECs can also result in improvement of a wide variety of models that do not yet depend directly on ECs.

In Chapter 3, I used satellite observations to examine variability in mean NO_x ECs for biomes and spatial variability within each biome. Here I focus instead on temporal variability and potential biogeophysical drivers of variability in emissions. Previous studies that have attempted to examine seasonal variability in EFs have relied on a small number of measured fires or inconsistent sampling strategies, e.g. comparing early-season measurements from one ecoregion to late-season measurements in another (Korontzi et al., 2003; Yokelson et al., 2011; Meyer et al., 2012). In Chapter 4 I demonstrated that there exists clear seasonally varying behavior in ECs for woody savannas in Africa, using measurements that offer continuous coverage throughout the fire season (Mebust and Cohen, 2013). Systematic differences in EFs as a function of local meteorological or biogeophysical properties e.g. precipitation, temperature, dry season length have been studied by van Leeuwen and van der Werf (2011), who used EFs from a wide range of previous studies to show that EFs for CO_2, CO and CH_4 were each correlated to some (statistically significant) degree with some of these likely drivers of a mechanism affecting fire behavior. A subsequent study found that the inclusion of a varying EF scheme in a global model resulted in significant differences in emissions as compared to the static EF scheme (van Leeuwen et al., 2013). These results emphasize the importance of identifying and quantifying drivers of EC and EF variability.

In this chapter, I examine seasonal variability in savanna ecoregions across the globe and compare to the observed seasonal patterns in Africa. I also explore correlations between ECs and wind speed at the biome scale.

5.2 Methods

The data and methods used here have been described previously (Chapter 3). Briefly, I combine observations of tropospheric NO_2 vertical column densities from the Ozone Monitoring Instrument (OMI) Standard Product (OMNO2, Level 2, Version 2.1, Collection 3; Bucsela et al., 2013), FRP from the Aqua Moderate Resolution Imaging Spectroradiometer (MODIS) Thermal Anomalies product (MYD14, Level 2, Collection 5; Kaufman et al., 1998; Justice et al., 2002; Giglio et al., 2003), and wind vectors at 850 hPa from the Climate Forecast System Reanalysis/version 2 (CFSR/CFSv2; Saha et al., 2010; Saha et al., submitted 2013). I include all

observations from the period of 2005-2011, subject to quality control as described in Mebust and Cohen (submitted 2013). I aggregate coincident OMI and MODIS pixels to identify individual fires and include observed fires with total FRP > 250 MW. I use OMI NO_2 column densities in conjunction with wind observations and fire pixel locations to determine a "mass emission rate" (MER in g s^{-1}) of NO_2 for each fire, and calculate ECs as the slope of a regression between FRP and MER (g MJ^{-1}). ECs and corresponding standard errors are derived via nonparametric bootstrap resampling with replacement.

I include observations of land cover from the MODIS Land Cover product (MCD12Q1, Level 3, Collection 5.1; Friedl et al., 2010), as well as Köppen-Geiger climate classification data at 0.5°×0.5° (Kottek et al., 2006), to differentiate between biomes and within biomes (e.g. savannas vs. woody savannas). To further divide biomes into ecoregions, I perform a spatial aggregation, in which observations of forest, grass, shrub or agricultural fires are grouped according to proximity (within 100 km for grasses). For the results presented here, only grass ecoregions are used. Fires are considered to be "grass" if at least 75% of FRP comes from fire pixels determined to be "grassland", "savanna" or "woody savanna" by the MODIS Land Cover product. As a result, ECs can also be determined for sub-categories of grasses (grasslands, savannas, and woody savannas). In all work here, ECs are only presented when based on a minimum of 100 observations and the standard error of the EC is less than 75%.

5.3 Results and discussion

5.3.1 Seasonal variability in savanna biomes

In Chapter 4, I demonstrated that ECs for woody savanna fires in Africa decrease throughout the fire season, while ECs for savanna fires have no distinct seasonal pattern. Here I examine seasonal variations in ECs in savannas across the globe. I separately assess seasonal behavior in ecoregions as defined in Mebust and Cohen (submitted 2013) with substantial sampling of savanna and/or woody savanna fires. A map of grassland ecoregions is shown in Fig. 5.1; I find that Regions M, N, O, and Q sample woody savanna fires at a sufficiently high rate such that it is possible to examine seasonal variability in ECs. In all figures showing seasonally resolved ECs, I show the number of observations for each month as light grey bars; this also provides an approximate sense of the fire season. Note that the sample size scales vary between the different figure panels.

In tropical ecoregions, ECs in woody savanna or mixed savanna/woody savanna biomes decrease systematically throughout the fire season. This behavior appears to be due almost exclusively to woody savannas. Figure 5.2 shows the seasonal behavior in these tropical ecoregions (Regions M, N, O, and Q): across all ecoregions there is a distinct decreasing pattern in ECs across the fire season. Additionally, when ECs in these mixed savanna/woody savanna regions are calculated separately for each of the two biomes, strong seasonal decreases are apparent for woody savanna ECs while little to no decrease is observed in ECs for savannas (Fig. 5.3). This result is consistent with the previous observation of seasonal behavior in woody savannas and not in savannas in Africa (Mebust and Cohen, 2013).

I suggest that this biome-specific process is a result of long term ecological adaptation to frequent fire exposure. The ecoregions in which the seasonal pattern is observed generally contain large numbers of observations, sugggesting that fire occurs at regular intervals (i.e. every

few years) in areas within these ecoregions and it would be appropriate to consider them fire-adapted. In contrast, it is not possible to fully characterize seasonal behavior in ECs in temperate and polar woody savanna regions, but the limited evidence suggests that ECs in those regions are consistent or increasing throughout the season. Such regions contain substantially fewer observations of fires as compared to the tropical savanna regions, suggesting that they may not be adapted to frequent fire. While there is no direct evidence that fire adaptation accounts for this pattern, I suggest it as a possible and plausible explanation.

5.3.2 Wind speed dependence of ECs

I evaluate the relationship with wind speed by binning observations into 2 m s^{-1} bins and measuring an EC for each bin. The results for such an analysis on the biome scale are shown in Fig. 5.4. In most biomes, there appears to be a relationship between wind speed and ECs, with higher wind speeds correlated with increasing ECs. The relationship is approximately linear and is stronger in some biomes than in others. This result is consistent with our previous knowledge about the effects of wind on fires. It is commonly known that high winds can impact fire intensity, rate of spread, etc. High wind speeds might be correlated with increased MCE which could result in increased NO_x emissions. It has also been previously proposed that high wind speeds could also induce green, live vegetation to burn under flaming conditions, as opposed to the smoldering combustion normally associated with live vegetation (Yokelson et al., 2011); since green (live) vegetation generally contains more N than senesced (dead) vegetation (Ratnam et al., 2008), this could also result in increased NO_x emissions in high wind conditions.

I do not show individual ecoregion analyses here, because on the ecoregion scale this relationship exhibits greater variability. In some ecoregions there is a strong correlation; in others ECs appear relatively constant with wind speed; and in still others ECs peak at moderate wind speed and are smaller at low and high wind speeds. It is possible that different mechanisms influence how wind speed impacts emissions from ecoregion to ecoregion. Reduced statistics due to smaller sample sizes can also affect the reliability of any conclusions for individual ecoregions.

I note that the observed correlations with wind speed must be viewed with caution, as wind speeds are directly used in the process of deriving ECs. I have investigated the possibility that the correlation between wind speed and ECs is an artifact of the analysis, but I can find no evidence that it is; on the other hand, it is difficult to rule that effect out completely. Other processes not related to emissions may also play a role. For example, wind speeds will likely affect the rate of plume mixing with background ozone, and thus might impact our measured ECs by affecting the amount of NO_x present as NO_2 or by affecting aerosol loading which can influence the NO_2 retrieval. In low-wind scenarios, mixing with background ozone will be slow, and thus a greater percentage of NO_x might be present as NO, meaning that our analysis may underestimate the EC under these conditions. Correlations between wind speed and boundary layer height theoretically may also play a role. Higher wind speeds could indicate a higher boundary layer height, increasing the signal of NO_2 as measured by the satellite due to increased sensitivity at higher altitudes. This would not be accounted for by the satellite retrieval which assumes an invariant vertical profile, resulting in a high bias.

5.4 Conclusions

I present observations of systematic variability in NO_x ECs from fires including seasonal variability in ECs in savanna and woody savanna ecoregions and correlations with wind speed. I find that ECs for five separate tropical woody savannas exhibit clear linear decreasing behavior across the season, while savannas in four of the same regions do not exhibit this same behavior and neither do more temperate woody savannas. I suggest that this is the result of biogeophysical fire adaptation processes in woody savannas. I also find that for most biomes, increasing wind speeds are correlated with increasing ECs, consistent with processes suggested by a previous analysis (Yokelson et al., 2011).

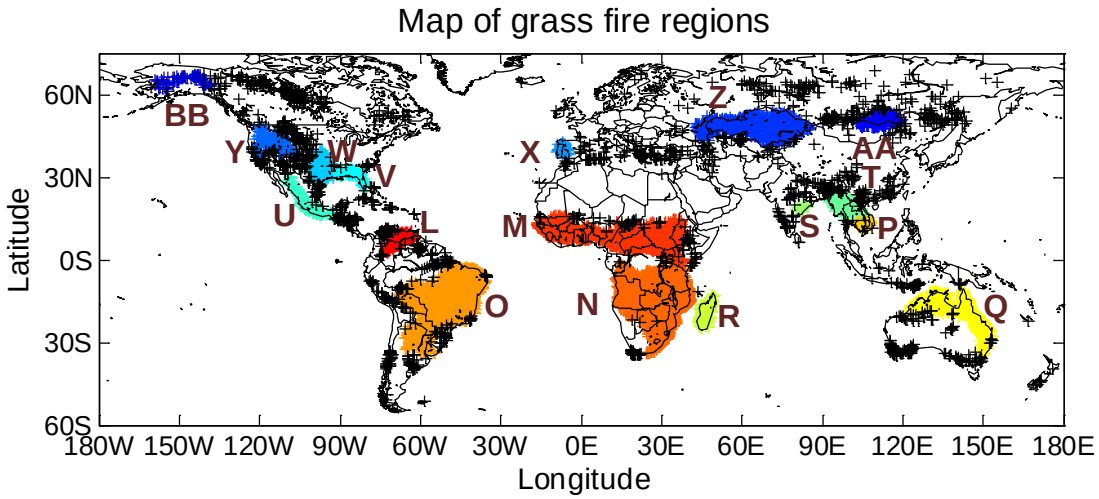

Figure 5.1. A map of grass fire ecoregions as developed in Chapter 3.

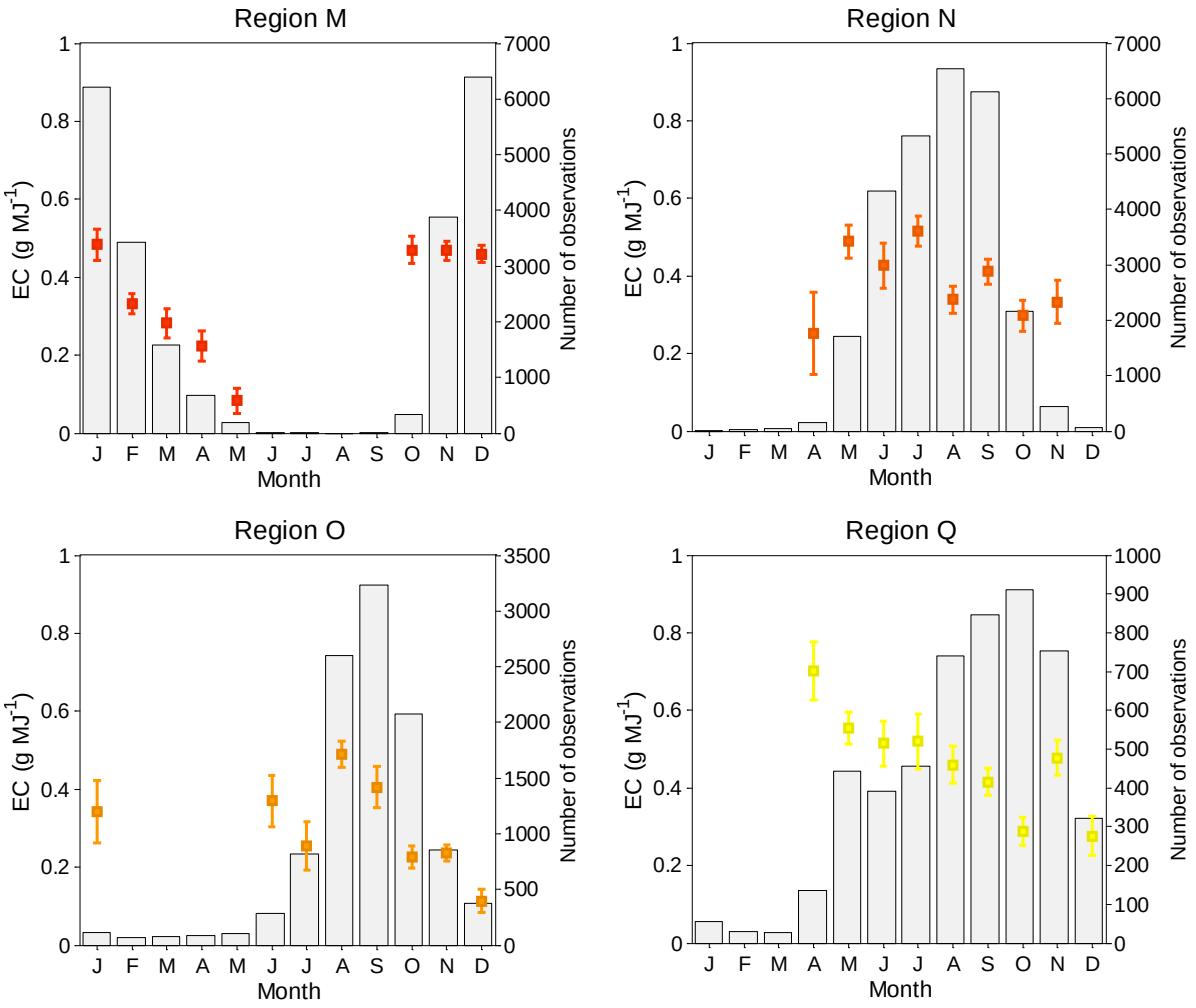

Figure 5.2. Seasonal patterns for ECs in four ecoregions that contain a mix of savanna and woody savanna fires.

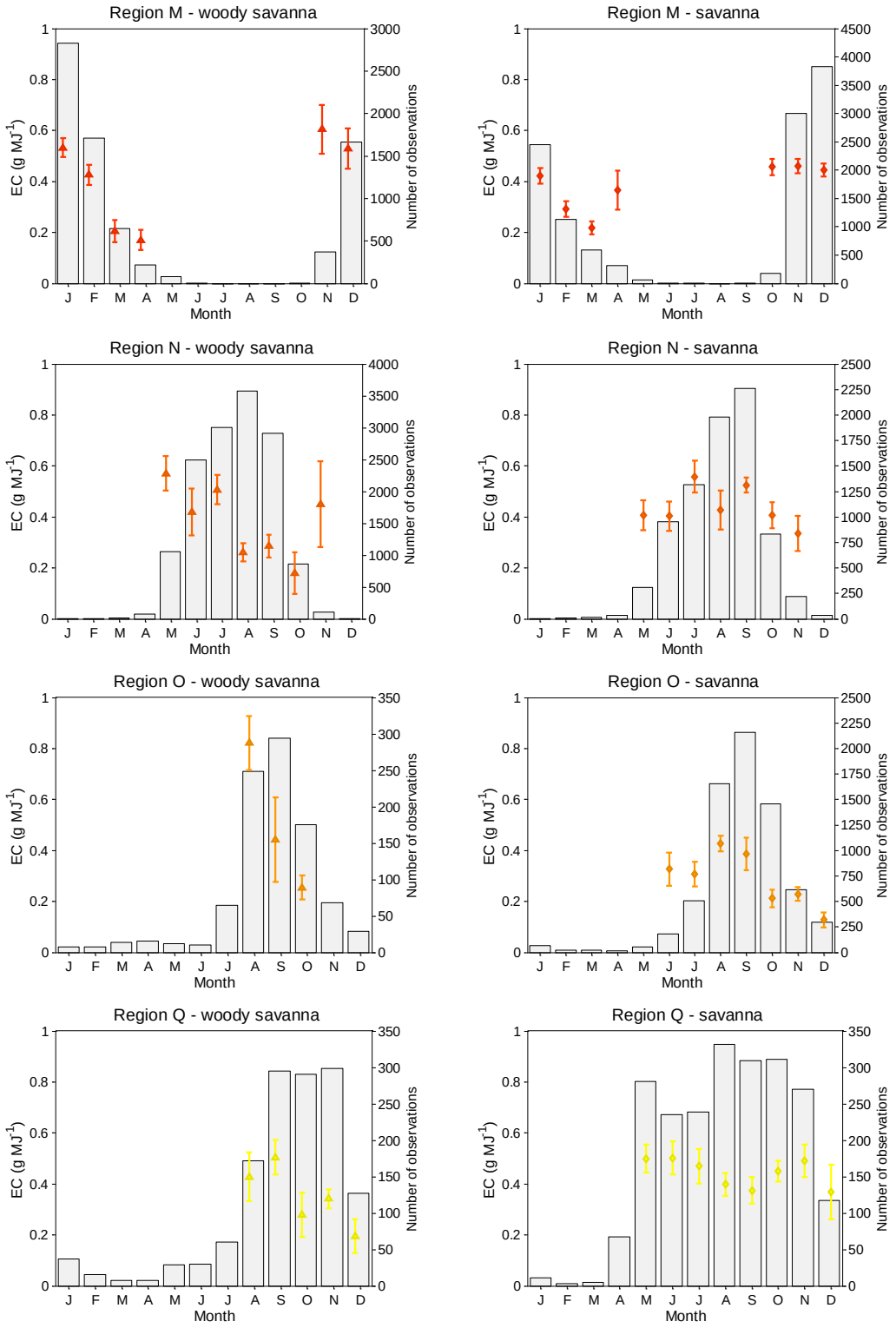

Figure 5.3. Seasonally resolved ECs from four ecoregions (Regions M, N, O and Q) separately calculated for savanna and for woody savanna fires. Woody savanna ECs exhibit a clear decreasing pattern throughout the season, while savanna fires have little or no seasonal pattern.

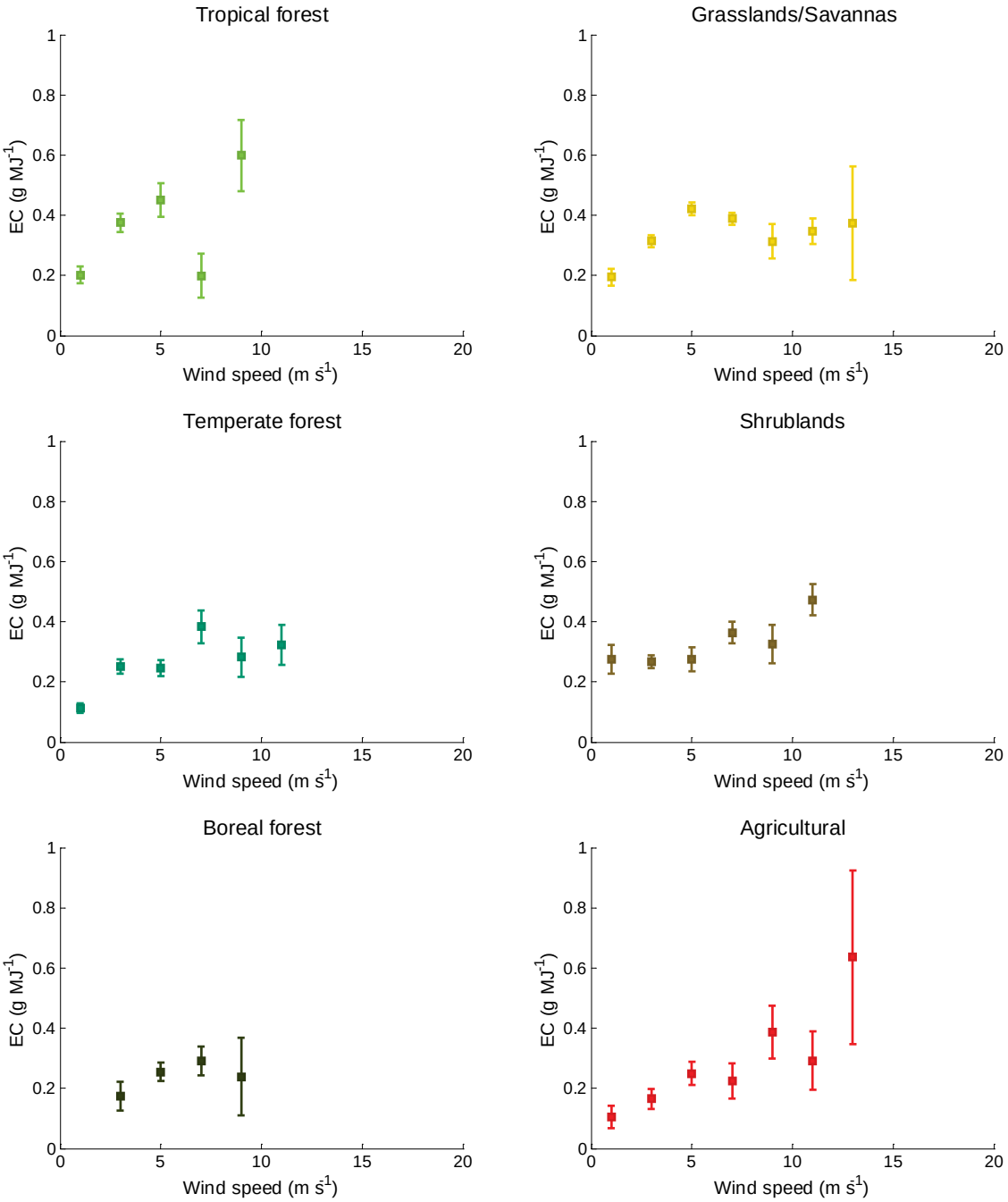

Figure 5.4. ECs as a function of wind speed for six primary biome types (tropical, temperate, and boreal forests, grasslands, shrublands, and agricultural fires).

Chapter 6

Future directions for wildfire NO_x emission research

6.1 Introduction

In this dissertation, I have presented a new strategy for analyzing variability in wildfire NO_x emissions using space-based observations. This strategy has enabled the study of systematic variability in NO_x ECs at a scale never even approached in previous in situ research. As a result, I have been able to produce the first large-scale within-biome comparisons in emission parameters, discovering important spatial differences (Chapter 3); I also presented the first complete seasonally resolved emission parameters for savannas and woody savannas, providing conclusive evidence that emissions from some biomes vary seasonally in a way that has never been possible to observe through laboratory or in situ measurements (Chapters 4 and 5). Despite these important contributions, however, there remains significant untapped power in applying these observations to explore systematic variability in fire NO_x emissions. Here I present some ideas for future work in which the strategy presented here can be used to provide a wealth of process-oriented information regarding variability in emissions.

6.2 Future directions

6.2.1 Seasonal variability

Building on the observed seasonally dependent behavior of ECs in tropical woody savanna environments (Chapters 4 and 5; Mebust and Cohen, 2013), I suggest that future efforts should attempt to provide seasonally resolved measurements of ECs for other biomes. I have made some preliminary observations of seasonal behavior in non-grassland biomes. Results suggest that there are two kinds of patterns observed in forested ecoregions, while shrubland and agricultural ecoregions behave in a less consistent manner, with seasonal patterns differing substantially between ecoregions of the same biome. Some of the difficulties in evaluating seasonal behavior in these biomes are due to the much smaller sample size per ecoregion relative to the savanna biomes. In cases where the sample size is large, typically there is some sort of visible seasonal pattern (see e.g. Fig. 6.1), but in many cases there are insufficient data to provide rigorous seasonally-resolved ECs across the full fire season. One way to overcome this would be to normalize observations in each ecoregion to the peak month of the fire season and then combine all observations from similar ecoregions. This would increase the sample size and allow characterization of ECs throughout the season.

6.2.2 Interannual variability

The extent to which emission parameters vary between different years has not been explored in any previous analysis. Such an analysis could prove very useful in identifying driving processes when combined with observations about each year's fire season (length, drought

record, biomass loading, etc.). The multiyear satellite record can prove very useful in such an analysis. Initial observations suggest that interannual differences in ECs can be observed. In most cases where ECs were derived for 6 or more years, the difference between the minimum and maximum yearly ECs in a single ecoregion is approximately a factor of 2, with these ECs differing from each other by more than one standard deviation. This suggests that there is information that could be extracted from annually resolved ECs, especially in combination with observations about the fire season during these years. For example, I separately determine annually resolved ECs for tropical and temperate forests in two mixed forest ecoregions (Fig. 6.2). ECs for tropical forest fires in Region F are consistently higher than ECs for temperate forest fires, and this difference is approximately the same regardless of year—in other words, the ECs vary together, presumably with some sort of large-scale biogeophysical process that affects both biomes. Tropical forest fires in Region E, on the other hand, are not consistently higher or lower than temperate forest fires, and the interannual variations in the two fuel types are not correlated (either positively or negatively). That suggests that in Region E, factors driving interannual variability in these two biomes are specific to each biome.

6.2.3 Observations of local vegetation and meteorology

Modified combustion efficiency (MCE) and fuel nitrogen (N) are both suggested to correlate with NO_x emissions (e.g. Andreae and Merlet, 2001; Battye and Battye, 2002). Since MCE can be impacted by fuel thickness/density (e.g. logs burn with lower MCE than leaves), fuel moisture, and other properties; and fuel N is variable both within the plant (e.g., logs vs. leaves) and as a function of plant conditions (e.g., senesced or dry, dead plant material will generally contain less nitrogen); a logical plan of action would be to test ECs for correlation with meteorological and/or vegetation observations. Some potentially relevant observations include precipitation records, vegetation indices (e.g., EVI, NDVI), surface temperature, relative humidity, soil moisture, soil N, or percent tree cover. Many of these observations are available at a global scale either as satellite observations or assimilated observations (e.g., from the CFSR). Preliminary tests with precipitation and vegetation indices suggest that biome-scale ECs vary as a function of these factors, but the relationships tend to be complicated (e.g., not necessarily linear) and different behavior is observed with different months (e.g., ECs might be positively correlated with precipitation from 3 months previous to the fire and negatively correlated with precipitation from 6 months previous).

6.2.4 The next generation of satellite instruments

Future efforts can make use of upcoming launches of new space-based observing instruments, including those launched on polar-orbiting satellites with higher spatial resolution than OMI (e.g., TROPOMI) and instruments deployed on geostationary satellites (e.g., TEMPO). Improvements in the technology on which the satellite observations are based can help reduce certain sources of uncertainty and can also prove better at isolating emissions from proximate fires and allow characterization of how the NO_2 column changes downwind of the fire source. Geostationary satellite observations would also allow diurnal resolution of emission parameters, which is not possible with polar orbiting satellite observations given that observations are made at the same local time globally.

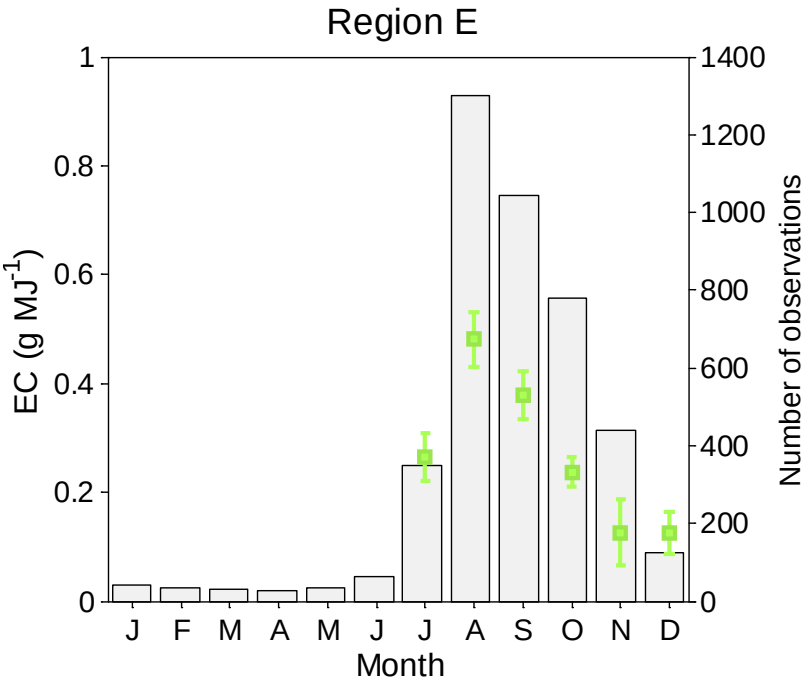

Figure 6.1. Seasonally resolved ECs for Region E, a mixed tropical-temperate forest region in South America.

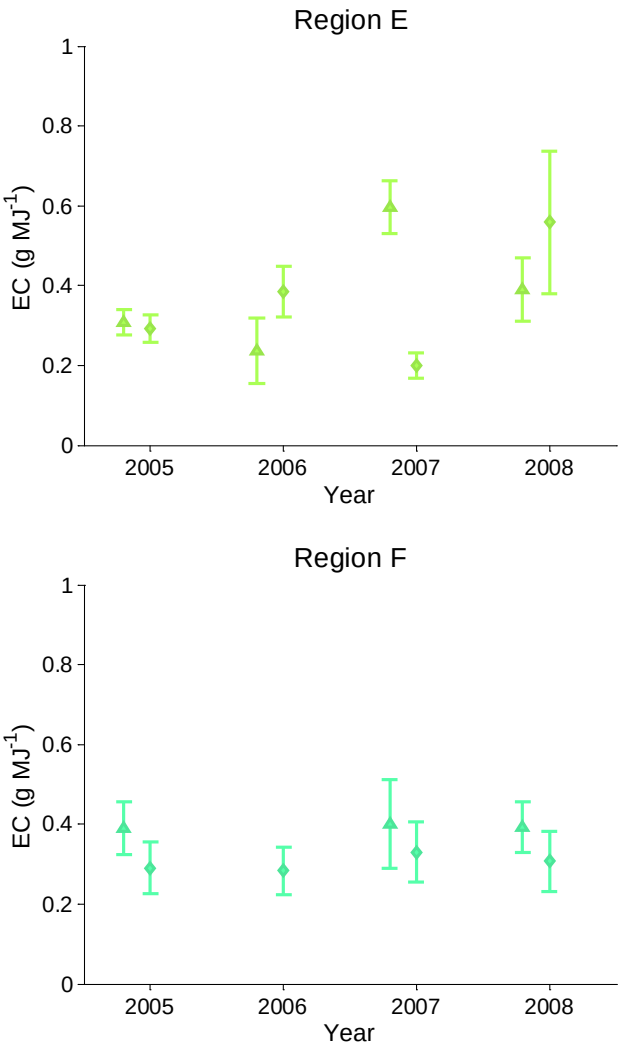

Figure 6.2. ECs calculated by year (2005-2008) and biome for Regions E and F, both mixed tropical-temperate forests. Triangles indicate ECs for tropical forests, while diamonds indicate ECs for temperate forests. In Region E, interannual variability in ECs varies significantly for the two biomes, while in Region F the interannual variability is small and is similar between the two biomes.

References

Akagi, S. K., Yokelson, R. J., Wiedinmyer, C., Alvarado, M. J., Reid, J. S., Karl, T., Crounse, J. D., and Wennberg, P. O.: Emission factors for open and domestic biomass burning for use in atmospheric models, Atmos. Chem. Phys., 11, 4039-4072, 2011.

Akagi, S. K., Yokelson, R. J., Burling, I. R., Meinardi, S., Simpson, I., Blake, D. R., McMeeking, G. R., Sullivan, A., Lee, T., Kreidenweis, S., Urbanski, S., Reardon, J., Griffith, D. W. T., Johnson, T. J., and Weise, D. R.: Measurements of reactive trace gases and variable O_3 formation rates in some South Carolina biomass burning plumes, Atmos. Chem. Phys., 13, 1141-1165, 2013.

Alvarado, M. J. and Prinn, R. G.: Formation of ozone and growth of aerosols in young smoke plumes from biomass burning: 1. Lagrangian parcel studies, J. Geophys. Res., 114, D09306, doi:10.1029/2008JD011144, 2009.

Alvarado, M. J., Logan, J. A., Mao, J., Apel, E., Riemer, D., Blake, D., Cohen, R. C., Min, K.-E., Perring, A. E., Browne, E. C., Wooldridge, P. J., Diskin, G. S., Sachse, G. W., Fuelberg, H., Sessions,W. R., Harrigan, D. L., Huey, G., Liao, J., Case-Hanks, A., Jimenez, J. L., Cubison, M. J., Vay, S. A., Weinheimer, A. J., Knapp, D. J., Montzka, D. D., Flocke, F. M., Pollack, I. B., Wennberg, P. O., Kurten, A., Crounse, J., Clair, J. M. St., Wisthaler, A., Mikoviny, T., Yantosca, R. M., Carouge, C. C., and Le Sager, P.: Nitrogen oxides and PAN in plumes from boreal fires during ARCTAS-B and their impact on ozone: an integrated analysis of aircraft and satellite observations, Atmos. Chem. Phys., 10, 9739–9760, doi:10.5194/acp-10-9739-2010, 2010.

Andreae, M. O. and Merlet, P.: Emission of trace gases and aerosols from biomass burning, Global Biogeochem. Cy., 15, 955–966, 2001.

Battye, W. and Battye, R.: Development of emissions inventory methods for wildland fire, US Environmental Protection Agency, Research Triangle Park, NC, USA, Contract 68-D-98-046, 2002.

Boersma, K. F., Bucsela, E., Brinksma, E., and Gleason, J. F.: NO_2, in: OMI Algorithm Theoretical Basis Document, Volume IV: OMI Trace Gas Algorithms, 2 ed., edited by: Chance, K., Smithsonian Astrophysical Observatory, Cambridge, MA, 13-36, 2002.

Boersma, K. F., Eskes, H. J., and Brinksma, E. J.: Error analysis for tropospheric NO_2 retrieval from space, J. Geophys. Res.-Atmos., 109, D04311, doi:10.1029/2003JD003962, 2004.

Boersma, K. F., Eskes, H. J., Veefkind, J. P., Brinksma, E. J., van der A, R. J., Sneep, M., van den Oord, G. H. J., Levelt, P. F., Stammes, P., Gleason, J. F., and Bucsela, E. J.: Near-real time retrieval of tropospheric NO_2 from OMI, Atmos. Chem. Phys., 7, 2103-2118, 2007.

Boersma, K. F., Eskes, H. J., Dirksen, R. J., van der A, R. J., Veefkind, J. P., Stammes, P., Huijnen, V., Kleipool, Q. L., Sneep, M., Claas, J., Leitao, J., Richter, A., Zhou, Y., and Brunner, D.: An improved tropospheric NO_2 column retrieval algorithm for the Ozone Monitoring Instrument, Atmos. Meas. Tech., 4, 1905-1928, 2011.

Boschetti, L., and Roy, D. P.: Strategies for the fusion of satellite fire radiative power with burned area data for fire radiative energy derivation, J. Geophys. Res. Atmos., 114, D20302, 2009.

Bowman, D. M. J. S., Balch, J. K., Artaxo, P., Bond, W. J., Carlson, J. M., Cochrane, M. A., D'Antonio, C. M., DeFries, R. S., Doyle, J. C., Harrison, S. P., Johnston, F. H., Keeley, J. E., Krawchuk, M. A., Kull, C. A., Marston, J. B., Moritz, M. A., Prentice, I. C., Roos, C. I., Scott, A. C., Swetnam, T. W., van der Werf, G. R., and Pyne, S. J.: Fire in the Earth System, Science, 324, 481-484, 2009.

Bucsela, E. J., Celarier, E. A., Wenig, M. O., Gleason, J. F., Veefkind, J. P., Boersma, K. F., and Brinksma, E. J.: Algorithm for NO_2 vertical column retrieval from the ozone monitoring instrument, IEEE Trans. Geosci. Remote Sens., 44, 1245–1258, 2006.

Bucsela, E. J., Krotkov, N. A., Celarier, E. A., Swartz, L. N. L. W. H., Bhartia, P. K., Boersma, K. F., Veefkind, J. P., Gleason, J. F., and Pickering, K. E.: A new stratospheric and tropospheric NO_2 retrieval algorithm for nadir-viewing satellite instruments: applications to OMI, Atmos. Meas. Tech. Disc., 6, 1361-1407, 2013.

Burling, I. R., Yokelson, R. J., Akagi, S. K., Urbanski, S. P., Wold, C. E., Griffith, D. W. T., Johnson, T. J., Reardon, J., and Weise, D. R.: Airborne and ground-based measurements of the trace gases and particles emitted by prescribed fires in the United States, Atmos. Chem. Phys., 11, 12197-12216, 2011.

Celarier, E. A., Brinksma, E. J., Gleason, J. F., Veefkind, J. P., Cede, A., Herman, J. R., Ionov, D., Goutail, F., Pommereau, J. P., Lambert, J. C., van Roozendael, M., Pinardi, G., Wittrock, F., Schonhardt, A., Richter, A., Ibrahim, O. W., Wagner, T., Bojkov, B., Mount, G., Spinei, E., Chen, C. M., Pongetti, T. J., Sander, S. P., Bucsela, E. J., Wenig, M. O., Swart, D. P. J., Volten, H., Kroon, M., and Levelt, P. F.: Validation of ozone monitoring instrument nitrogen dioxide columns, J. Geophys. Res., 113, D15S15, doi:10.1029/2007JD008908, 2008.

Cook, P. A., Savage, N. H., Turquety, S., Carver, G. D., O'Connor, F. M., Heckel, A., Stewart, D., Whalley, L. K., Parker, A. E., Schlager, H., Singh, H. B., Avery, M. A., Sachse, G. W., Brune, W., Richter, A., Burrows, J. P., Purvis, R., Lewis, A. C., Reeves, C. E., Monks, P. S., Levine, J. G., and Pyle, J. A.: Forest fire plumes over the North Atlantic: p-TOMCAT model simulations with aircraft and satellite measurements from the ITOP/ICARTT campaign, J. Geophys. Res., 112, D10S43, doi:10.1029/2006JD007563, 2007.

Denman, K. L., Brasseur, A., Chidthaisong, A., Ciais, P., Cox, P. M., Dickinson, R. E., Hauglustaine, D., Heinze, C., Holland, E., Jacob, D., Lohmann, U., Ramachandran, S., da Silva Dias, P. L., Wofsy, S. C., and Zhang, X.: Couplings Between Changes in the Climate System and Biogeochemistry, in: Climate Change 2007: The Physical Science Basis, Contribution of Working Group I to the Fourth Assessment Report of the Intergovernmental Panel on Climate Change, edited by: Solomon, S., Qin, D., Manning, M., Chen, Z., Marquis, M., Averyt, K. B., Tignor, M., and Miller, H. L., Cambridge University Press, Cambridge, UK and New York, NY, USA, 499–588, 2007.

Ellicott, E., Vermote, E., Giglio, L., and Roberts, G.: Estimating biomass consumed from fire using MODIS FRE, Geophys. Res. Lett., 36, L13401, doi:10.1029/2009GL038581,2009.

Ferek, R. J., Reid, J. S., Hobbs, P. V., Blake, D. R., and Liousse, C.: Emission factors of hydrocarbons, halocarbons, trace gases and particles from biomass burning in Brazil, J. Geophys. Res. Atmos., 103, 32107-32118, 1998.

Fiore, A. M., Naik, V., Spracklen, D. V., Steiner, A., Unger, N., Prather, M., Bergmann, D., Cameron-Smith, P. J., Cionni, I., Collins, W. J., Dalsoren, S., Eyring, V., Folberth, G. A., Ginoux, P., Horowitz, L. W., Josse, B., Lamarque, J. F., MacKenzie, I. A., Nagashima, T., O'Connor, F. M., Righi, M., Rumbold, S. T., Shindell, D. T., Skeie, R. B., Sudo, K., Szopa, S., Takemura, T., and Zeng, G.: Global air quality and climate, Chem. Soc. Rev., 41, 6663-6683, 2012.

Freeborn, P. H.,Wooster, M. J., Hao,W. M., Ryan, C. A., Nordgren, B. L., Baker, S. P., and Ichoku, C.: Relationships between energy release, fuel mass loss, and trace gas and aerosol emissions during laboratory biomass fires, J. Geophys. Res., 113, D01301, doi:10.1029/2007JD008679 , 2008.

Freeborn, P. H., Wooster, M. J., and Roberts, G.: Addressing the spatiotemporal sampling design of MODIS to provide estimates of the fire radiative energy emitted from Africa, Remote Sens. Environ., 115, 475-489, 2011.

Friedl, M. A., Sulla-Menashe, D., Tan, B., Schneider, A., Ramankutty, N., Sibley, A., and Huang, X. M.: MODIS Collection 5 global land cover: Algorithm refinements and characterization of new datasets, Remote Sens. Environ., 114, 168–182, 2010.

Giglio, L., Descloitres, J., Justice, C. O., and Kaufman, Y. J.: An enhanced contextual fire detection algorithm for MODIS, Remote Sens. Environ., 87, 273–282, 2003.

Giglio, L., Csiszar, I., and Justice, C. O.: Global distribution and seasonality of active fires as observed with the Terra and Aqua Moderate Resolution Imaging Spectroradiometer (MODIS) sensors, J. Geophys. Res., 111, G02016, 2006.

Giglio, L.: Characterization of the tropical diurnal fire cycle using VIRS and MODIS observations, Remote Sens. Environ., 108, 407–421, 2007.

Goode, J. G., Yokelson, R. J., Susott, R. A., and Ward, D. E.: Trace gas emissions from laboratory biomass fires measured by open-path Fourier transform infrared spectroscopy: Fires in grass and surface fuels, J. Geophys. Res.-Atmos., 104, 21237–21245, 1999.

Goode, J. G., Yokelson, R. J., Ward, D. E., Susott, R. A., Babbitt, R. E., Davies, M. A., and Hao, W. M.: Measurements of excess O_3, CO_2, CO, CH_4, C_2H_4, C_2H_2, HCN, NO, NH_3, HCOOH, CH_3COOH, HCHO, and CH_3OH in 1997 Alaskan biomass burning plumes by airborne fourier transform infrared spectroscopy (AFTIR), J. Geophys. Res., 105, 22147–22166, 2000.

Granier, C., Bessagnet, B., Bond, T., D'Angiola, A., van der Gon, H. D., Frost, G. J., Heil, A., Kaiser, J. W., Kinne, S., Klimont, Z., Kloster, S., Lamarque, J. F., Liousse, C., Masui, T., Meleux, F., Mieville, A., Ohara, T., Raut, J. C., Riahi, K., Schultz, M. G., Smith, S. J., Thompson, A., van Aardenne, J., van der Werf, G. R., and van Vuuren, D. P.: Evolution of anthropogenic and biomass burning emissions of air pollutants at global and regional scales during the 1980-2010 period, Climatic Change, 109, 163-190, 2011.

Hoelzemann, J. J., Schultz, M. G., Brasseur, G. P., Granier, C., and Simon, M.: Global Wildland Fire Emission Model (GWEM): Evaluating the use of global area burnt satellite data, J. Geophys. Res.-Atmos, 109, D14S04, doi:10.1029/2003JD003666, 2004.

Hoffa, E. A., Ward, D. E., Hao, W. M., Susott, R. A., and Wakimoto, R. H.: Seasonality of carbon emissions from biomass burning in a Zambian savanna, J. Geophys. Res., 104, 13841-13853, 1999.

Hudman, R. C., Murray, L. T., Jacob, D. J., Turquety, S., Wu, S., Millet, D. B., Avery, M., Goldstein, A. H., and Holloway, J.: North American influence on tropospheric ozone and the effects of recent emission reductions: Constraints from ICARTT observations, J. Geophys. Res., 114, D07302, doi:10.1029/2008JD010126, 2009.

Ichoku, C. and Kaufman, Y. J.: A method to derive smoke emission rates from MODIS fire radiative energy measurements, IEEE Trans. Geosci. Remote Sens., 43, 2636–2649, 2005.

Jacob, D. J., Wofsy, S. C., Bakwin, P. S., Fan, S. M., Harriss, R. C., Talbot, R. W., Bradshaw, J. D., Sandholm, S. T., Singh, H. B., Browell, E. V., Gregory, G. L., Sachse, G. W., Shipham, M. C., Blake, D. R., and Fitzjarrald, D. R.: Summertime Photochemistry of the Troposphere at High Northern Latitudes, J. Geophys. Res., 97, 16421–16431, 1992.

Jacob, D. J., Crawford, J. H., Maring, H., Clarke, A. D., Dibb, J. E., Emmons, L. K., Ferrare, R. A., Hostetler, C. A., Russell, P. B., Singh, H. B., Thompson, A. M., Shaw, G. E., McCauley, E., Pederson, J. R., and Fisher, J. A.: The Arctic Research of the Composition of the Troposphere from Aircraft and Satellites (ARCTAS) mission: design, execution, and first results, Atmos. Chem. Phys., 10, 5191-5212, 2010.

Jaeglé, L., Steinberger, L., Martin, R. V., and Chance, K.: Global partitioning of NO_x sources using satellite observations: Relative roles of fossil fuel combustion, biomass burning and soil emissions, Faraday Disc., 130, 407–423, 2005.

Jaffe, D. A., and Wigder, N. L.: Ozone production from wildfires: A critical review, Atmos. Environ., 51, 1-10, 2012.

Jordan, N. S., Ichoku, C., and Hoff, R. M.: Estimating smoke emissions over the US Southern Great Plains using MODIS fire radiative power and aerosol observations, Atmos. Environ., 42, 2007–2022, 2008.

Justice, C. O., Giglio, L., Korontzi, S., Owens, J., Morisette, J. T., Roy, D., Descloitres, J., Alleaume, S., Petitcolin, F., and Kaufman, Y.: The MODIS fire products, Remote Sens. Environ., 83, 244–262, 2002.

Kaufman, Y. J., Justice, C. O., Flynn, L. P., Kendall, J. D., Prins, E. M., Giglio, L., Ward, D. E., Menzel, W. P., and Setzer, A. W.: Potential global fire monitoring from EOS-MODIS, J. Geophys. Res., 103, 32215–32238, 1998.

Kopacz, M., Jacob, D. J., Fisher, J. A., Logan, J. A., Zhang, L., Megretskaia, I. A., Yantosca, R. M., Singh, K., Henze, D. K., Burrows, J. P., Buchwitz, M., Khlystova, I., McMillan, W. W., Gille, J. C., Edwards, D. P., Eldering, A., Thouret, V., and Nedelec, P.: Global estimates of CO sources with high resolution by adjoint inversion of multiple satellite datasets (MOPITT, AIRS, SCIAMACHY, TES), Atmos. Chem. Phys., 10, 855–876, doi:10.5194/acp-10-855-2010, 2010.

Korontzi, S., Ward, D. E., Susott, R. A., Yokelson, R. J., Justice, C. O., Hobbs, P. V., Smithwick, E. A. H., and Hao, W. M.: Seasonal variation and ecosystem dependence of emission factors for selected trace gases and $PM_{2.5}$ for southern African savanna fires, J. Geophys. Res., 108, 4758, 2003.

Kottek, M., Grieser, J., Beck, C., Rudolf, B., and Rubel, F.: World map of the Köppen-Geiger climate classification updated, Meteorol. Z., 15, 259-263, 2006.

Lacaux, J. P., Delmas, R., Jambert, C., and Kuhlbusch, T. A. J.: NO_x emissions from African savanna fires, J. Geophys. Res., 101, 23585-23595, 1996.

Lamsal, L. N., Martin, R. V., van Donkelaar, A., Celarier, E. A., Bucsela, E. J., Boersma, K. F., Dirksen, R., Luo, C., and Wang, Y.: Indirect validation of tropospheric nitrogen dioxide retrieved from the OMI satellite instrument: Insight into the seasonal variation of nitrogen oxides at northern midlatitudes, J. Geophys. Res.-Atmos., 115, D05302, doi:10.1029/2009JD013351, 2010.

Lapina, K., Honrath, R. E., Owen, R. C., Val Martin, M., Hyer, E. J., and Fialho, P.: Late summer changes in burning conditions in the boreal regions and their implications for NO_x and CO emissions from boreal fires, J. Geophys. Res., 113, D11304, doi:10.1029/2007JD009421, 2008.

Laursen, K. K., Hobbs, P. V., Radke, L. F., and Rasmussen, R. A.: Some Trace Gas Emissions from North-American Biomass Fires with an Assessment of Regional and Global Fluxes from Biomass Burning, J. Geophys. Res., 97, 20687–20701, 1992.

Leitão, J., Richter, A., Vrekoussis, M., Kokhanovsky, A., Zhang, Q. J., Beekmann, M., and Burrows, J. P.: On the improvement of NO_2 satellite retrievals - aerosol impact on the airmass factors, Atmos. Meas. Tech., 3, 475-493, 2010.

Leung, F. Y. T., Logan, J. A., Park, R., Hyer, E., Kasischke, E., Streets, D., and Yurganov, L.: Impacts of enhanced biomass burning in the boreal forests in 1998 on tropospheric chemistry and the sensitivity of model results to the injection height of emissions, J. Geophys. Res., 112, D10313, doi:10.1029/2006JD008132, 2007.

Liousse, C., Guillaume, B., Gregoire, J. M., Mallet, M., Galy, C., Pont, V., Akpo, A., Bedou, M., Castra, P., Dungall, L., Gardrat, E., Granier, C., Konare, A., Malavelle, F., Mariscal, A., Mieville, A., Rosset, R., Serca, D., Solmon, F., Tummon, F., Assamoi, E., Yoboue, V., and Van Velthoven, P.: Updated African biomass burning emission inventories in the framework of the AMMAIDAF program, with an evaluation of combustion aerosols, Atmos. Chem. Phys., 10, 9631–9646, doi:10.5194/acp-10-9631-2010, 2010.

Mauzerall, D. L., Logan, J. A., Jacob, D. J., Anderson, B. E., Blake, D. R., Bradshaw, J. D., Heikes, B., Sachse, G. W., Singh, H., and Talbot, B.: Photochemistry in biomass burning plumes and implications for tropospheric ozone over the tropical South Atlantic, J. Geophys. Res., 103, 8401–8423, 1998.

McMeeking, G. R., Kreidenweis, S. M., Baker, S., Carrico, C. M., Chow, J. C., Collett, J. L., Hao, W. M., Holden, A. S., Kirchstetter, T. W., Malm, W. C., Moosmuller, H., Sullivan, A. P., and Wold, C. E.: Emissions of trace gases and aerosols during the open combustion of biomass in the laboratory, J. Geophys. Res., 114, D19210, doi:10.1029/2009JD011836, 2009.

Mebust, A. K., Russell, A. R., Hudman, R. C., Valin, L. C., and Cohen, R. C.: Characterization of wildfire NO_x emissions using MODIS fire radiative power and OMI tropospheric NO_2 columns, Atmos. Chem. Phys., 11, 5839-5851, 2011.

Mebust, A. K., and Cohen, R. C.: Observations of a seasonal cycle in NO_x emissions from fires in African woody savannas, Geophys. Res. Lett., 40, 1451-1455, 2013.

Mebust, A. K., and Cohen, R. C.: Space-based observations of fire NO_x emission coefficients: a global biome-scale comparison, Atmos. Chem. Phys., submitted 2013.

Mesinger, F., DiMego, G., Kalnay, E., Mitchell, K., Shafran, P. C., Ebisuzaki, W., Jovic, D., Woollen, J., Rogers, E., Berbery, E. H., Ek, M. B., Fan, Y., Grumbine, R., Higgins, W., Li, H., Lin, Y., Manikin, G., Parrish, D., and Shi, W.: North American regional reanalysis, B. Am. Meteorol. Soc., 87, 343–360, 2006.

Meyer, C. P., Cook, G. D., Reisen, F., Smith, T. E. L., Tattaris, M., Russell-Smith, J., Maier, S. W., Yates, C. P., and Wooster, M. J.: Direct measurements of the seasonality of emission factors from savanna fires in northern Australia, Journal of Geophysical Research-Atmospheres, 117, D20305, 2012.

Monfreda, C., Ramankutty, N., and Foley, J. A.: Farming the planet: 2. Geographic distribution of crop areas, yields, physiological types, and net primary production in the year 2000, Global Biogeochem. Cycles, 22, GB1022, 2008.

Mu, M., Randerson, J. T., van der Werf, G. R., Giglio, L., Kasibhatla, P., Morton, D., Collatz, G. J., DeFries, R. S., Hyer, E. J., Prins, E. M., Griffith, D. W. T., Wunch, D., Toon, G. C., Sherlock, V., and Wennberg, P. O.: Daily and 3-hourly variability in global fire emissions and consequences for atmospheric model predictions of carbon monoxide, Journal of Geophysical Research-Atmospheres, 116, 2011.

Nicholson, S. E.: The nature of rainfall variability over Africa on time scales of decades to millenia, Global and Planetary Change, 26, 137-158, 2000.

Pfister, G. G., Wiedinmyer, C., and Emmons, L. K.: Impacts of the fall 2007 California wildfires on surface ozone: Integrating local observations with global model simulations, Geophys. Res. Lett., 35, L19814, doi:10.1029/2008GL034747, 2008.

Radke, L. F., Hegg, D. A., Hobbs, P. V., Nance, J. D., Lyons, J. H., Laursen, K. K., Weiss, R. E., Riggan, P. J., and Ward, D. E.: Particulate and trace gas emissions from large biomass fires in North America, in: Global biomass burning – Atmospheric, climatic, and biospheric implications, MIT Press, Cambridge, MA, 209-224, 1991.

Ratnam, J., Sankaran, M., Hanan, N. P., Grant, R. C., and Zambatis, N.: Nutrient resorption patterns of plant functional groups in a tropical savanna: variation and functional significance, Oecologia, 157, 141-151, 2008.

Real, E., Law, K. S., Weinzierl, B., Fiebig, M., Petzold, A., Wild, O., Methven, J., Arnold, S., Stohl, A., Huntrieser, H., Roiger, A., Schlager, H., Stewart, D., Avery, M., Sachse, G., Browell, E., Ferrare, R., and Blake, D.: Processes influencing ozone levels in Alaskan forest

fire plumes during long-range transport over the North Atlantic, J. Geophys. Res., 112, D10S41, doi:10.1029/2006JD007576, 2007.

Roberts, G., Wooster, M. J., Perry, G. L. W., Drake, N., Rebelo, L.-M., and Dipotso, F.: Retrieval of biomass combustion rates and totals from fire radiative power observations: Application to southern Africa using geostationary SEVIRI imagery, J. Geophys. Res., 110, D21111, doi:10.1029/2005JD006018, 2005.

Russell, A. R., Perring, A. E., Valin, L. C., Bucsela, E. J., Browne, E. C., Min, K. E., Wooldridge, P. J., and Cohen, R. C.: A high spatial resolution retrieval of NO_2 column densities from OMI: method and evaluation, Atmos. Chem. Phys., 11, 8543-8554, 2011.

Russell, A. R., Valin, L. C., and Cohen, R. C.: Trends in OMI NO_2 observations over the United States: effects of emission control technology and the economic recession, Atmos. Chem. Phys., 12, 12197-12209, 2012.

Saha, S., Moorthi, S., Pan, H. L., Wu, X. R., Wang, J. D., Nadiga, S., Tripp, P., Kistler, R., Woollen, J., Behringer, D., Liu, H. X., Stokes, D., Grumbine, R., Gayno, G., Wang, J., Hou, Y. T., Chuang, H. Y., Juang, H. M. H., Sela, J., Iredell, M., Treadon, R., Kleist, D., Van Delst, P., Keyser, D., Derber, J., Ek, M., Meng, J., Wei, H. L., Yang, R. Q., Lord, S., Van den Dool, H., Kumar, A., Wang, W. Q., Long, C., Chelliah, M., Xue, Y., Huang, B. Y., Schemm, J. K., Ebisuzaki, W., Lin, R., Xie, P. P., Chen, M. Y., Zhou, S. T., Higgins, W., Zou, C. Z., Liu, Q. H., Chen, Y., Han, Y., Cucurull, L., Reynolds, R. W., Rutledge, G., and Goldberg, M.: The NCEP Climate Forecast System Reanalysis, Bull. Am. Meteorol. Soc., 91, 1015-1057, 2010.

Saha, S., Moorthi, S., Wu, X., Wang, J., Nadiga, S., Tripp, P., Behringer, D., Hou, Y.-T., Chuang, H.-y., Iredell, M., Ek, M., Meng, J., Yang, R., Mendez, M. P., Dool, H. v. d., Zhang, Q., Wang, W., Chen, M., and Becker, E.: The NCEP Climate Forecast System Version 2, J. Climate, submitted 2013.

Seiler, W. and Crutzen, P. J.: Estimates of Gross and Net Fluxes of Carbon between the Biosphere and the Atmosphere from Biomass Burning, Clim. Change, 2, 207–247, 1980.

Simpson, I. J., Akagi, S. K., Barletta, B., Blake, N. J., Choi, Y., Diskin, G. S., Fried, A., Fuelberg, H. E., Meinardi, S., Rowland, F. S., Vay, S. A., Weinheimer, A. J., Wennberg, P. O., Wiebring, P., Wisthaler, A., Yang, M., Yokelson, R. J., and Blake, D. R.: Boreal forest fire emissions in fresh Canadian smoke plumes: C_1-C_{10} volatile organic compounds (VOCs), CO_2, CO, NO_2, NO, HCN and CH_3CN, Atmos. Chem. Phys., 11, 6445-6463, 2011.

Spichtinger, N., Wenig, M., James, P., Wagner, T., Platt, U., and Stohl, A.: Satellite detection of a continental-scale plume of nitrogen oxides from boreal forest fires, Geophys. Res. Lett., 28, 4579-4582, 2001.

Val Martin, M., Honrath, R. E., Owen, R. C., Pfister, G., Fialho, P., and Barata, F.: Significant enhancements of nitrogen oxides, black carbon, and ozone in the North Atlantic lower free troposphere resulting from North American boreal wildfires, J. Geophys. Res., 111, D23S60, doi:10.1029/2006JD007530, 2006.

Val Martin, M., Logan, J. A., Kahn, R. A., Leung, F.-Y., Nelson, D. L., and Diner, D. J.: Smoke injection heights from fires in North America: analysis of 5 years of satellite observations, Atmos. Chem. Phys., 10, 1491–1510, doi:10.5194/acp-10-1491-2010, 2010.

van der Werf, G. R., Randerson, J. T., Giglio, L., Collatz, G. J., Mu, M., Kasibhatla, P. S., Morton, D. C., DeFries, R. S., Jin, Y., and van Leeuwen, T. T.: Global fire emissions and the contribution of deforestation, savanna, forest, agricultural, and peat fires (1997-2009), Atmos. Chem. Phys., 10, 11707-11735, 2010.

van Leeuwen, T. T. and van der Werf, G. R.: Spatial and temporal variability in the ratio of trace gases emitted from biomass burning, Atmos. Chem. Phys., 11, 3611–3629, doi:10.5194/acp-11-3611-2011, 2011.

van Leeuwen, T. T., Peters, W., Krol, M. C., and van der Werf, G. R.: Dynamic biomass burning emission factors and their impact on atmospheric CO mixing ratios, J. Geophys. Res. Atmos., 118, 2013.

Vermote, E., Ellicott, E., Dubovik, O., Lapyonok, T., Chin, M., Giglio, L., and Roberts, G. J.: An approach to estimate global biomass burning emissions of organic and black carbon from MODIS fire radiative power, J. Geophys. Res., 114, D18205, doi:10.1029/2008JD011188, 2009.

Wiedinmyer, C., Quayle, B., Geron, C., Belote, A., McKenzie, D., Zhang, X. Y., O'Neill, S., and Wynne, K. K.: Estimating emissions from fires in North America for air quality modeling, Atmos. Environ., 40, 3419–3432, 2006.

Wooster, M. J.: Small-scale experimental testing of fire radiative energy for quantifying mass combusted in natural vegetation fires, Geophys. Res. Lett., 29, 2027, doi:10.1029/2002GL015487, 2002.

Wooster, M. J., Zhukov, B., and Oertel, D.: Fire radiative energy for quantitative study of biomass burning: derivation from the BIRD experimental satellite and comparison to MODIS fire products, Remote Sens. Environ., 86, 83–107, 2003.

Wooster, M. J., Roberts, G., Perry, G. L. W., and Kaufman, Y. J.: Retrieval of biomass combustion rates and totals from fire radiative power observations: FRP derivation and calibration relationships between biomass consumption and fire radiative energy release, J. Geophys. Res., 110, D24311, doi:10.1029/2005JD006318, 2005.

Yokelson, R. J., Goode, J. G., Ward, D. E., Susott, R. A., Babbitt, R. E., Wade, D. D., Bertschi, I., Griffith, D. W. T., and Hao, W. M.: Emissions of formaldehyde, acetic acid, methanol, and other trace gases from biomass fires in North Carolina measured by airborne Fourier transform infrared spectroscopy, J. Geophys. Res.-Atmos., 104, 30109–30125, 1999.

Yokelson, R. J., Urbanski, S. P., Atlas, E. L., Toohey, D. W., Alvarado, E. C., Crounse, J. D., Wennberg, P. O., Fisher, M. E., Wold, C. E., Campos, T. L., Adachi, K., Buseck, P. R., and Hao, W. M.: Emissions from forest fires near Mexico City, Atmos. Chem. Phys., 7, 5569–5584, doi:10.5194/acp-7-5569-2007, 2007.

Yokelson, R. J., Christian, T. J., Karl, T. G., and Guenther, A.: The tropical forest and fire emissions experiment: laboratory fire measurements and synthesis of campaign data, Atmos. Chem. Phys., 8, 3509–3527, doi:10.5194/acp-8-3509-2008, 2008.

Yokelson, R. J., Burling, I. R., Urbanski, S. P., Atlas, E. L., Adachi, K., Buseck, P. R., Wiedinmyer, C., Akagi, S. K., Toohey, D. W., and Wold, C. E.: Trace gas and particle

emissions from open biomass burning in Mexico, Atmos. Chem. Phys., 11, 6787-6808, 2011.

Yokelson, R. J., Burling, I. R., Gilman, J. B., Warneke, C., Stockwell, C. E., de Gouw, J., Akagi, S. K., Urbanski, S. P., Veres, P., Roberts, J. M., Kuster, W. C., Reardon, J., Griffith, D. W. T., Johnson, T. J., Hosseini, S., Miller, J. W., Cocker, D. R., Jung, H., and Weise, D. R.: Coupling field and laboratory measurements to estimate the emission factors of identified and unidentified trace gases for prescribed fires, Atmos. Chem. Phys., 13, 89-116, 2013.

Zhang, X. Y. and Kondragunta, S.: Temporal and spatial variability in biomass burned areas across the USA derived from the GOES fire product, Remote Sens. Environ., 112, 2886–2897, 2008.